General Disclaimer

One or more of the Following Statements may affect this Document

- This document has been reproduced from the best copy furnished by the organizational source. It is being released in the interest of making available as much information as possible.

- This document may contain data, which exceeds the sheet parameters. It was furnished in this condition by the organizational source and is the best copy available.

- This document may contain tone-on-tone or color graphs, charts and/or pictures, which have been reproduced in black and white.

- This document is paginated as submitted by the original source.

- Portions of this document are not fully legible due to the historical nature of some of the material. However, it is the best reproduction available from the original submission.

Produced by the NASA Center for Aerospace Information (CASI)

F78-03

ELECTRONIC SWITCHING SPHERICAL ARRAY ANTENNA

This type of antenna provides uniform gain (8-25 db depending on size and type) throughout extremely large coverage areas.

Final Report For Period June 1976 - March 1978

(NASA-CR-156757) ELECTRONIC SWITCHING SPHERICAL ARRAY ANTENNA Final Report, Jun. 1976 - Mar. 1978 (Ball Bros. Research Corp.) 160 p HC A08/MF A01 CSCL 09C

N78-24461

G3/33 Unclas 21149

Ron Stockton

Ball Aerospace Systems Division
P.O. Box 1062
Boulder, Colorado 80306

APRIL 1978

Prepared for
GODDARD SPACE FLIGHT CENTER
RF Technology Branch
Greenbelt, Maryland 20771

Ball Aerospace Systems Division

TECHNICAL REPORT STANDARD TITLE PAGE

1. Report No.	2. Government Accession No.	3. Recipient's Catalog No.
F78-03		

4. Title and Subtitle	5. Report Date
Electronic Switching Spherical Array Antenna	15 March 1978
	6. Performing Organization Code: B7300
7. Author(s): Ron Stockton	8. Performing Organization Report No.: F78-03
9. Performing Organization Name and Address: Ball Brothers Research Corporation, P.O. Box 1062, Boulder, Colorado 80306	10. Work Unit No.
	11. Contract or Grant No.: NAS5-23518
	13. Type of Report and Period Covered: Final, June 1976 - March 1978
12. Sponsoring Agency Name and Address: Goddard Space Flight Center, Greenbelt, MD 20771, Technical Monitor: Richard P. Hockensmith	14. Sponsoring Agency Code

15. Supplementary Notes

16. Abstract

This work was conducted to demonstrate the performance levels attainable with an ESSA (Electronic Switching Spherical Array) antenna by designing and testing an engineering model. The antenna was designed to satisfy general spacecraft environmental requirements and built to provide electronically commandable beam pointing capability throughout a hemisphere. Constant gain and beam shape throughout large volumetric coverage regions are the principle characteristics. The model is intended to be a prototype of a standard communications and data handling antenna for User scientific spacecraft with the Tracking and Data Relay Satellite System (TDRSS). Some additional testing was conducted to determine the feasibility of an integrated TDRSS and GPS (Global Positioning System) antenna system.

17. Key Words (Selected by Author(s))	18. Distribution Statement
Electronic Switching Spherical Array; Hemispherical Coverage Antenna; TDRSS User Antenna Switching Power Divider	

19. Security Classif. (of this report)	20. Security Classif. (of this page)	21. No. of Pages	22. Price*
UNCLASSIFIED	UNCLASSIFIED	150	UNKNOWN

*For sale by the Clearinghouse for Federal Scientific and Technical Information, Springfield, Virginia 22151.

ELECTRONIC SWITCHING SPHERICAL ARRAY ANTENNA

FINAL REPORT
F78-03

Period
June 1976 - March 1978

Prepared for

National Aeronautics & Space Administration
Goddard Space Flight Center
Greenbelt Road
Greenbelt, Maryland 20771

Prepared by:

Ron Stockton

Ron Stockton, Manager
Antenna Projects

Approved by:

R E Munson

R. E. Munson, Manager
Antenna Systems

BALL BROTHERS RESEARCH CORPORATION
P.O. Box 1062
Boulder, Colorado 80306

PREFACE

This report describes the development of an Electronic Switching Spherical Array Antenna (ESSA) formerly referred to as a Hemispherical Coverage Medium Gain Antenna. This work was conducted by Ball Brothers Research Corporation (BBRC), Boulder, Colorado, between 1 June 1976 and 1 March 1978, for the Goddard Space Flight Center, Greenbelt, Maryland under NASA Contract NAS5-23518.

The purpose of this work was to demonstrate the performance levels attainable with an ESSA antenna by designing and testing an engineering model unit (EMU). The antenna was designed to satisfy general spacecraft environmental requirements and built to provide commandable beam pointing capability throughout a hemisphere. The model is intended to be a prototype of a standard communications and data handling antenna for user scientific spacecraft with the Tracking and Data Relay Satellite System (TDRSS). Supplementary tests were conducted to: 1) examine the feasibility of an integrated TDRSS and GPS (Global Positioning System) antenna system, and 2) to determine the coverage angle limits when the ESSA antenna is deployed a short distance from a simulated spacecraft.

The engineering model developed on this contract provided a gain of 12.85 dB over the predominance of the coverage hemisphere. Further analysis documented in this report indicates that a coverage gain of 14 dB will be attainable in a Flight Qualification unit. Coverage areas greater than 90% spherical or $\pm 155^{0}$ cone angle coverage are practical using an ESSA type antenna. A unique, new technology component called a switching power divider was developed. This simple low-loss device with one input and 120 output ports has enabled the ESSA concept to be successfully implemented. The results of the combined TDRSS/GPS antenna system indicated that the integrated antenna system concept is practical.

Recommendations regarding future development work include the following: 1) determine the operational limits of the EMU ESSA for directive, omni and multibeam modes and develop a microprocessor controller for the acquisition/track mode, 2) reconfigure the switching power divider for 200 output ports, 3) investigate collapsible ESSA antenna configurations, 4) develop a phase corrected ESSA for increased gain, 5) pursue the development of an integrated antenna system concept.

TABLE OF CONTENTS

Section		Page
	PREFACE	
1.0	HEMISPHERICAL COVERAGE MEDIUM GAIN ANTENNA DEV.	1
	1.1 Introduction	1
	1.2 Summary	2
	1.3 Technical Description	8
	1.3.1 Spherical Array Considerations	8
	1.3.1.1 Element Distribution	10
	1.3.1.2 Subarray Selection	11
	1.3.1.3 Spherical Array Efficiencies	11
	1.3.2 Mechanical Details	14
	1.3.3 Switching Power Divider	19
	1.3.4 Other Component Details	24
	1.3.4.1 Radiating Element	24
	1.3.4.2 Controller	24
	1.4 Performance Projections for Flight Qualification Unit	26
	1.4.1 Gain Estimate for Same Size ESSA	26
	1.4.1.1 Enlarge Spherical Array	27
	1.4.1.2 Optimize Subarray	27
	1.4.1.3 Single Frequency Design	28
	1.4.1.4 Switching Power Divider Iso-Isolation	28
	1.4.1.5 Lower Loss Coax	28
	1.4.2 Gain Estimates for Different Size ESSA Antennas	30
	1.5 Future Development Recommendations	33
	1.5.1 Determine Operational Limits	33
	1.5.2 Develop Microprocessor Controller	33
	1.5.3 Increase Switching Power Divider Output Ports	33
	1.5.4 Investigate Collapsible Configurations	34
	1.5.5 Develop Phase Corrected ESSA	34
	1.5.6 Continue Development of Integrated Antenna Concept	34

TABLE OF CONTENTS (Cont'd)

Section		Page
	1.6 Data Summary and Examples	35
	1.6.1 Composite Patterns	35
	1.6.2 Ellipticity	68
	1.6.3 VSWR	68
	1.6.4 Phase Variation	68
	1.6.5 Switching Power Divider	68
2.0	SUPPLEMENTARY TESTS	73
	2.1 ESSA/GPS Performance Degradation Tests	73
	2.1.1 Description of Tests	73
	2.1.1.1 Turnstile Array	73
	2.1.1.2 Microstrip Array	74
	2.1.2 Test Results	76
	2.1.3 Conclusions	85
	2.2 Volumetric Coverage Tests	87
	2.2.1 Description of Tests	87
	2.2.2 Test Results	89
	2.2.3 Conclusions	92

ILLUSTRATIONS

Figure		Page
1-1	Engineering Model ESSA Antenna	3
1-2	Switching Power Divider	5
1-3	Phase Error on Spherical Array	9
1-4	Element Pointing Error on Spherical Array	9
1-5	Optimum Subarray Configuration	12
1-6	Computed Radiation Pattern of Optimum Subarray	12
1-7	Beam Crossover Levels	15
1-8	Spherical Array Element Orientation	15
1-9	ESSA EMU Outline and Mounting Details	17
1-10	Element Mechanical Details	18
1-11	Switching Power Divider Schematic	20
1-12	Switching Power Divider Construction Details	22
1-13	Sidelobe Level Comparison	23
1-14	Element Performance	25
1-15	Recommended Element Feed Pin Attachment	31
1-16	ESSA Coverage Gain -vs- Size	32
1-17	Coverage Area Characterized by Acceptance Tests	36
1-18	Typical ESSA EMU Pattern	37
1-19	Composite Pattern for $\phi = 150^{o}$	39
1-20	Composite Pattern for $\phi = 156^{o}$	40
1-21	Composite Pattern for $\phi = 162^{o}$	41
1-22	Composite Pattern for $\phi = 168^{o}$	42
1-23	Composite Pattern for $\phi = 174^{o}$	43
1-24	Composite Pattern for $\phi = 180^{o}$	44
1-25	Composite Pattern for $\phi = 186^{o}$	45
1-26	Composite Pattern for $\phi = 192^{o}$	46
1-27	Composite Pattern for $\phi = 198^{o}$	47
1-28	Composite Pattern for $\phi = 204^{o}$	48
1-29	Composite Pattern for $\phi = 210^{o}$	49
1-30	Composite Pattern for $\phi = 216^{o}$	50

ILLUSTRATIONS (Cont'd)

Figure		Page
1-31	Composite Pattern for $\phi = 222^{o}$	51
1-32	Composite Pattern for $\phi = 228^{o}$	52
1-33	Composite Pattern for $\phi = 234^{o}$	53
1-34	Composite Pattern for $\theta = 6^{o}$	54
1-35	Composite Pattern for $\theta = 11^{o}$	55
1-36	Composite Pattern for $\theta = 17^{o}$	56
1-37	Composite Pattern for $\theta = 22^{o}$	57
1-38	Composite Pattern for $\theta = 27^{o}$	58
1-39	Composite Pattern for $\theta = 33^{o}$	59
1-40	Composite Pattern for $\theta = 39^{o}$	60
1-41	Composite Pattern for $\theta = 45^{o}$	61
1-42	Composite Pattern for $\theta = 50^{o}$	62
1-43	Composite Pattern for $\theta = 56^{o}$	63
1-44	Composite Pattern for $\theta = 62^{o}$	64
1-45	Composite Pattern for $\theta = 67^{o}$	65
1-46	Composite Pattern for $\theta = 73^{o}$	66
1-47	Composite Pattern for $\theta = 77^{o}$	67
1-48	Typical Beam Ellipticity	69
1-49	Typical Input VSWR	70
1-50	Typical Beam to Beam Phase Variations	71
1-51	Switching Power Divider Amplitude and Phase Data	72
2-1	GPS Turnstile Element on ESSA	75
2-2	GPS Microstrip Element on ESSA	77
2-3	ESSA Degradation Due to GPS Turnstile	81
2-4	ESSA Configuration for Coverage Limit Tests	88
2-5	Coverage Gain Limit for 53 cm Spacing	90
2-6	Coverage Gain Limit for 145 cm Spacing	91
2-7	Coverage Gain Anomaly at 53 cm Spacing	93
2-8	Axial Ratio at 53 cm Spacing	94
2-9	Axial Ratio at 145 cm Spacing	95

TABLES

		Page
1-1	Comparative Loss Budget for ESSA Antenna	7
1-2	Electrical and Mechanical Characteristics of Engineering Model ESSA Antenna	6
1-3	Spherical Array Efficiencies	13
1-4	ESSA EMU Weight Budget	19
1-5	Projected Loss Budget for Flight Qualification ESSA Antenna	29
1-6	Projected Electrical and Mechanical Characteristics for a Flight Qualification ESSA Antenna	29
2-1	Turnstile Array Performance on Smooth Hemisphere	76
2-2	Turnstile Array Performance on ESSA Antenna	78
2-3	ESSA/GPS Turnstile Performance Summary	82
2-4	Microstrip Array Performance on Smooth Hemisphere	82
2-5	Microstrip Array Performance on ESSA Antenna	83
2-6	GPS Array Trade-Offs	85
2-7	Coverage Limits Data Summary	89

1.0 HEMISPHERICAL COVERAGE MEDIUM GAIN ANTENNA DEVELOPMENT

1.1 Introduction

With the advent of the Tracking and Data Relay Satellite System (TDRSS), user satellite antennas must provide directed gain in order to transmit even moderate data rates through the multiple access return link. Omnidirectional and low gain antennas are inadequate for data rates over 500 b/s, hence the need for high gain.

This new requirement for higher gain over large coverage angles prompted the development of the Electronic Switching Spherical Array (ESSA) Antenna, which is expected to be the forerunner of a standard integrated antenna system for scientific satellites. This antenna will satisfy coverage gain requirements between 8 and 25 dB depending on type and size. ESSA I is a simple non-phase corrected aperture approach with gain between 8 and 15 dB. Corresponding radii range from 12 to 50 cm. ESSA II is a phase corrected aperture with improved gain and very low sidelobes. Gains between 15 and 25 dB are practical for ESSA II antennas with radii between 30 and 90 cm.

This development work was performed on NASA Contract NAS5-23518. The primary objective of the contract was to design, fabricate and test an engineering model ESSA antenna to satisfy the User command and telemetry data requirement when operating with TDRSS. The antenna is a fixed mounted, electronically scanned array, capable of generating 551 beams one at a time to sufficiently cover a hemisphere with a minimum gain of 13 dB and a design goal of 14 dB or greater. The size, weight and costs of the antenna are compatible with Scout launched satellites. Spacecraft experiment compatibility is assured through the selection of non-magnetic materials with low outgassing properties and a construction technique that prohibits electrostatic build-up.

For future User Satellites or shuttle payloads an integrated ESSA antenna system mentioned above could include all or parts of a S-band transponder, a Global Positioning System (GPS) antenna, receiver and processor assembly and/or

experiment packages. A key consideration regarding the practicality of an integrated TDRSS/GPS antenna system is that the performance, weight and size will be compatible with scientific spacecraft. As an initial step in evaluating these factors, several L-band GPS antennas were added to the EMU ESSA antenna. A series of tests were performed to characterize any interaction between the two antenna systems. A second contract objective, then, was to make performance degradation assessment for each antenna system in this integrated configuration.

Further testing was conducted to evaluate the volumetric coverage limits of an ESSA type antenna when deployed from a simulated AEM spacecraft chassis. The objective of these tests was to verify that 90% spherical coverage can be achieved.

The following sections of this report describe the antenna and components developed to demonstrate the practicality of the ESSA concept. A technical summary is provided in Section 1.2. Section 1.3 describes the technical details of the Engineering Model ESSA antenna. Section 1.4 discusses the projected performance for a future iteration or Flight Qualification Unit, while Section 1.6 contains a summary of the EMU test data with typical examples. Section 2.0 describes the supplementary tests involving the ESSA EMU antenna. Specifically, Section 2.1 contains the results of the ESSA/GPS performance degradation tests and Section 2.2 covers the volumetric coverage tests.

1.2 Summary

An engineering model of the hemispherical coverage medium gain antenna was built and tested and is shown in Figure 1-1. The major system components included an array of 120 radiating elements configured on a 74 cm diameter hemispherical shell, a solid-state RF switching power divider and an electronic control box for beam selection.

The antenna was designed to satisfy general spacecraft environmental requirements and built to demonstrate commandable beam pointing performance throughout

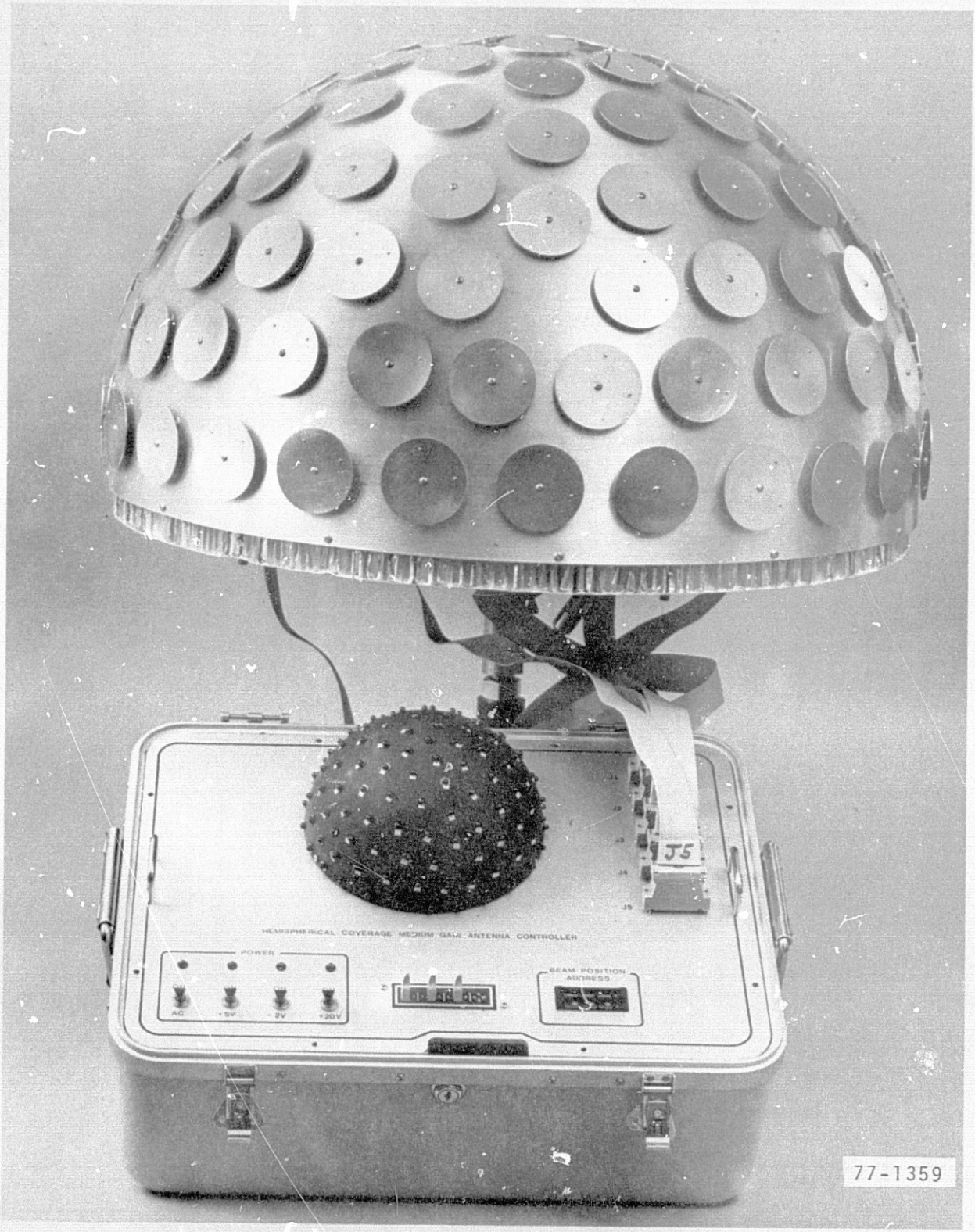

Figure 1-1 Engineering Model ESSA Antenna

REPRODUCIBILITY OF THE
ORIGINAL PAGE IS POOR

a hemisphere. The materials used are non-magnetic with low outgassing properties and the construction technique assures electrostatic cleanliness for spacecraft experiment compatibility. The model is expected to be a forerunner of a standard integrated antenna system for scientific spacecraft.

A directional beam with 13 dBi gain is formed by exciting a 12-element subarray which approximates a circular aperture. Pointing direction is changed electronically by selecting another such subarray. Angular beam steering increments and beam cross-over levels are determined by the degree of overlap between adjacent subarrays. This scanning technique is implied in the title Electronic Switching Spherical Array (ESSA) which describes this class of antennas. The ESSA antenna developed on the contract achieves hemispherical coverage with 551 beams. The primary performance characteristic is uniformity of gain throughout a hemisphere.

A series of tests were performed to demonstrate that other antenna types can be satisfactorily integrated onto the spherical surface. One type of GPS antenna showed a worse case gain degradation of 2 dB. Supplementary tests also verified that $\pm 155^{0}$ cone angle coverage (95% spherical) is achieved when the antenna is deployed 1.5 meters from a simulated AEM spacecraft.

The ESSA concept was successfully implemented by the development of a new technology component called a switching power divider (SPD) shown in Figure 1-2. This is a single low-loss device which distributes the RF input power to any 12-element subarray within the entire 120-element array. It has a single input and a 120 PIN diode controlled outputs. The control logic and diode drivers for the SPD are in the electronic control box. The 12-element subarrays for each of the 551 beams are pre-programmed and stored by means of a programmable read-only memory (PROM) contained in the control box. Beams are selected manually with a hexadecimal thumbwheel switch on the control panel. The small dome on the control box has a light emitting diode (LED) corresponding to each radiating element on the antenna and visually displays the location and make-up of the 12-element subarray for each beam position.

Figure 1-2 Switching Power Divider (with one ground plane removed)

REPRODUCIBILITY OF THE
ORIGINAL PAGE IS POOR

The individual array elements are right hand circular polarized microstrip patches as described by Munson (1). In order to increase the bandwidth the elements are mounted 0.635 cm above the hemispherical ground plane. Inter-element spacings vary between 0.6 λ - 0.8 λ.

A loss budget for the ESSA engineering model is given in Table 1-1. This table compares the computed theoretical losses with the actual losses for each entry. Coverage gain in Table 1-1 is defined as the actual gain at the lowest beam crossover level and represents the minimum achievable gain within the specified coverage limits. Coverage gain can be interpreted as a gain surface which passes through all the beam crossover levels throughout the coverage volume. The peaks of all the beams protrude above this minimum gain surface. A detailed explanation of each parameter listed in the table is given in Section 1.3 Performance projections for a Flight Qualified ESSA antenna are presented in Section 1.4. A summary of significant electrical and mechanical characteristics of the engineering model is presented in Table 1-2.

Table 1-2
ELECTRICAL AND MECHANICAL CHARACTERISTICS
OF ENGINEERING MODEL ESSA ANTENNA

ELECTRICAL	
Frequency Range	2.0 - 2.3 GHz
Beamwidth at -3 dB	26^{o}
Polarization	RHC
Input VSWR	1.5:1 maximum
Phase Variation (Beam to Beam)	3^{o} Typical, 7^{o} maximum
Switching Time (Beam to Beam)	0.6 μsec maximum
Beam Pointing Power (pin diodes + drivers)	.55 W
MECHANICAL	
Diameter	76 cm
Volume	.150 m^3
Weight	6.5 Kg
Mounting	6 pt. Circumferential
Materials	generally non-magnetic with low outgassing properties

Table 1-1

COMPARATIVE LOSS BUDGET FOR ESSA ANTENNA

(Diameter - 5.3 λ)

CONSIDERATION	PREDICTED	ENGINEERING MODEL ACTUALS
GAIN FOR FLAT APERTURE	17.8 dB	17.8 dB
LOSS DUE TO PHASE ERRORS	0.55	0.75
LOSS DUE TO ELEMENT ORIENTATION ERRORS	Negligible	Negligible
LOSS DUE TO POINTING ERRORS	0.25	0.35
- DIRECTIVITY	17.0 dB	16.7 dB
ELEMENT MISMATCH LOSS	0.1	0.5
COUPLER LOSS	0.3	0.3
BEAM CROSSOVER LOSS	0.7	0.8
SWITCH LOSSES ("ON" PORTS)	0.8	0.8
IMPERFECT SWITCH ISOLATION ("OFF" PORTS)	0.1	0.25
LOSS DUE TO NON-UNIFORM APERTURE ILLUMINATION (ASYMMETRIC SWITCH LOADING)	*	0.5
CABLE LOSSES	0.7	0.7
- TOTAL LOSSES	3.6	4.95
TOTAL COVERAGE GAIN	14.3 dB	12.85 dB

*Not predicted

1.3 Technical Description

1.3.1 Spherical Array Considerations

Spherical arrays have natural properties that solve many antenna system problems. The very large solid cone coverage (on the order of 300 degrees by one antenna) is the principle property. Within the solid cone, the antenna can have single or multiple beams which are nearly constant in shape and gain (2). Other properties are very high front to back ratios, constant impedance and mutual coupling as a function of scan angle.

The Electronic Switching Spherical Array (ESSA) is an antenna which takes advantage of all the above properties. It consists of three essential components: microstrip radiator elements, a truncated spherical surface, and a switching power divider. A directive beam is formed by turning on the appropriate set of elements or subarray. Beam steering is accomplished by switching from one subarray to another.

In general, as the size of a uniformly illuminated aperture is increased, the directivity also increases. However, if the aperture is a curved surface, the individual elements do not add in phase, Figure 1-3, and the element patterns do not point in the same direction, Figure 1-4. As a result, the variation of directivity with increasing spherical aperture size will reach a peak and then decline for a fixed radius. A computer program was developed to calculate the directivity and far - field patterns of a non-phase compensated spherical subarray. Given the θ, ϕ coordinates of the elements and the individual element radiation pattern, analysis of an ESSA antenna is straightforward. A description and listing of this program is given in Appendix A.

The steps are as follows:

- Select size or radius of spherical array
- Determine the number of elements
- Specify element distribution on spherical surface
- Computer determines subarray size and elements for optimum directivity

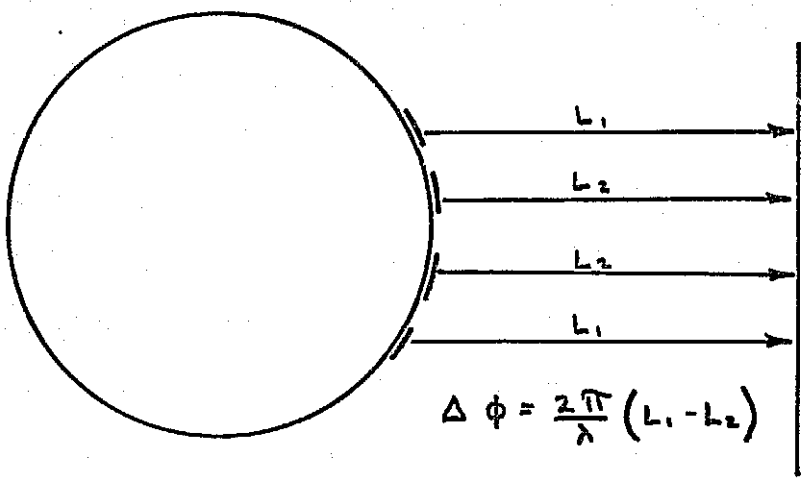

Figure 1-3
Phase Error on Spherical Array

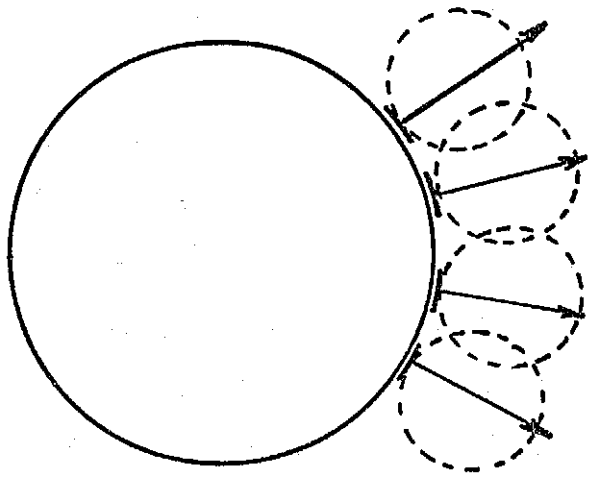

Figure 1-4
Element Pointing Error on Spherical Array

This procedure was used for the design of the engineering model ESSA antenna. The baseline array design assumed the maximum allotted volume of 0.153 m^3 which corresponds to a hemisphere with a radius of approximately 38 cm.

The number of elements would normally be determined by the element distribution, however, in this case the number was limited to 120 which corresponds to a convenient 3° angular segment for each output port on the switching power divider.

1.3.1.1 Element Distribution

The choice of element distribution on the spherical surface is governed by the desire to maintain a constant directivity and pattern while scanning. Ideally, the element distribution should appear to be the same from any far-field observation point. This condition is not realizable for a spherical array since a large number of elements cannot be spaced equidistant on a sphere. However, a large number of elements may be placed almost uniformly by utilizing the symmetry properties of the icosahedron geometry (3). The icosahedron is a three-dimensional figure with 20 faces and 12 vertices. Each face is an equilateral triangle and can be broken down into additional faces as required by the desired frequency. For a given diameter, the higher the frequency, the more sphere-like the icosahedron becomes. The five-frequency icosahedron was selected because it has 126 vertices or element locations on a hemisphere.

The total number of elements reduces to exactly 120, since elements are deleted at the 6 icosahedron vertices. The inter-element spacings are so close at these intersections that a center element would degrade the performance of the surrounding elements. Using this geometry for the element distribution the inter-element spacing only varies from 0.61 λ to 0.68 λ.

This element distribution provides adequate coverage for all portions of the hemisphere except in the vicinity of the equator or $\theta = 90°$. In an effort to improve the equatorial coverage each of the 5-frequency icosahedrons which originate at the zenith were "stretched" down toward the equator so that the bottom row of elements is at $\theta = 88°$. Therefore, the actual element distribution for the engineering model is based on a modified 5-frequency icosahedron

geometry. One of the consequences of this elongation is an increase in the range of inter-element spacings which now varies from 0.65 λ to 0.78 λ. This non-ideal element distribution was employed on the EMU antenna so that the number of elements did not exceed the number of switching power divider output ports.

1.3.1.2 Subarray Selection

Once the radius of the sphere and frequency of the icosahedron have been specified, the edge lengths can be computed (4). These distances are the actual inter-element spacings and are used to define the exact θ, ϕ location of each element in the spherical array. With this information the directivity of any subarray can be computed. The subarray with the highest directivity becomes the active portion of the array. The subarray approximates a circular aperture to achieve a symmetrical beam with a constant beamwidth. This characteristic is necessary to ensure uniform beam crossover levels for any direction of scan.

Analysis of the spherical array described above indicated that the subarray illustrated in Figure 1-5 provides the optimum performance.

1.3.1.3 Spherical Array Efficiencies

The computed far field radiation pattern for the optimum subarray (Figure 1-5) using "unstretched" icosahedron geometry is shown in Figure 1-6. The theoretical directivity is 17.0 dB. The computed directivity for an equivalent flat circular array is 17.8 dB. The 0.8 dB difference is attributable to 0.55 dB phase error loss and 0.25 dB element pointing error loss. The computed directivity for the optimum subarray based on the elongated or modified icosahedron element distribution has a slightly lower value of 16.7 dB. The consequence of expanding the aperture size beyond the optimum is increased phase error loss and element pointing error loss. The magnitude of these losses is 0.75 dB and 0.35 dB respectively. The directivity of the equivalent flat circular array remains at 17.8 dB even though the area has increased because the aperture is no longer uniformly illuminated.

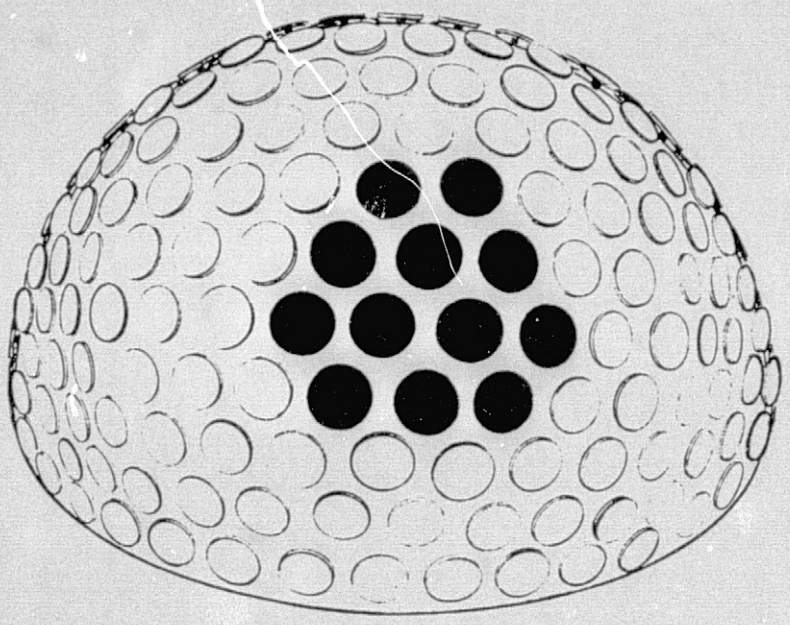

Figure 1-5 Optimum Subarray Configuration

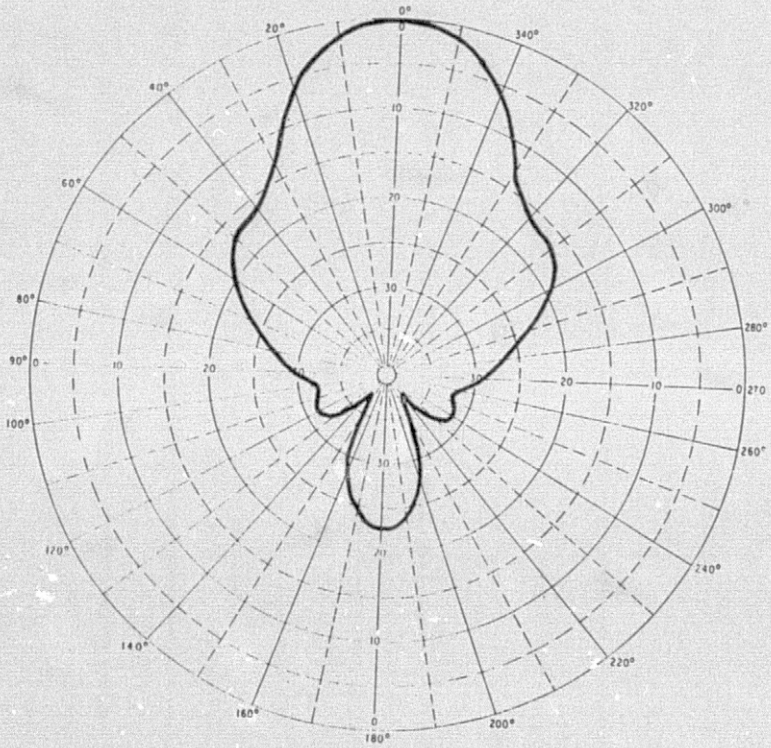

Figure 1-6 Computed Radiation Pattern of Optimum Subarray

It should be emphasized that the 16.7 dB directivity figure is based on the best subarray. In practice, however, this ideal subarray configuration cannot be used for every beam position. Angular beam steering increments and beam crossover levels are determined by the degree of overlap between adjacent subarrays. If the ideal subarray were used for every beam position, the beam steering increments would be quantized to 17° or one element arc spacing. Beam crossovers would then occur at 8.5° either side of the main beam at -1.6 dB or at the 15.1 dB directivity level. Since feed system losses are greater than 2.1 dB, 13 dB gain could not be realized with this approach. An alternative then is to use non-optimum subarrays with reduced gain to provide fill-in coverage and higher beam crossover levels. It was decided that the engineering model ESSA antenna would use two beams to obtain the required fill-in coverage. This reduces the angular beam steering granularity from 17° to 5.6°. The resulting beam crossovers are shown in Figure 1-7. Beams A and A' are the optimum subarray beams located at 0° and 17° respectively. Beams B and B' are the two fill-in beams at 5.6° and 11.2° with a directivity of 16.2 dB or 0.5 dB below that of the optimum subarray. The lowest beam crossover level occurs between beams B and B' and is 0.7 dB down for a directivity of 16.0 dB. This 0.7 dB is attributed to the 0.5 dB lower directivity of the fill-in beams and 0.2 dB crossover loss at 2.8° off the peak of these beams. The directivity for the lowest beam crossover level defines the coverage directivity for an ESSA antenna.

The efficiencies associated with the spherical array configured on the engineering model is given in Table 1-3.

Table 1-3
SPHERICAL ARRAY EFFICIENCIES

PARAMETER	VALUE (dB)
Gain for Flat Aperture	17.8
Loss Due to Phase Errors	0.75
Loss Due to Element Pointing Errors	0.35
Loss Due to Element Orientation Errors	Negligible
Beam Crossover Losses	0.7
TOTAL COVERAGE DIRECTIVITY	16.0

Element orientation errors have a negligible effect on the overall array efficiency. Orientation errors arise from the spherical geometry. The polarization vector of each element must be properly oriented with respect to its position on the spherical surface. The polarization reference is a $\phi = 0$ line. Elements located on other constant ϕ lines have an orientation, Ψ , proportional to their location as shown in Figure 1-8. Every subarray, therefore, consists of elements which are not co-polarized. The resultant loss is negligible since this effect only skews the beam pointing direction.

The directivity in Table 1-3 represents an average for the majority of the array. As the beam is scanned down to the horizon or $\theta = 90°$, the absence of array elements below the equator causes a severe departure from the optimum subarray configuration. The subarray in this area is compressed in the θ direction and elongated in ϕ. Phase error losses, element pointing error losses, and the beam crossover levels in the ϕ direction increase as the 12-element subarray becomes more elliptical. This is only a limitation in the present engineering model spherical array. In future iterations the spherical array will represent a larger portion of a sphere so that the optimum subarray can be configured for all desired scan angles. This was not done on the engineering model because of the 120 element limit imposed by the switching power divider. A switching power divider with more output ports is considered in Section 1.5.3. The spherical array technology developed for the engineering model and described in this section is not limited to a hemispherical antenna, but is applicable to any spherical surface.

1.3.2 Mechanical Details

An overall outline of the EMU ESSA antenna including the mounting ring is shown in Figure 1-9. Details of the individual components and materials are provided in Appendix C. The major mechanical component is the spherical support structure which also provides the ground plane for the microstrip radiating elements. During the design study phase of the program several techniques were considered for the design and fabrication of a hemispherical surface. A System Engineering Report describing all the candidate approaches is included in Appendix B. Using the criteria of structural integrity, lightweight and

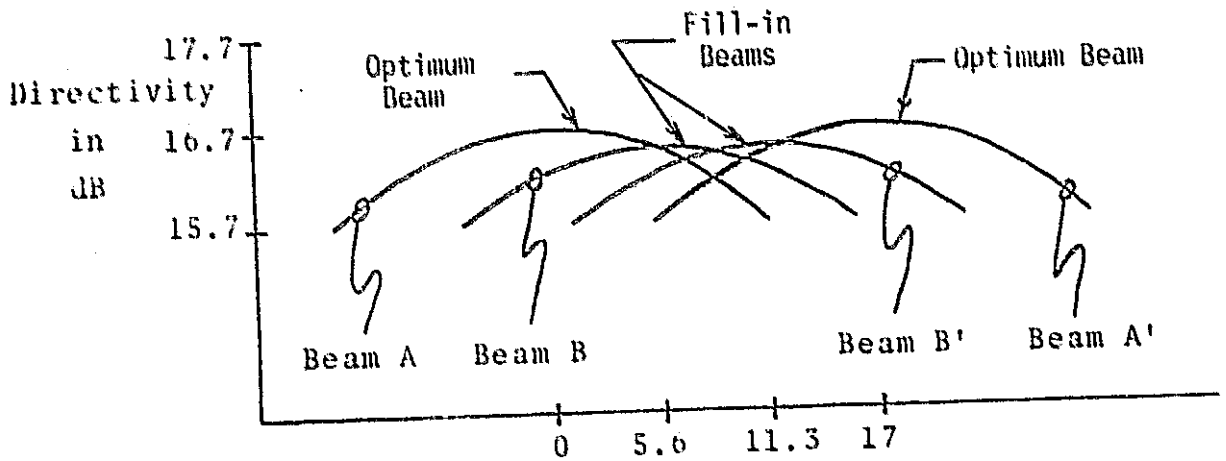

Figure 1-7 Beam Crossover Levels

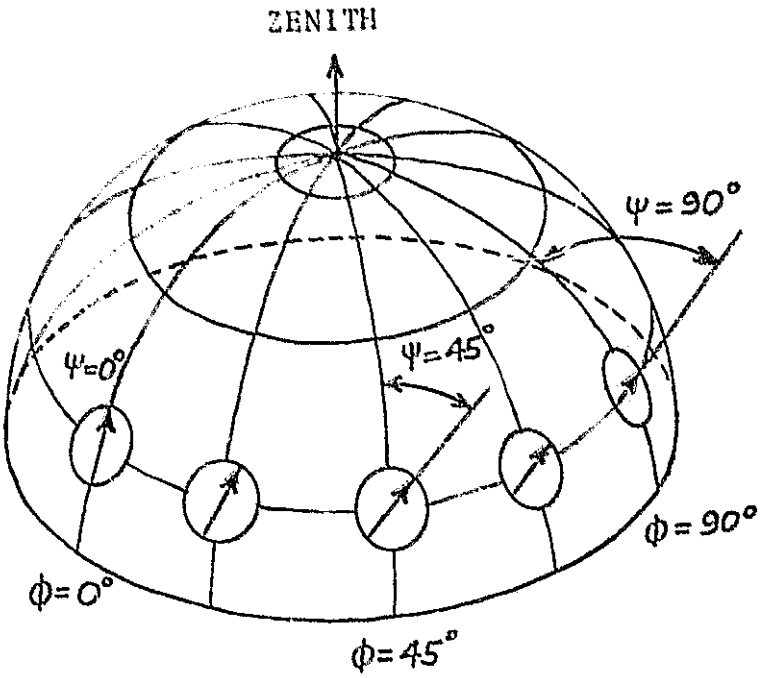

Figure 1-8 Spherical Array Element Orientation

cost effectiveness, a shear spun aluminum dome was selected. With this fabrication technique a thin flat sheet was spun and formed over a mandrel. The thickness varies from the original value of 1.27 mm at the north pole to 0.9 mm in the equatorial region. These domes weigh approximately 2.9 kg.

For future units where minimum weight is essential, the shell thickness could be reduced to a uniform value by chemical milling. The minimum thickness required for structural integrity is 0.57 mm.

Additional weight reduction could be achieved by using a magnesium dome rather than aluminum. However, none of the forming vendors contacted expressed any enthusiasm or encouragement for spinning the hemisphere from magnesium. The concensus was that a spinning of this size from magnesium would become a development program. The weight of a shear spun magnesium dome with a uniform thickness of 0.57 mm would be 1 kg.

A peripheral ring on the interior major diameter provides mechanical stiffening and a means to mount the antenna. This ring was fabricated from magnesium for the EMU and weighs 1 kg. Three spokes converge at the center to provide a mounting platform for the switching power divider as shown in Figure 1-9. The antenna is mounted using the six threaded holes provided on circumference of the ring. The holes are equally spaced on a 70.8 cm bolt circle and are tapped for #10-32 machine screws.

The metallic radiating elements are attached to the hemispherical shell using 0.635 cm metallic standoffs and #6-32 machine screws. Metallic spacers are used to ground the elements to the supporting shell to eliminate static build-up.

Mechanical details of the element-coupler configuration are shown in Figure 1-10. The stripline coupler is supported beneath the element inside the shell by the two transformer housings. The spacing is approximately 2.5 cm which is determined by electrical impedance matching requirements. The other end of the coax cable connects the element to the switching power divider.

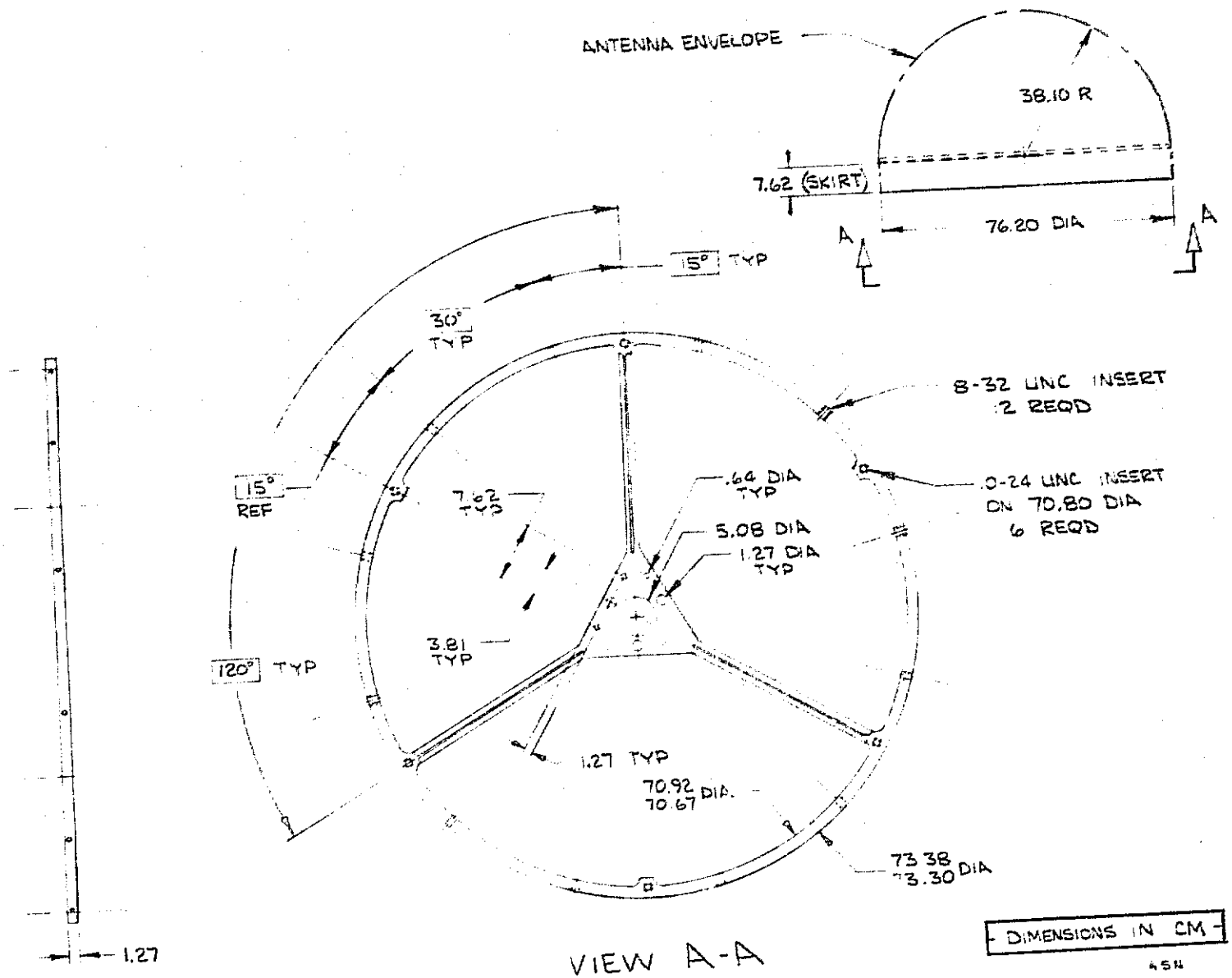

Figure 1-9 ESSA EMU Outline and Mounting Details

REPRODUCIBILITY OF THE
ORIGINAL PAGE IS POOR

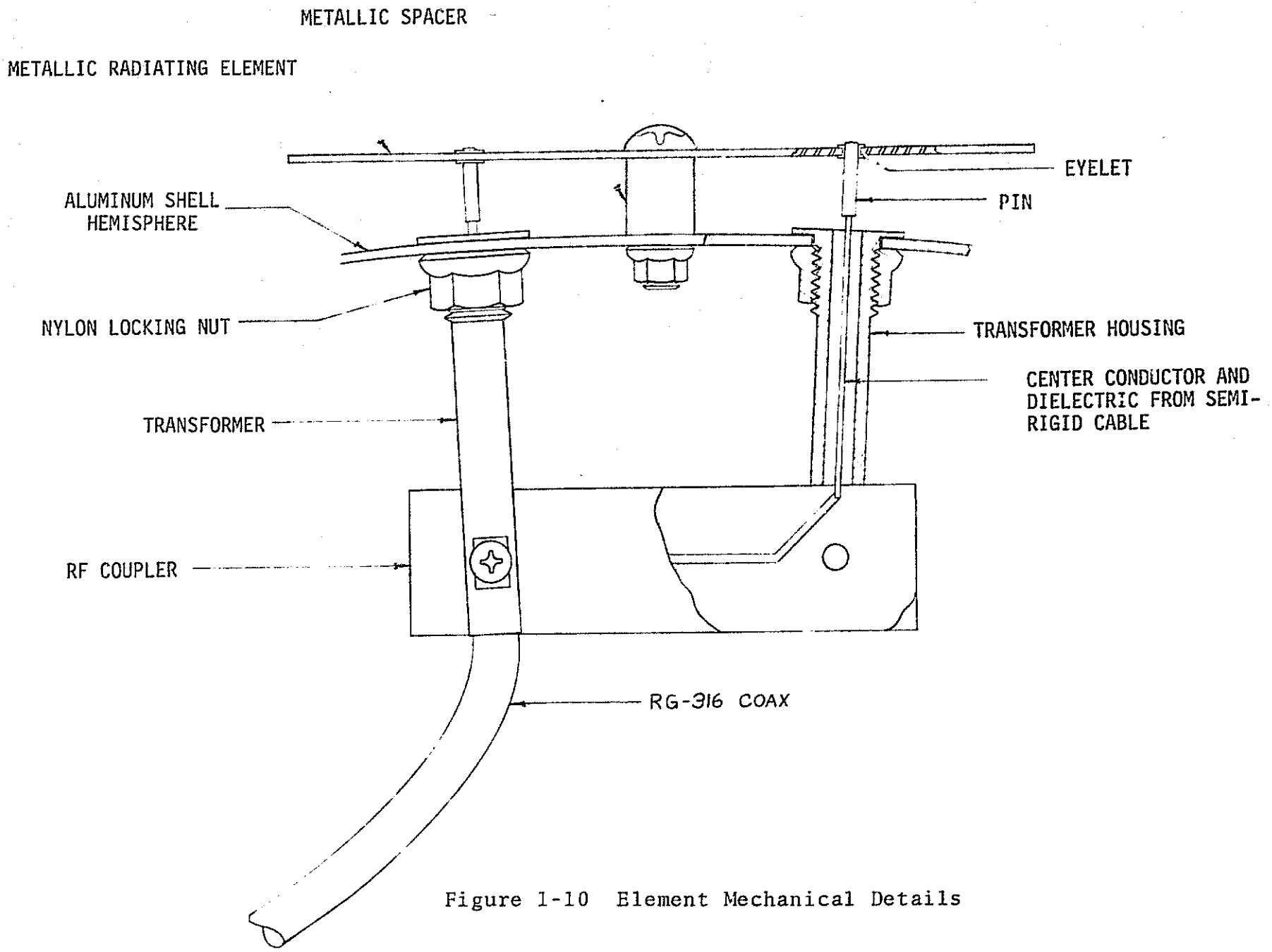

Figure 1-10 Element Mechanical Details

A weight budget for the EMU is given in Table 1-4.

Table 1-4

ESSA EMU Weight Budget

Component	Unit Weight (g)	Quantity Required	Total Weight (g)
Hemispherical Shell	2900	1	2900
Peripheral Ring	1000	1	1000
Element	7.15	120	858
Element Support	1.19	120	143
Element Support Fastener	2.0	120	240
Coupler	2.64	120	317
$\lambda/4$ Transformer	2.36	240	566
Coupler Fastener	0.36	240	86
RG-316 Coax (50 cm)	8.95	120	1074
Switching Power Divider	865	1	865
TOTAL EMU WEIGHT			8049 (g)

1.3.3 Switching Power Divider

The ESSA antenna forms a beam by exciting a 12-element subarray and changes pointing direction by selecting another subarray. This procedure imposes two requirements. First, that the input power be distributed with equal phase and amplitude to each element of the subarray; and, second, that this feed network be capable of exciting any 12-element subarray within the entire 120-element array. A simple means of satisfying both of these requirements with a single low loss component has enabled the ESSA concept to be implemented more efficiently. This component is a switching power divider having 120 outputs and one input. The input is matched to 50 ohms for 12-way power division, while maintaining a 50 ohm impedance level at each output.

A physical schematic is shown in Figure 1-11. Each output is controlled by a series PIN diode switch. The dc blocking capacitors provide the required bias isolation. Bias chokes isolate the microwave signal from the dc bias lines.

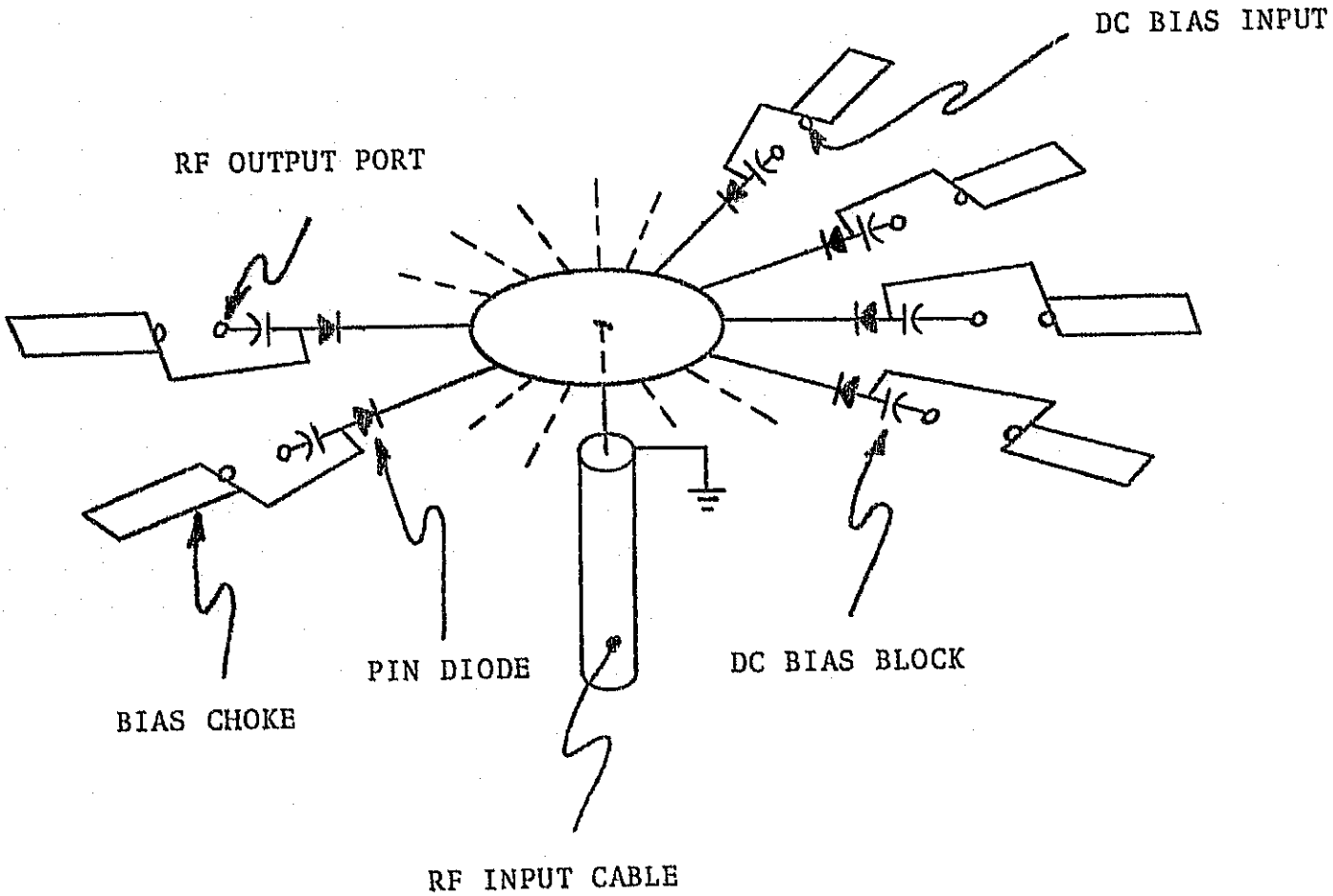

Figure 1-11 Switching Power Divider Schematic

Since the switching requirement can be met by existing PIN diode technology, the basic problem of providing a single-pole 120-throw switch with equal power division to 12 "on" ports is one of microwave physical realization. In this new approach a TEM radial line mode is excited between two parallel circular disks. The outer circumference of the disks is short circuited to create a standing wave in the cavity. A thin dielectric substrate containing 120 individual photoetched transmission lines is suspended between the two ground planes. This circuitry is used to intercept the field lines and transfer the power to an output port through a series PIN diode. A photograph of the completed switching power divider with one ground plane removed is shown in Figure 1-2. Figure 1-12 is a close-up showing the actual construction details. The high impedance section of the bias choke is photoetched on the dielectric. The low impedance coaxial section is fabricated radially in the lower ground plane. The output ports are 50 cm lengths of RG-316 coaxial cable. The inner and outer conductors are soldered to the photoetched board and the ground plane during assembly. The prototype of this new technology device is used in the EMU ESSA antenna. Typical performance levels are 0.8 dB insertion loss for the "on" condition and 12.5 dB isolation in the "off" state.

In the case of perfect isolation all the power is reflected from the "off" ports and is redistributed to the 12 "on" ports which feed the active portion of the array. For a switch with only 13 dB isolation, however, 0.25 dB of the total power is transmitted through the 108 "off" ports and is not redistributed to the active subarray. This appears as an overall system insertion loss. The energy which leaks out of these ports is radiated from the inactive portion of spherical array and appears as low level sidelobes. Figure 1-13 compares typical subarray beams for an ideal switch with perfect isolation and a non-ideal switch with 13 dB isolation.

An additional loss which could not be predicted prior to the switching power divider development is associated with asymmetric loading. Optimum 12-way power division is achieved when the 12 "on" ports are symmetrically distributed every 30^0 on the circumference. Deviations from this optimum distribution are unavoidable. The result is imperfect 12-way power division, and a corresponding nonuniform amplitude distribution across the subarray. In general,

REPRODUCIBILITY OF THE
ORIGINAL PAGE IS POOR

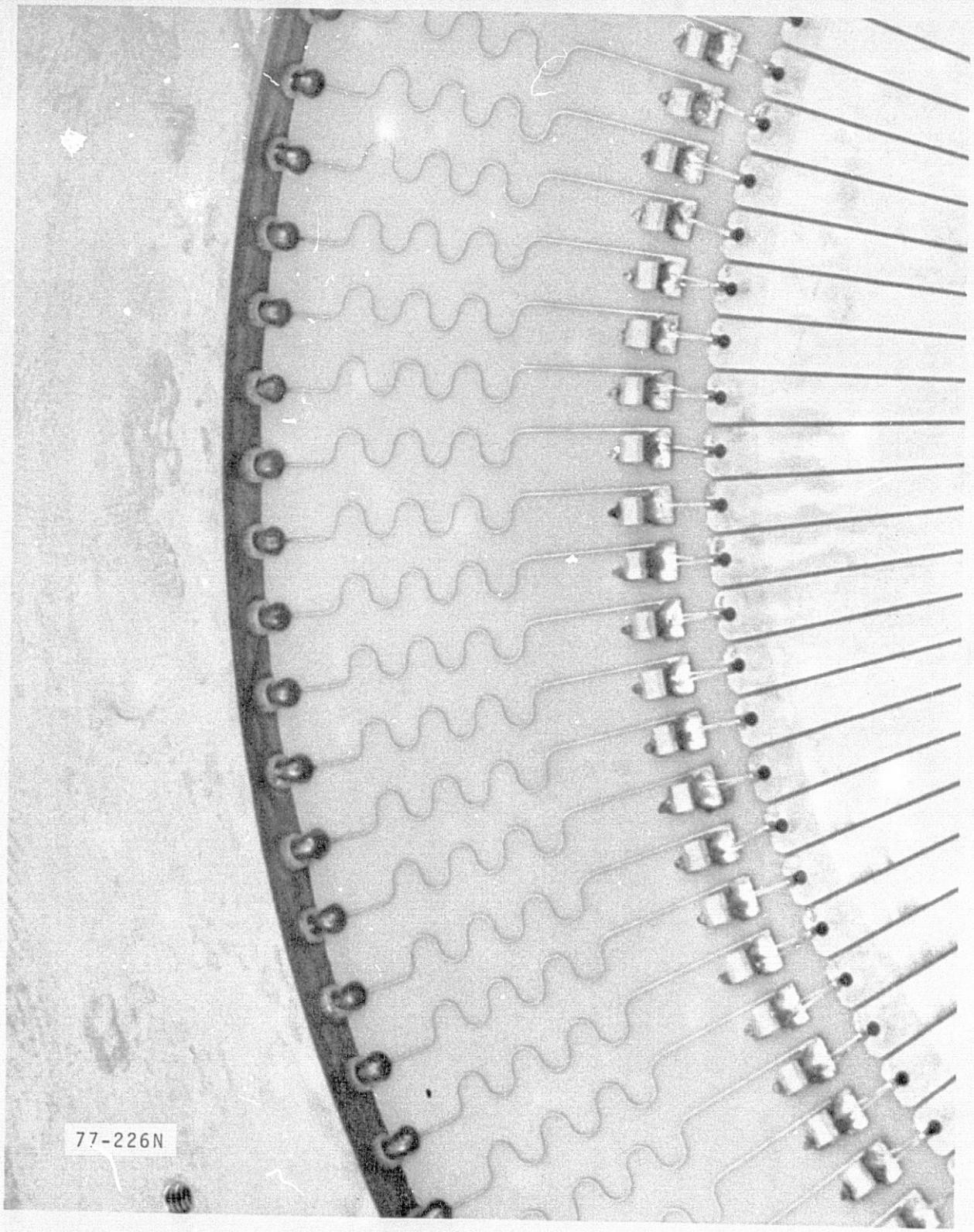

Figure 1-12 Switching Power Divider Construction Details

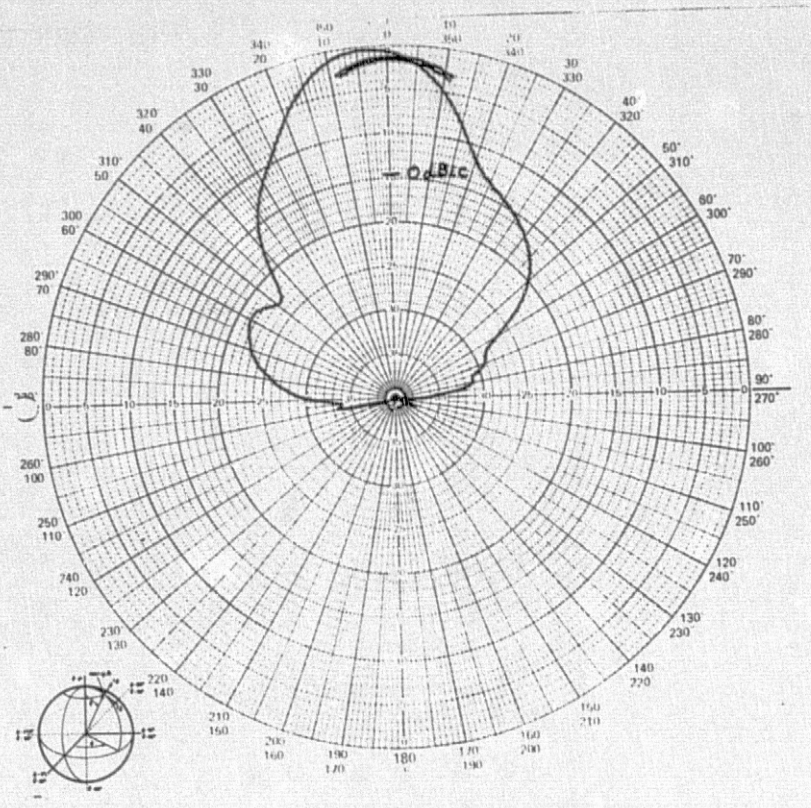

IDEAL SWITCH
WITH PERFECT
ISOLATION

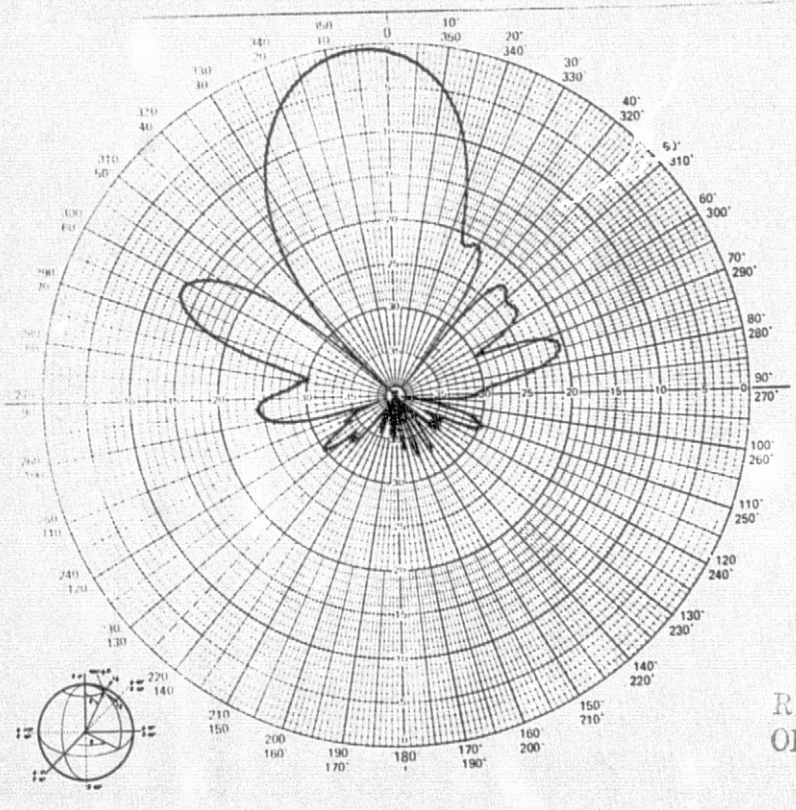

EMU SWITCH
WITH 13 dB
ISOLATION

REPRODUCIBILITY OF THE
ORIGINAL PAGE IS POOR

Figure 1-13 Sidelobe Level Comparison

this tends to reduce the gain of the subarray. In the case of a spherical array a change in the beam pointing direction usually occurs as well. Both of these effects were observed during acceptance testing of the EMU antenna. Measured gain variations of 1.0 dB and beam pointing errors of 10^{o} are directly attributable to asymmetric switch loading. On the average this nonuniform amplitude distribution reduced the subarray gain by 0.5 dB. Beam pointing errors altered the beam crossover points and lowered the total coverage gain by an additional 0.1 dB. In future ESSA antennas these losses could more than likely be minimized by replacing the random switch to element interconnection scheme with correlated interconnections.

The measured switching times for τ_{on} and τ_{off} are 0.18 μsec and 0.6 μsec respectively.

1.3.4 Other Component Details

1.3.4.1 Radiating Element

The individual array elements are right-hand circular (RHC) polarized microstrip patches. In order to increase the bandwidth, the elements are mounted 0.635 cm above the hemispherical ground plane. Two orthogonal modes are equally excited in phase quadrature by means of a stripline overlap coupler mounted inside the hemispherical shell. The quadrature hybrid is necessary to ensure polarization purity across the 2.0 - 2.3 GHz band. A 70 ohm quarterwave coaxial transformer is used to match the high impedance element to the 50 ohm coupler. Figure 1-10 illustrates how the element and quadrature hybrid are interconnected.

The RF characteristics of the element/coupler combination are summarized in Figure 1-14. The gain fall off at the band edges is primarily due to mismatch losses.

1.3.4.2 Controller

The engineering model ESSA antenna uses a control box for manual beam selection. The control box houses the power supplies, logic circuitry, programmable read

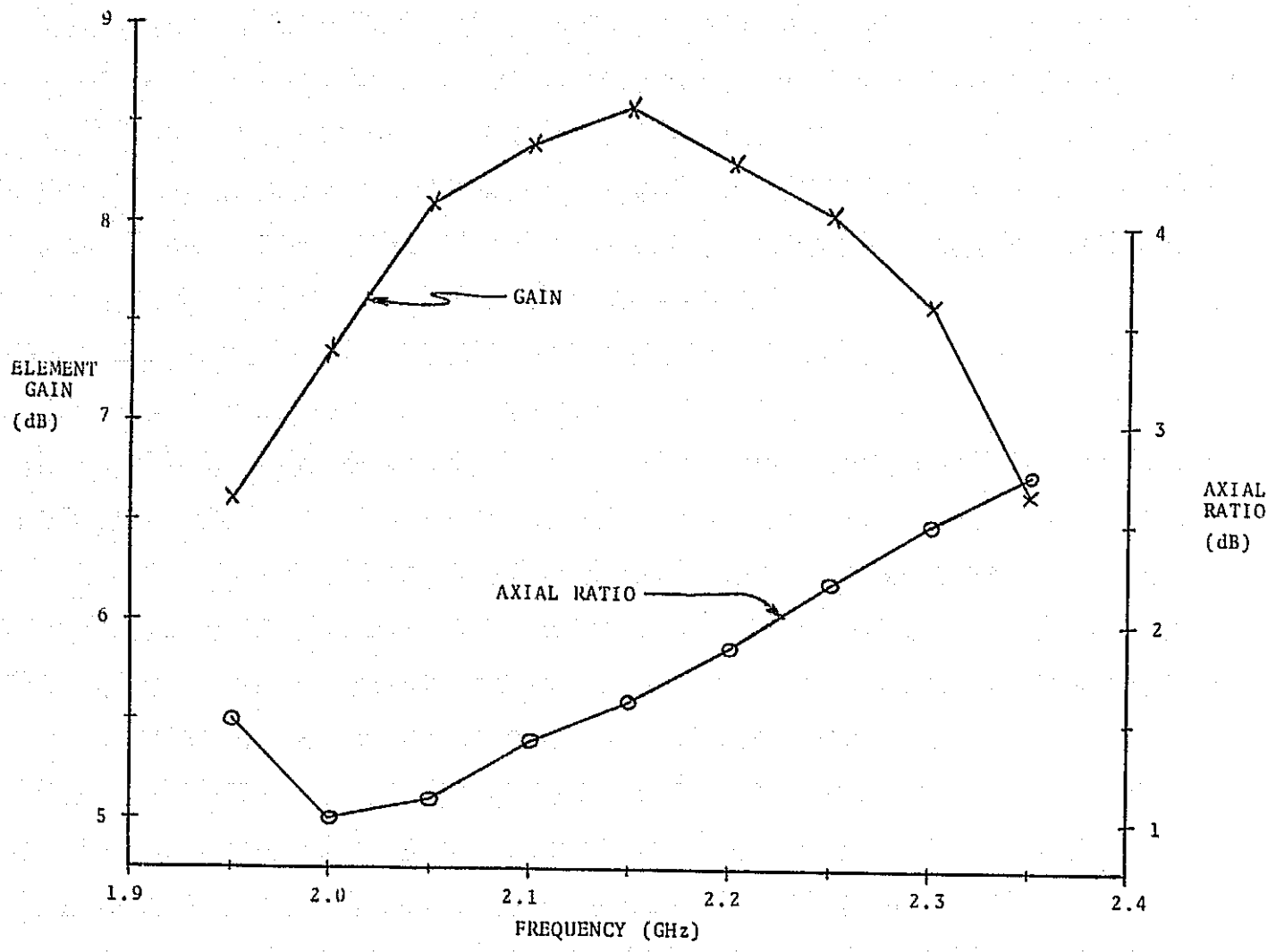

Figure 1-14 Element Performance

only memories (PROMs) and switching power divider diode drivers. For each beam the controller forward biases 12 PIN diodes in the "ON" condition with 25 mA. The remaining 108 diodes are reverse biased with -20 V. The total beam pointing power (drivers + switch diodes) is 0.3 watt. The PROMs require 29 watts to function.

A beam is selected by dialing in the appropriate hexadecimal code on the thumbwheel switch. The PROM interprets this code and determines which switching power divider ports are used and activates the drivers. A display dome on the front panel provides a visual display of the active portion of the spherical array. This display is a replica of the actual antenna array with light emitting diodes (LEDs) simulating the actual antenna elements. A cross reference between the thumbwheel hexadecimal code and the θ,ϕ coordinates for each of the 551 beams is included in Appendix D. A schematic diagram of the controller electronics is in Appendix E.

1.4 Performance Projections for Flight Qualification Unit

The engineering model unit developed on this program successfully demonstrated the feasibility of the ESSA antenna concept. Prior experience, however, suggests that more than one iteration of a model is frequently required to achieve ultimate performance. Using the experience and measured data obtained from this engineering model, performance projections are presented for subsequent ESSA models having 1) the same diameter, and 2) different diameters.

1.4.1 Gain Estimate for Same Size ESSA Antenna

A 1.15 dB improvement in coverage gain can be realized by refining the present EMU ESSA antenna design. The specific refinements and the associated benefits are summarized below:

Refinement	Benefit
• Enlarge spherical array	±150° cone angle coverage
• Use optimum subarray	Reduce subarray losses
• Design for return link band	Higher coverage gain
• Increase switch isolation	Higher coverage gain with reduced side-lobes
• Use low-loss coax	Higher coverage gain

The following paragraphs describe these improvements in detail.

1.4.1.1 Enlarge Spherical Array

The engineering model uses 120 elements for hemispherical coverage. In general, however, a spacecraft application requires long term spherical coverage. This reduces to a more practical value of $\pm 143^{o}$ cone angle coverage (90% spherical) when spacecraft blockage is considered. To achieve this coverage four-fifths of a spherical surface would be configured with approximately 200 elements. Element locations would be determined by 5-frequency icosahedron geometry. A switching power divider with 200 outputs would be configured for this enlarged array. The spherical array would extend beyond the maximum scan angle of $\theta = 143^{o}$ so that a subarray which approximates the optimum circular aperture can be maintained for all beam positions.

This change which is merely an extension of the existing spherical array will provide increased coverage with no directivity fall off at the beam scanning limits of $\theta = 143^{o}$. This will improve the beam crossover level average by 0.1 dB.

1.4.1.2 Optimize Subarray

From Table 1-1 it is clear that the elongated icosahedron geometry of the engineering model expanded the 12-element subarray beyond the optimum aperture size. The additional 0.2 dB phase error loss and 0.1 dB element pointing error loss can be recovered by returning to the optimum subarray.

A further benefit will be realized in the large array with the 200 port switching power divider. Increasing the number of output ports while maintaining 12-way power division will simplify the interconnections between the switch outputs and the elements. The resulting improvement in switch loading symmetry will provide more uniform aperture illumination. The 0.5 dB of loss attributed to this source in the engineering model will be reduced to 0.3 dB.

1.4.1.3 Single Frequency Design

For a TDRSS user spacecraft application it will be advantageous to design the ESSA array for the center of the return link frequency band, 2250 MHz. The engineering model was designed to operate over the entire 2.0 - 2.3 GHz band. As shown in Figure 1-14 peak performance of the radiating element occurs at 2150 MHz. The data for the EMU in Table 1-1, however, is for the test frequency of 2250 MHz. If the engineering model had been tested at design center frequency, the element mismatch loss would be 0.1 dB instead of 0.5 dB for a total coverage gain of 13.25 dB.

A flight qualification ESSA designed and tested at 2250 MHz will only have 0.1 dB mismatch loss.

The gain fall off at the center of the forward link band (2075 MHz) would be less than 1.5 dB.

1.4.1.4 Switching Power Divider Isolation

The switching power divider in the EMU ESSA has 12.5 dB of isolation for the 108 "OFF" ports. This isolation value corresponds to a loss of 0.25 dB. In a Flight Qualification unit the isolation will be greater than 16 dB so that the loss due to imperfect isolation is less than 0.1 dB.

1.4.1.5 Lower Loss Coax

The EMU antenna uses 50 cm of RG-316U coax cable between the switching power divider output ports and the element/coupler inputs. This cable was selected primarily on the basis of minimum weight and not loss. An optional improvement in coverage gain, therefore, involves a tradeoff between coax loss and weight. For example, if a 6.4 mm diameter coaxial cable (predominately air-filled) were used instead of RG-316U, the cable loss would be reduced from 0.7 dB to 0.1 dB but the total weight would increase from 1074 gms to 3222 gms. The tradeoff then is an 0.6 dB increase in gain with an associated increase in weight of 2148 gms. The ultimate decision, therefore, must be based on the spacecraft data rate requirement and weight limitations.

The coverage gain loss budget for subsequent ESSA antennas, specifically a flight qualification unit, is presented in Table 1-5. It is projected on the basis of the EMU measured performance and includes the design changes recommended above.

Table 1-5

Projected Loss Budget for Flight Qualification ESSA Antenna

Gain for flat aperture	17.8
Loss due to phase errors	0.55
Loss due to pointing errors	0.25
Directivity	17.0
Element mismatch loss	0.1
Coupler loss	0.3
Beam crossover loss	0.7
Switch loss ("ON" ports)	0.8
Imperfect switch isolation ("OFF" ports)	0.1
Loss due to nonuniform aperture illumination (result of asymmetric switch loading)	0.3
Cable losses (50 cm of RG-316U)	0.7
TOTAL LOSSES	3.8
TOTAL COVERAGE GAIN	14.0

A summary of the projected electrical and mechanical characteristics for a flight qualification model ESSA antenna is given in Table 1-6.

Table 1-6

PROJECTED ELECTRICAL AND MECHANICAL CHARACTERISTICS FOR A FLIGHT QUALIFICATION ESSA ANTENNA

Electrical

Coverage/Gain at 2250 MHz	14 dB throughout ±115° cone angle
Coverage/Gain at 2075 MHz	12.5 dB throughout ±115° cone angle
Beamwidth at -3 dB	26^{o}

Table 1-6 (Cont)

Electrical (Cont)	
Polarization	LHC or RHC
Input VSWR	1.5:1
Phase Variation (beam to beam)	4° typical, 10° maximum
Switching Time (beam to beam)	0.6 μsec
Beam Point Power (Pin Diodes & Drivers)	0.55 watt
Mechanical	
Diameter	76 cm
Volume	.194 m^3
Weight	6.5 kg
Materials	generally non-magnetic with low outgassing properties

The mechanical design of a Flight Qualification ESSA will in general be identical to the EMU. Mechanical design changes will reflect weight reduction techniques. The spherical shell will be shear spun and chemically milled for uniform thickness as described in Section 1.3.2. The recommended mechanical attachment between the radiating element feed pins and the quarterwave matching transformers is shown in Figure 1-15. This connection is not rigid and will survive vibrational distortions. The switching power divider can be mounted in the upper portion of the shell interior, with cabling dressed and routed to conform with the interior surface. The major portion of the ESSA interior volume could then be used for spacecraft payload. The tradeoff, however, is a slight increase in loss and weight due to increased cable length.

1.4.2 Gain Estimates for Different Size ESSA Antennas

The coverage gain as a function of diameter is given for the ESSA antenna concept in Figure 1-16. These gain figures are based on calculated directivities and realistic system losses for a Flight Qualification ESSA antenna.

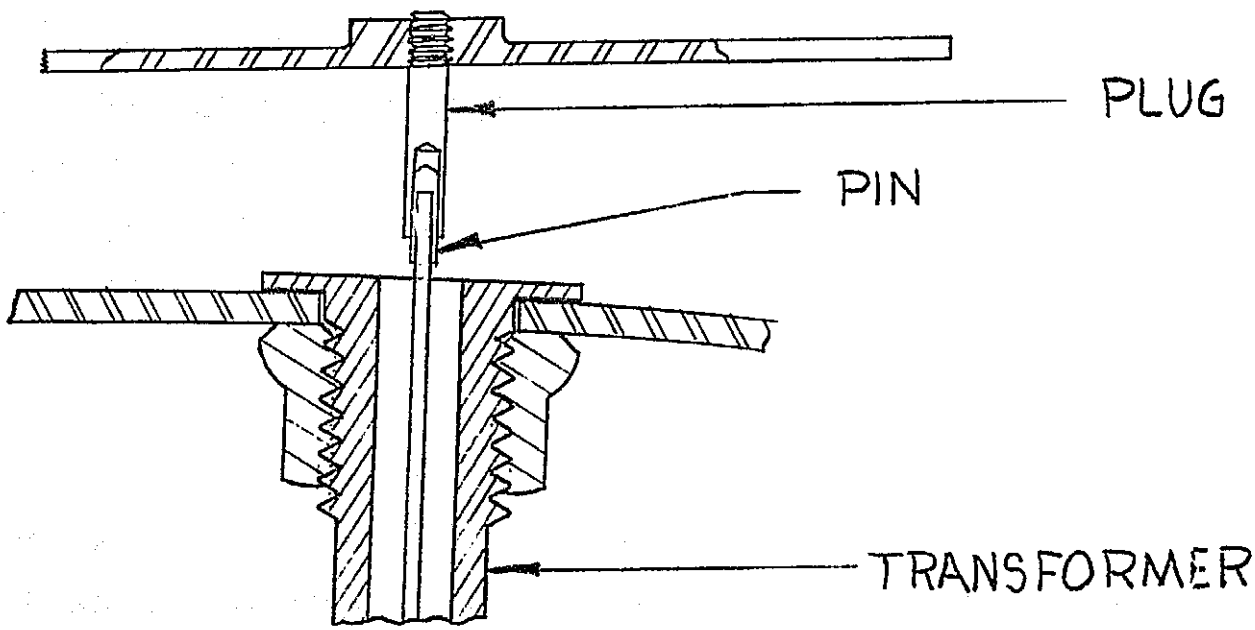

Figure 1-15 Recommended Element Feed Pin Attachment

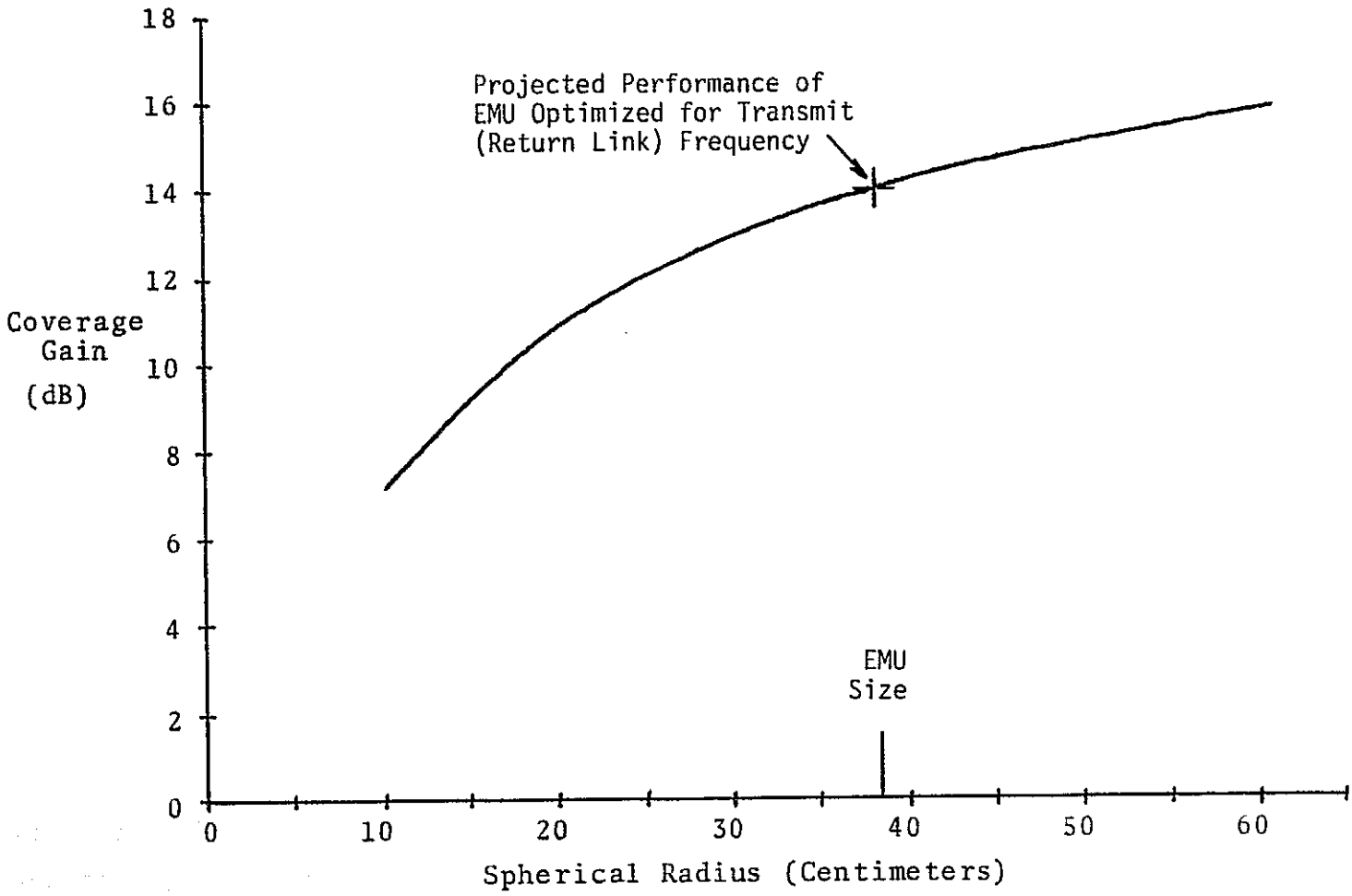

Figure 1-16 ESSA Coverage Gain -vs- Size

1.5 Future Development Recommendations

Although the ESSA concept was successfully demonstrated with the engineering model, there are many areas requiring additional work before the ESSA antenna system becomes a standard for scientific spacecraft. The primary future development areas as well as some others of interest are described in the following paragraphs.

1.5.1 Determine Operational Limits

In order to extend the capabilities of ESSA and make it a comprehensive solution to the TDRSS User spacecraft antenna problem, it is desirable to determine the optimum operating conditions and to demonstrate performance for the following modes of operation: 1) omnidirectional, 2) multi-beam, 3) TDRS acquisition and track. These modes have practical significance for typical satellite applications. Once the ESSA performance and operational limits have been characterized and documented, a general purpose TDRSS User antenna system with full acquisition and track capability can be defined and implemented.

1.5.2 Develop Microprocessor Controller

The engineering model requires a beam steering command from an external source, specifically a manual control box. However, in order to provide TDRS acquisition and track capability and operating mode versatility in a mission environment, it is necessary to control the antenna automatically. This can be done simply and effectively by the addition of a microprocessor controller and the appropriate control algorithms. Such a system would enable the ESSA antenna to fulfill the mission communication and data handling requirements regardless of spacecraft orientations and with very few ground commands.

1.5.3 Increase Switching Power Divider Output Ports

In order to achieve $\pm 143^{o}$ cone angle coverage (90% spherical coverage) a spherical array with roughly 200 elements would have to be configured. This imposes a 200 output port requirement on the switching power divider. Since

120 outputs is the maximum number achievable with the geometry used in the EMU, a new construction technique must be developed to provide 200 or more output port capability.

1.5.4 Investigate Collapsible Configurations

It has been suggested that a collapsible ESSA antenna, with the capability of being stowed during launch, may be a desirable feature for some missions where an integrated antenna system is not required. In order to determine the practicality of this concept and the envelope of the stowed configuration, a study effort would be required.

1.5.5 Develop Phase Corrected ESSA

The present ESSA does not use phase compensation across the aperture, therefore, the optimum directivity is uniquely related to the radius. If a phase corrected aperture is used, however, the directivity will continue to increase as the aperture size is increased. To realize this improvement the proper phase shift must be applied to each element. Preliminary calculations indicate that an improvement in directivity of approximately 3 dB is possible for a phase corrected ESSA having the same radius as the EMU.

The development of the phase compensated ESSA should be pursued so that the ESSA type antennas having gains from 7 to 20 dB will complement the range between the fixed omni systems (-7 to 3 dB) and the gimballed high gain antenna systems (20 - 50 dB).

1.5.6 Continue Development of Integrated Antenna Concept

The degradation tests performed on the EMU when configured with three L-band GPS antennas verified that the basic ESSA antenna can be integrated with other antennas or subsystems. This concept should be pursued so that a complete package for a User Satellite or shuttle payload consisting of an S-band transponder, ESSA antenna, GPS antenna, receiver and processor assembly is developed.

The antenna system could then provide accurate real-time position data to the spacecraft or experiment without ground support. Having this position information on-board would considerably simplify the ESSA/TDRS acquisition and track process as well.

1.6 Data Summary and Examples

1.6.1 Composite Patterns

A summary of the EMU test data and examples are presented in this section. The gain and principal radiation patterns were measured for all beams contained in the space $0^{o} \leq \theta \leq 90^{o}$ and $150^{o} \leq \phi \leq 240^{o}$ where $\phi = 144^{o}$ is the longitudinal centerline of the reference icosahedron and $\phi = 216^{o}$ is the centerline of the adjacent icosahedron.

This space is one-fifth of the total hemisphere, as shown in Figure 1-17, and is perfectly symmetrical with respect to each of the other four-fifths in terms of element locations. For this reason, the entire coverage can be characterized by measuring 20% of the total number of beams. This space includes all of the transition areas such as the Zenith, 72^{o} along the equator and the boundary between two adjacent icosahedrons.

Figure 1-18 shows a typical beam for the EMU ESSA 12-element subarray. Figure 1-19 through 1-33 are composite overlays of actual test data showing the beam peaks, gain and crossover levels. The θ composites are the super-position of all the beams in a plane defined by a constant ϕ value.

Figures 1-34 through 1-47 are composite patterns representing the super-position of all the beams for a constant θ value within the ϕ test sector, $150^{o} \leq \phi \leq 240^{o}$. The figures accurately depict the gain of each beam but not the coverage. Coverage in ϕ is a function of SIN θ. That is the number of beams required to cover a given sector in ϕ at $\theta = 90^{o}$ is greater than the

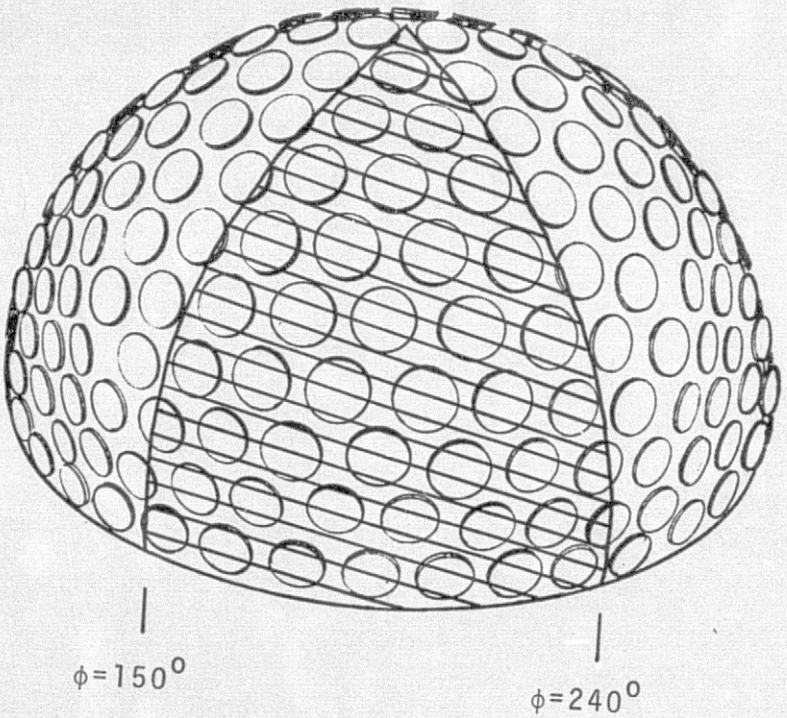

CROSS HATCHED TEST AREA IS 20% OF TOTAL SURFACE

Figure 1-17 Coverage Area Characterized by Acceptance Tests

REPRODUCIBILITY OF THE
ORIGINAL PAGE IS POOR

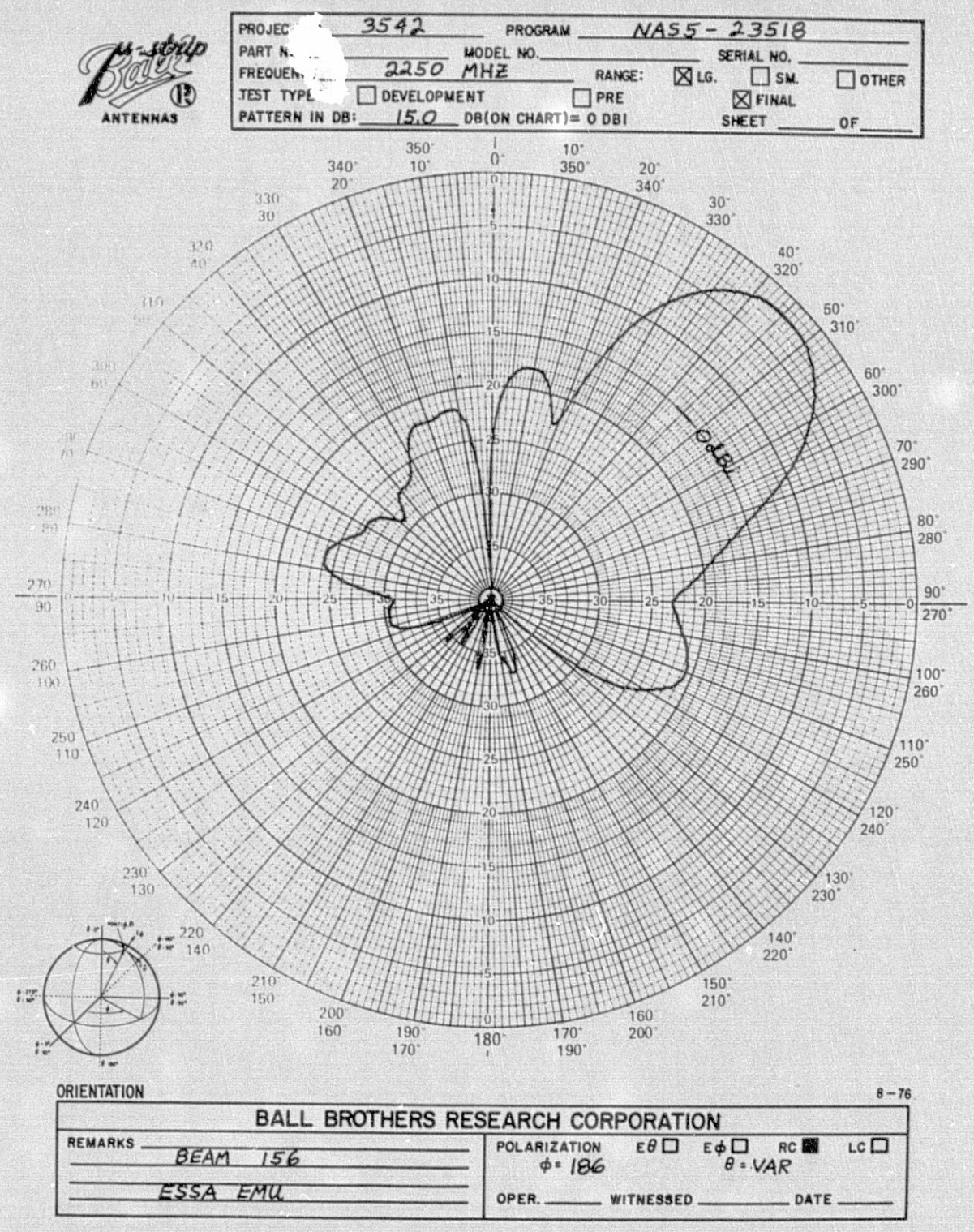

Figure 1-18 Typical ESSA EMU Pattern

number of beams required to cover that same sector for any value of θ less than 90^{o}. As an example of how this affects a two dimensional figure, examine Figure 1-34. If the four beams are moved radially inward they will eventually touch and still further inward they will overlap. The apparent beam crossover levels depend on how close to the center the beams are moved.

Although this factor affects all of the ϕ composites, Figures 1-41 through 1-47 (where θ is greater than 45^{o} and SIN θ is greater than 0.7) give fairly accurate representations of the coverage and beam crossover levels. Figures 1-34 through 1-40 on the other hand do not due to the small θ values. All of the ϕ composites are presented, however, for completeness and gain comparisons.

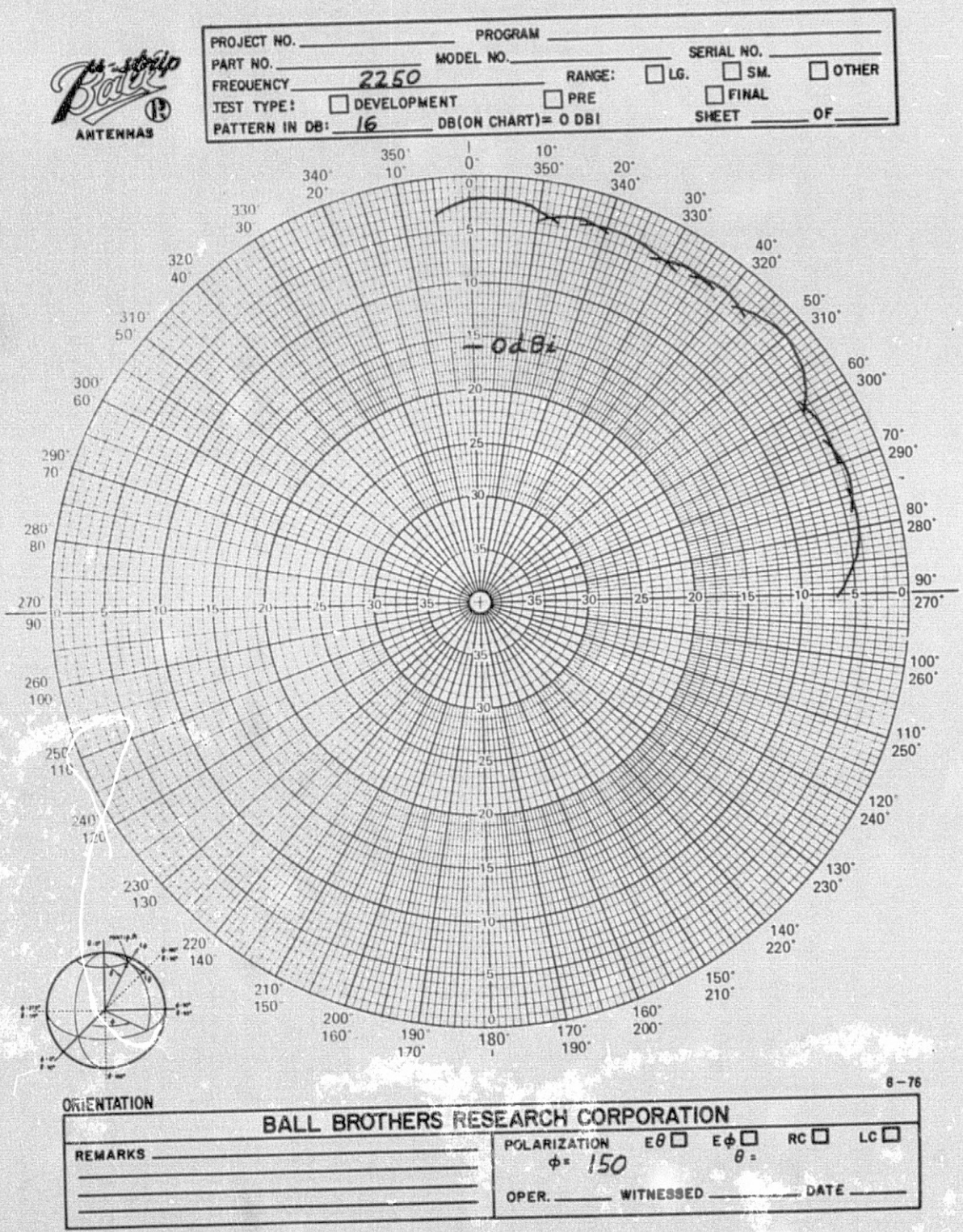

Figure 1-19 Composite Pattern for $\phi = 150^{o}$

REPRODUCIBILITY OF THE
ORIGINAL PAGE IS POOR

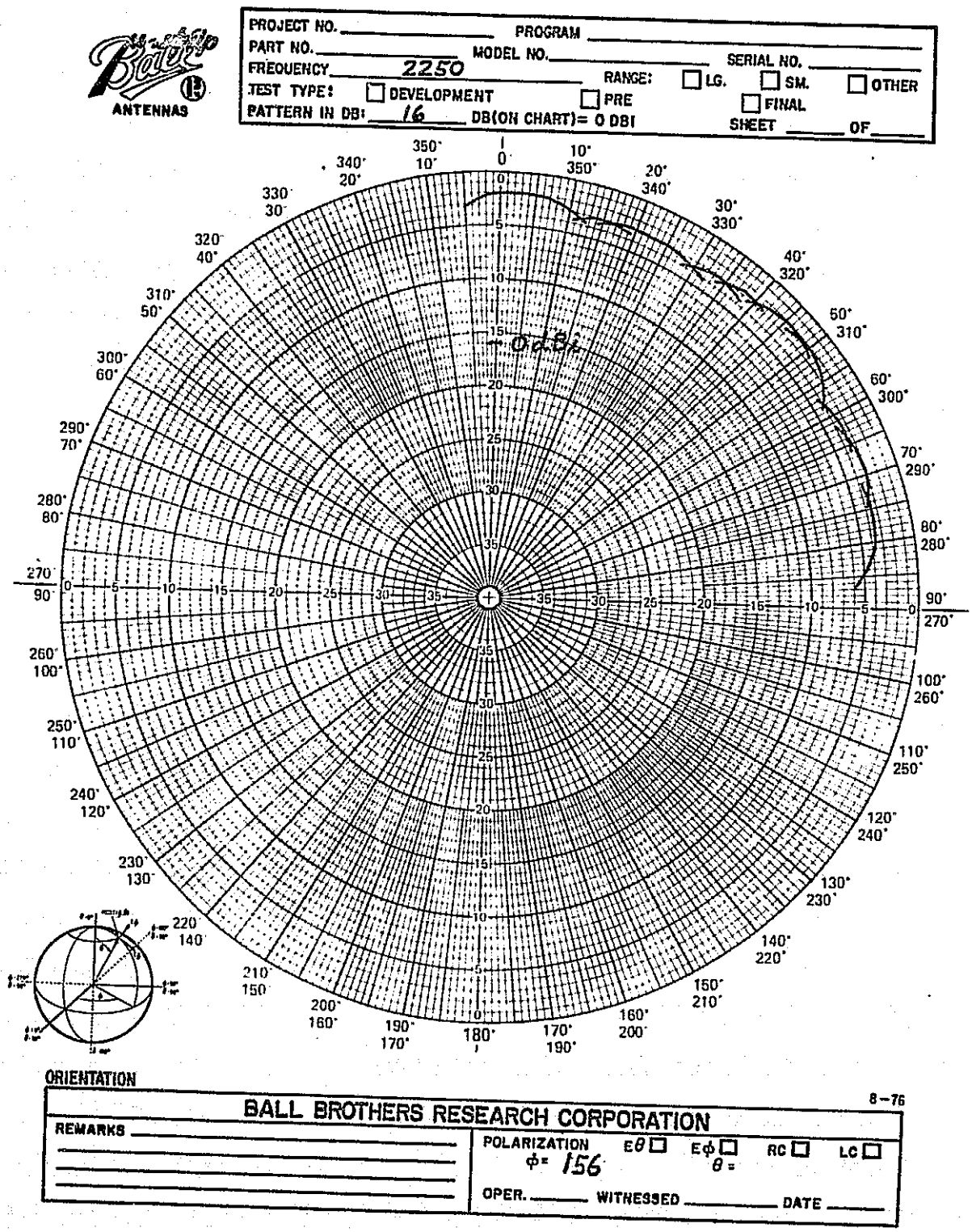

Figure 1-20 Composite Pattern for $\phi = 156^{o}$

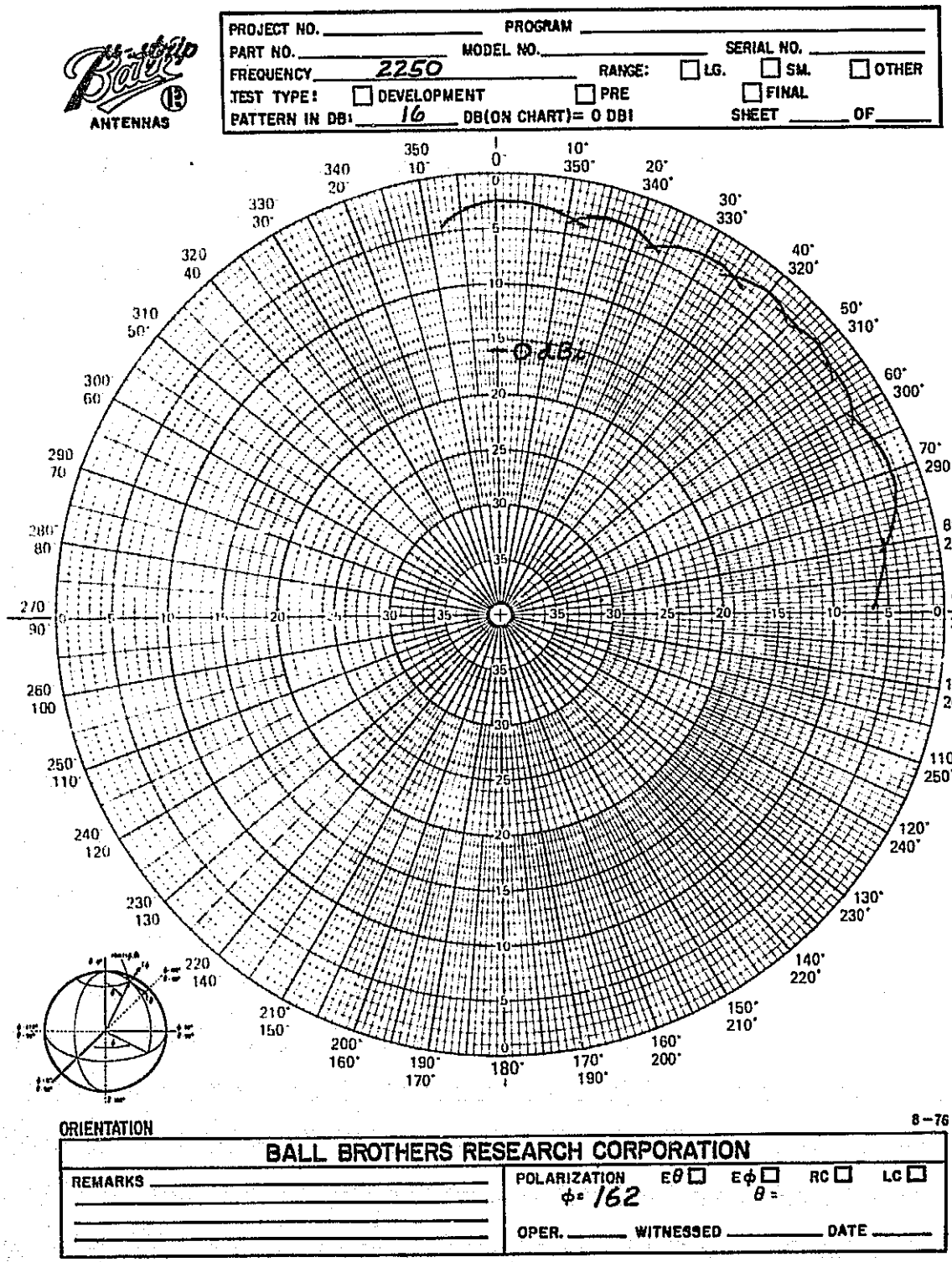

Figure 1-21 Composite Pattern for $\phi = 162^{\circ}$

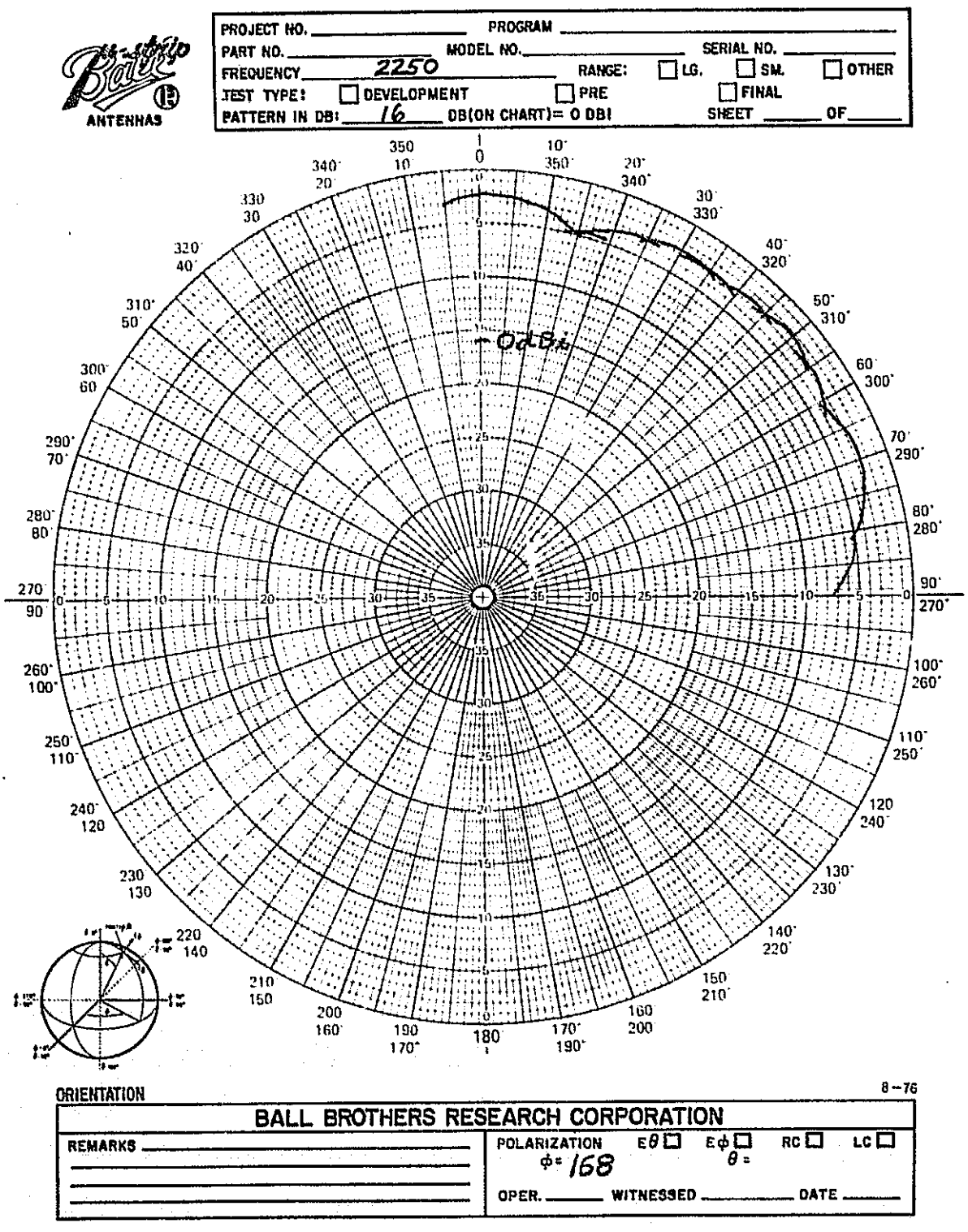

Figure 1-22 Composite Pattern for $\phi = 168^{o}$

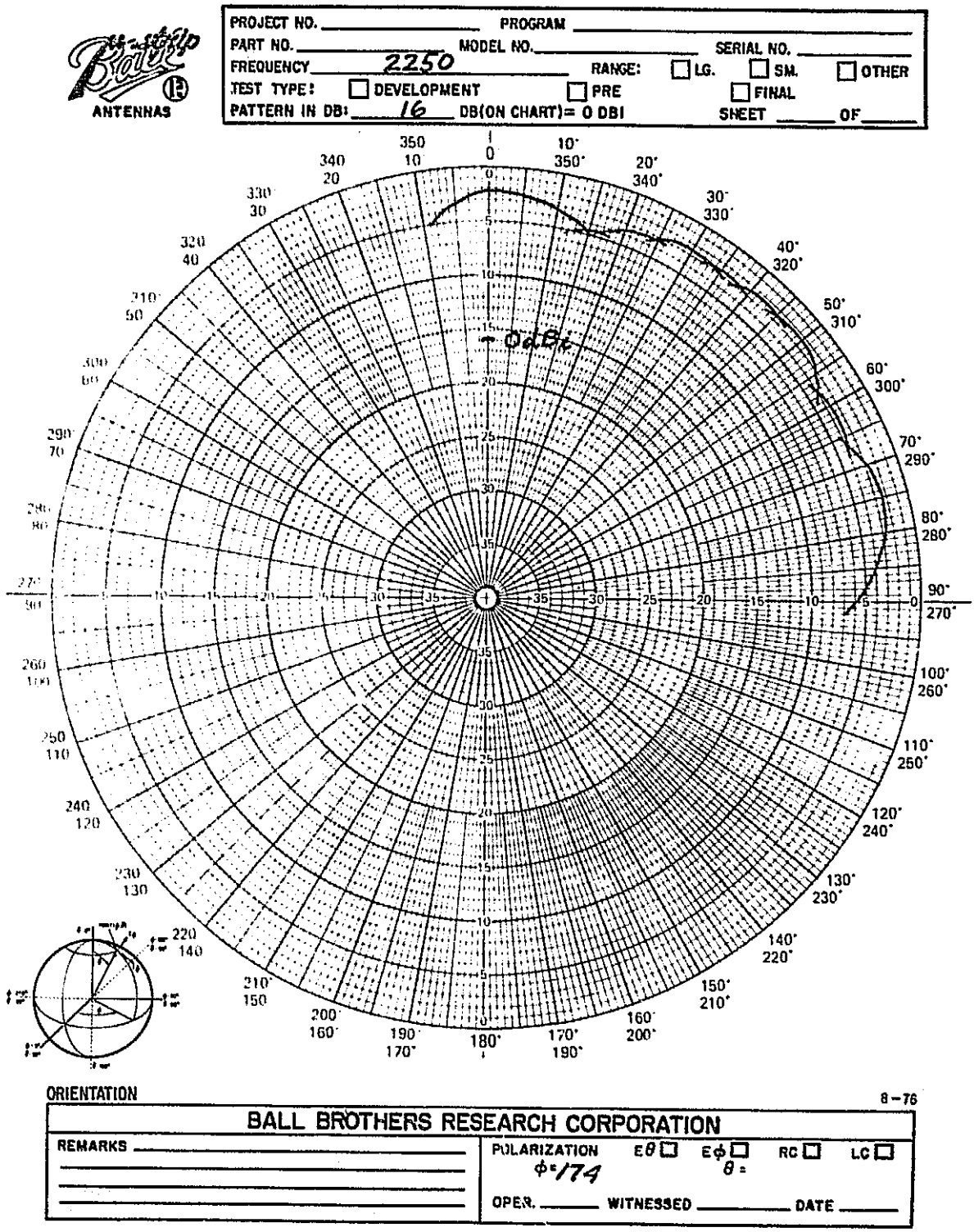

Figure 1-23 Composite Pattern for $\phi = 174^{o}$

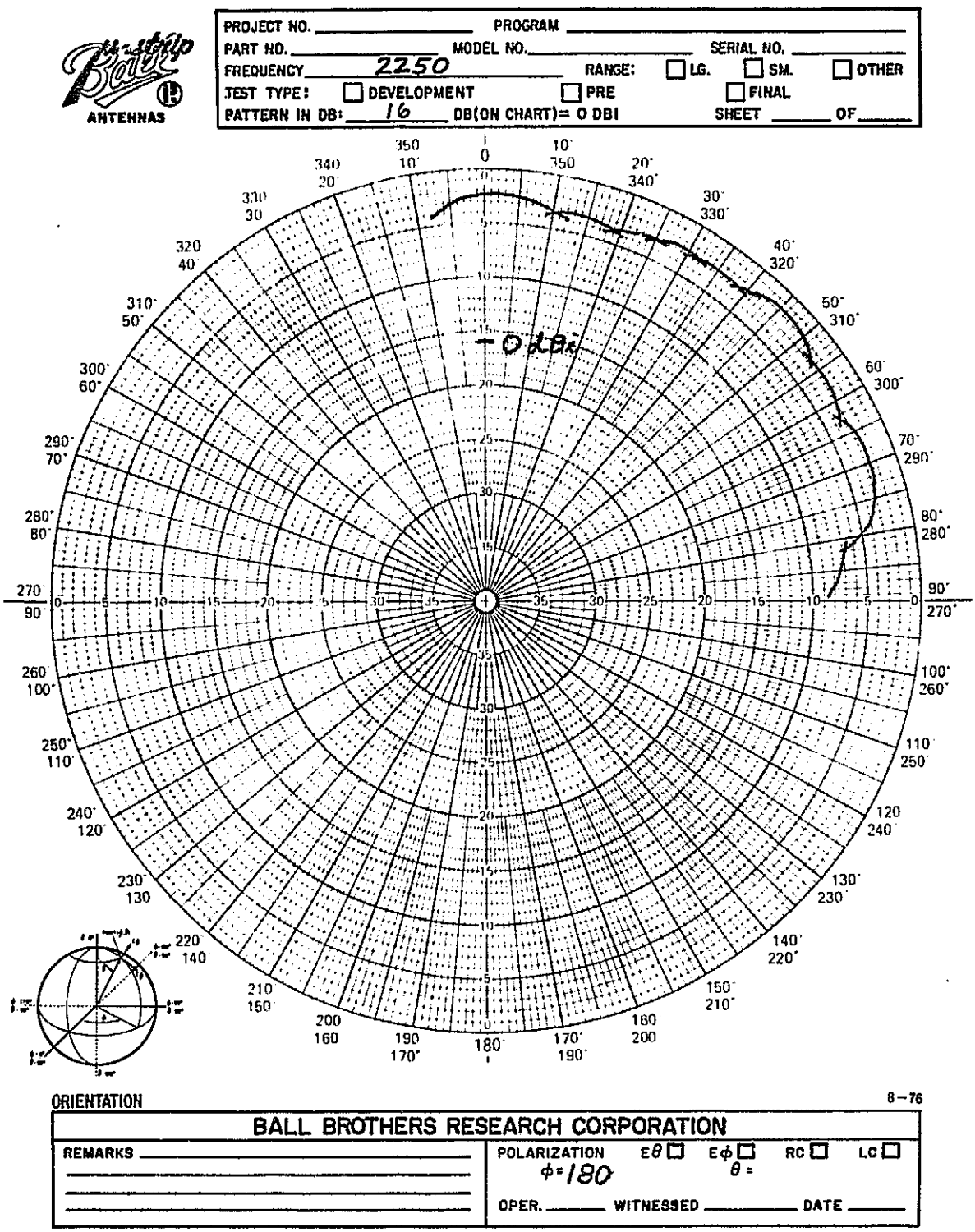

Figure 1-24 Composite Pattern for $\phi = 180^{o}$

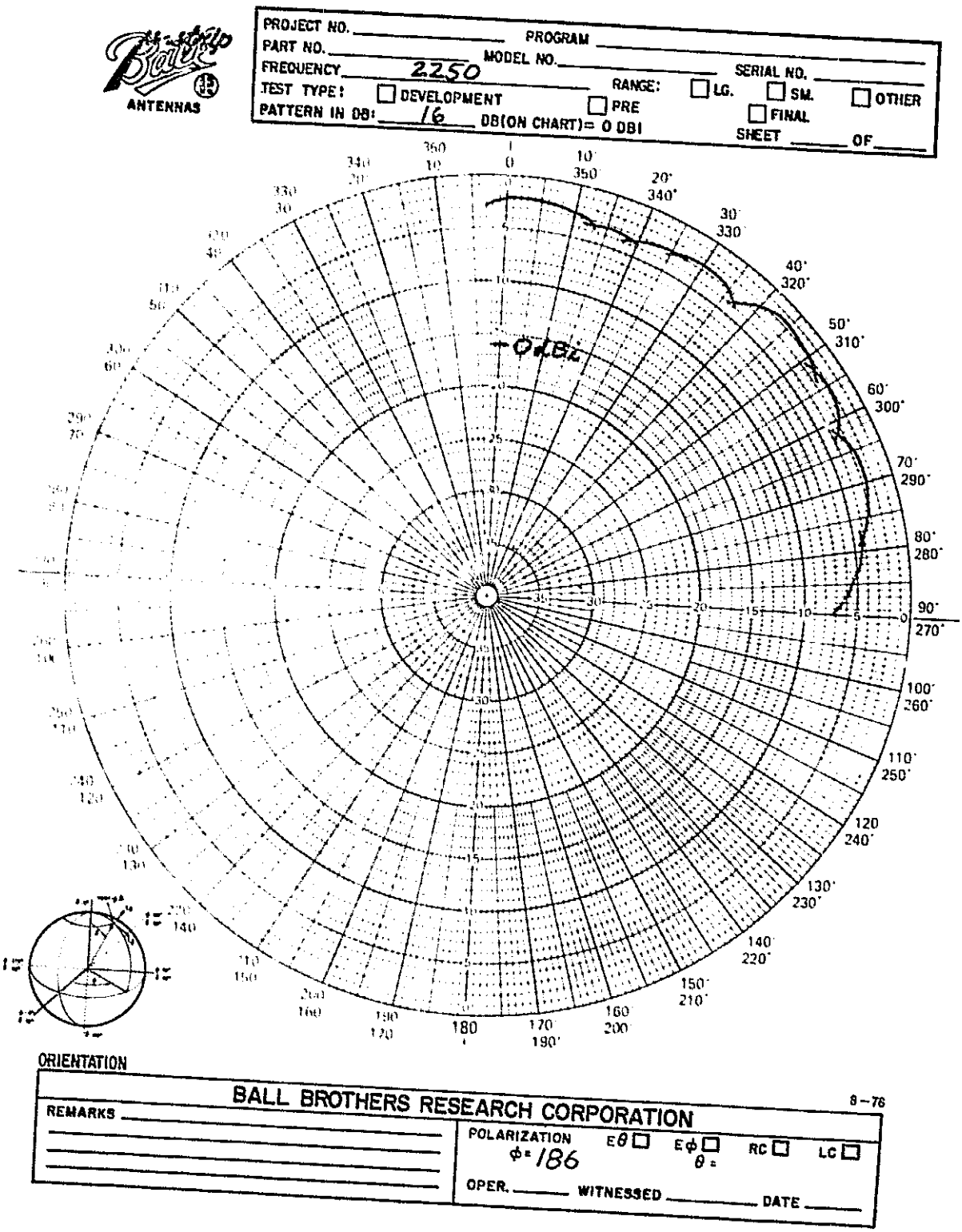

Figure 1-25 Composite Pattern for $\phi = 186^{\circ}$

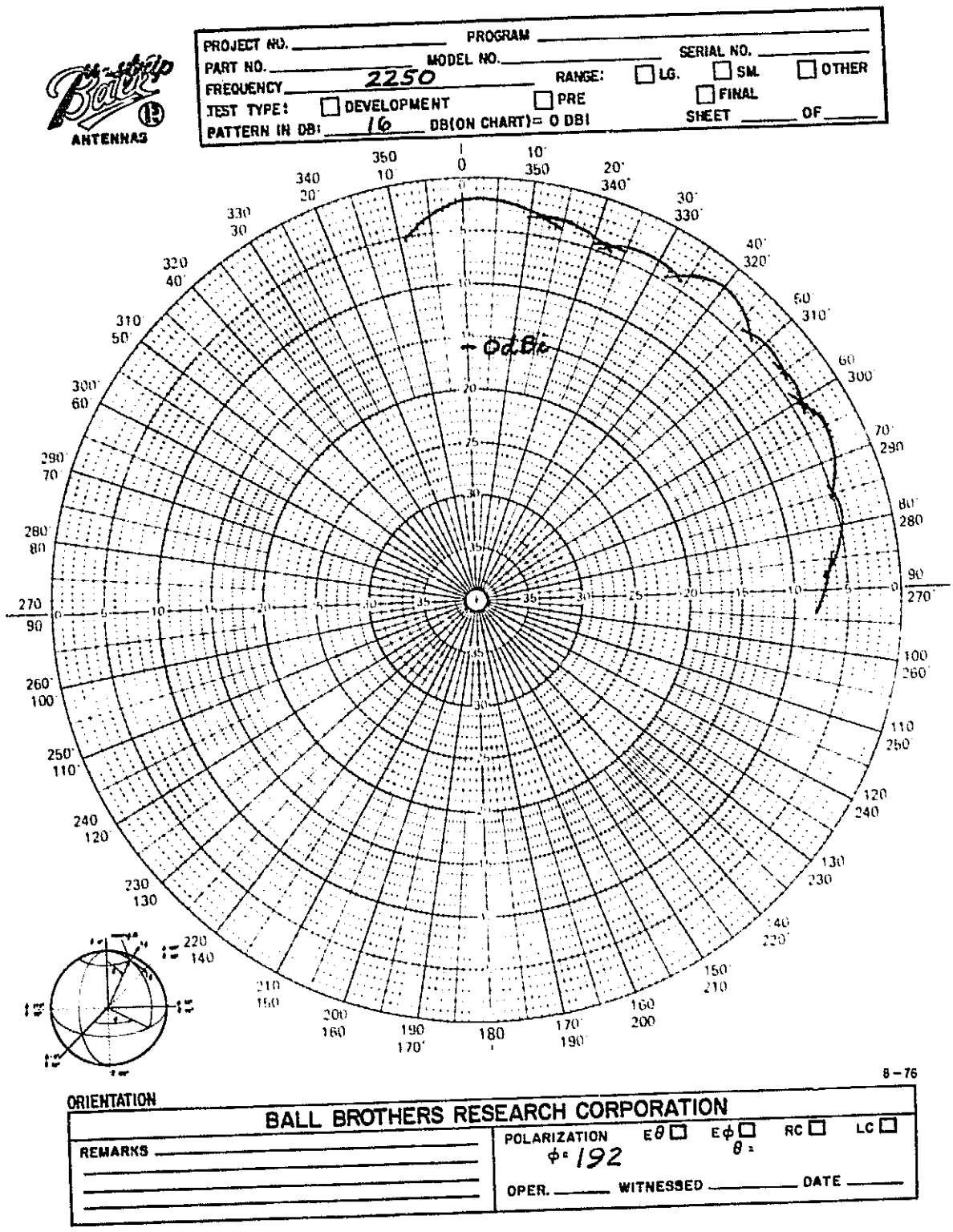

Figure 1-26 Composite Pattern for $\phi = 192^{o}$

REPRODUCIBILITY OF THE
ORIGINAL PAGE IS POOR

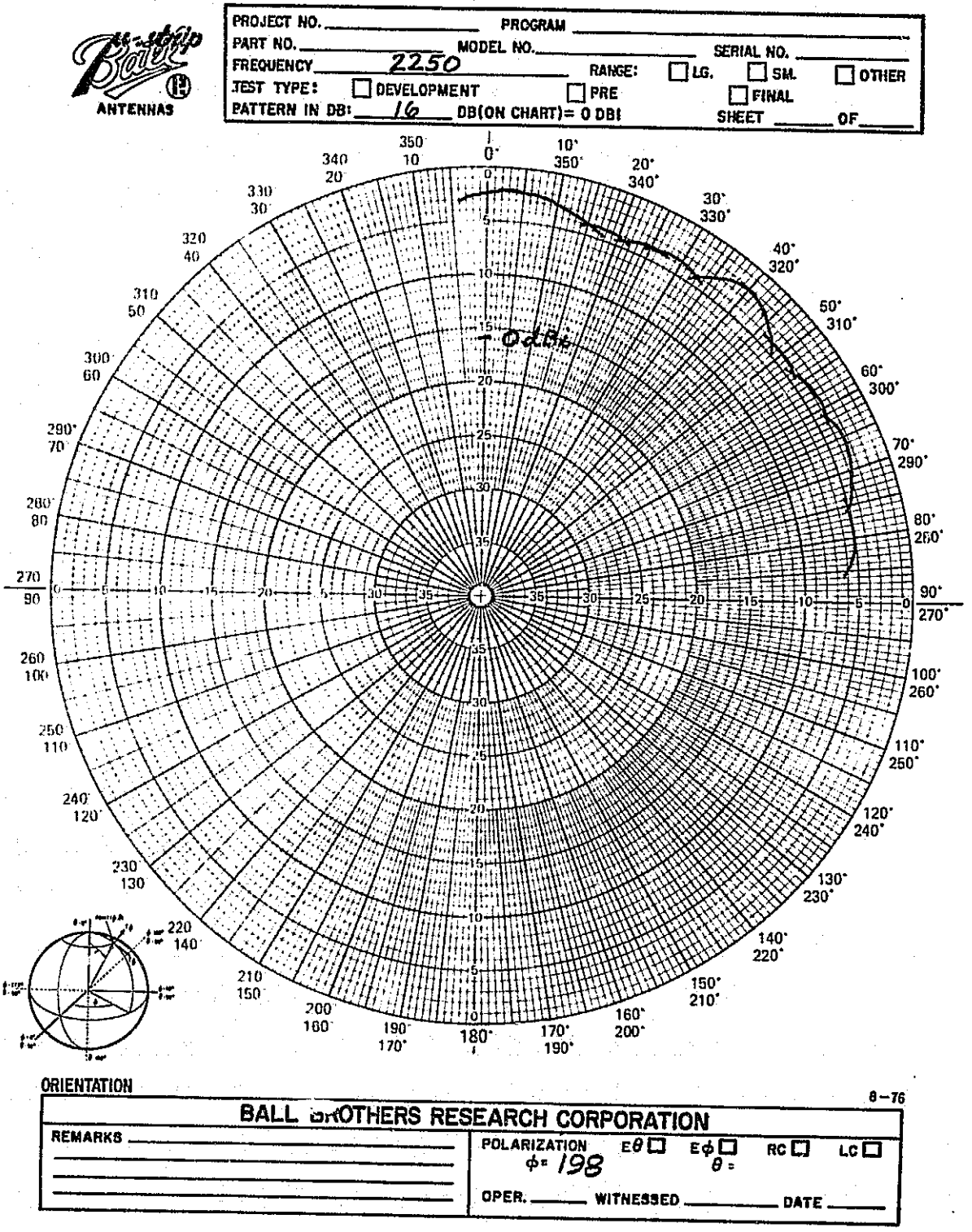

Figure 1-27 Composite Pattern for $\phi = 198^{\circ}$

REPRODUCIBILITY OF THE
ORIGINAL PAGE IS POOR

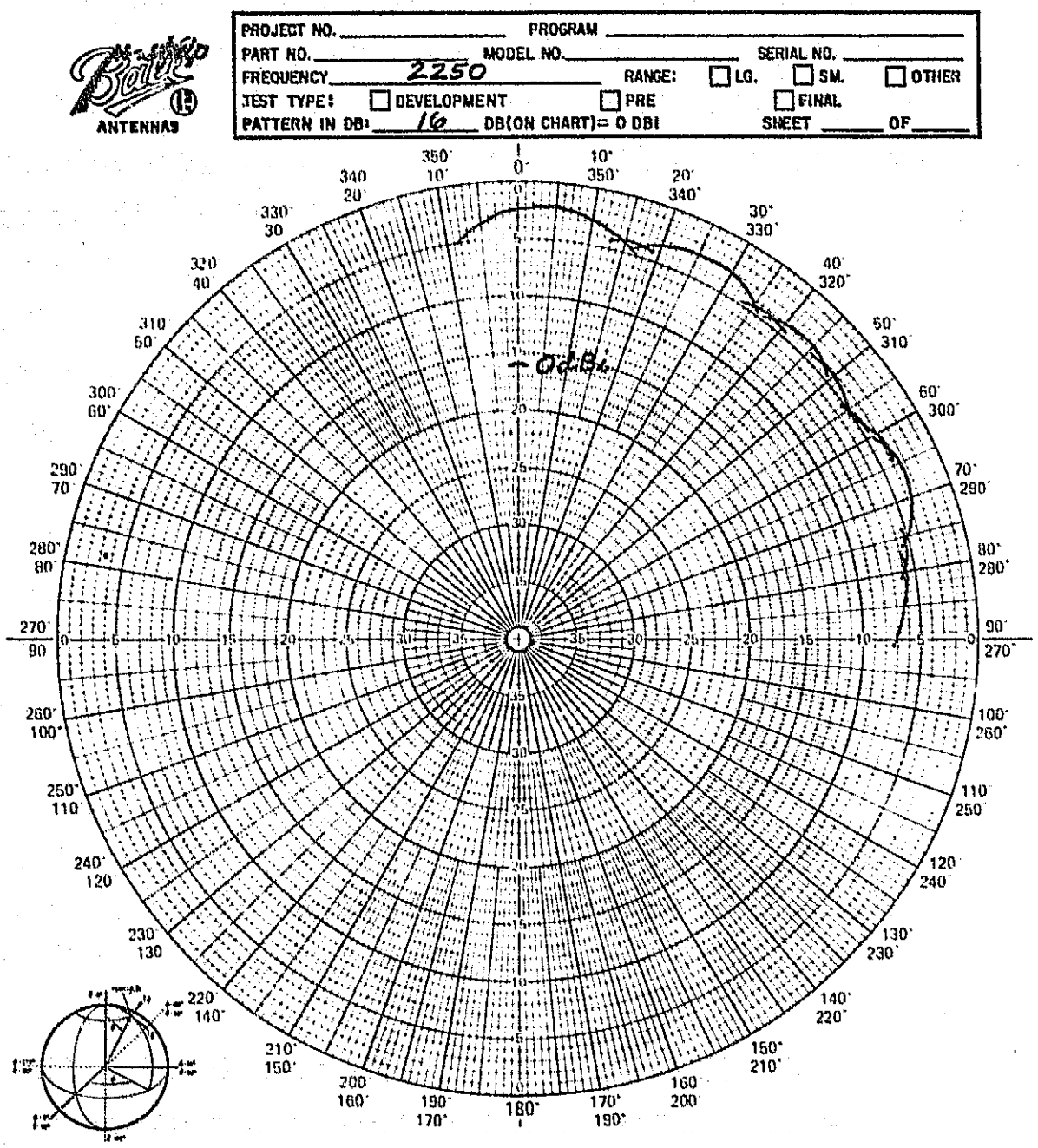

Figure 1-28 Composite Pattern for $\phi = 204^{\circ}$

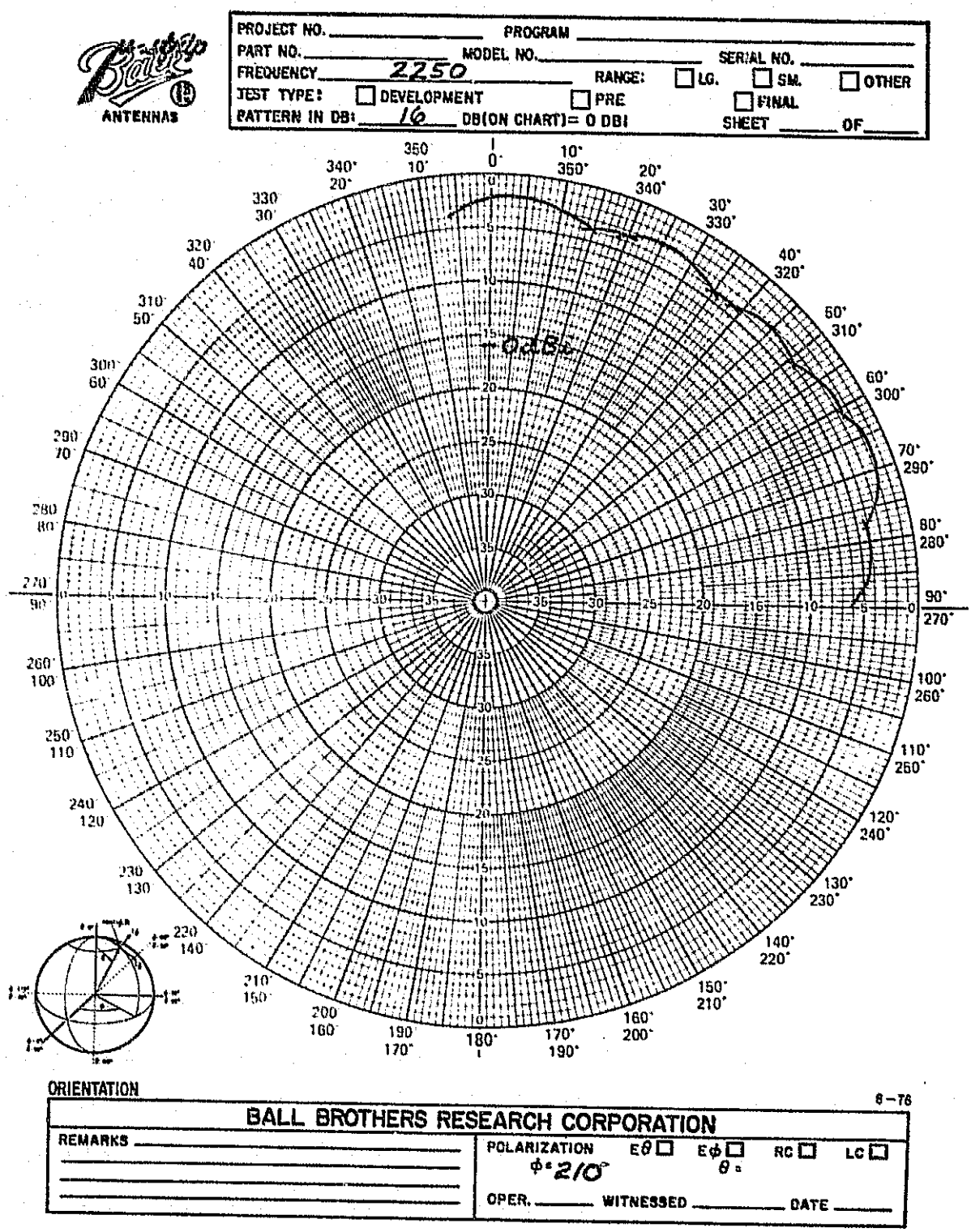

Figure 1-29 Composite Pattern for $\phi = 210^{o}$

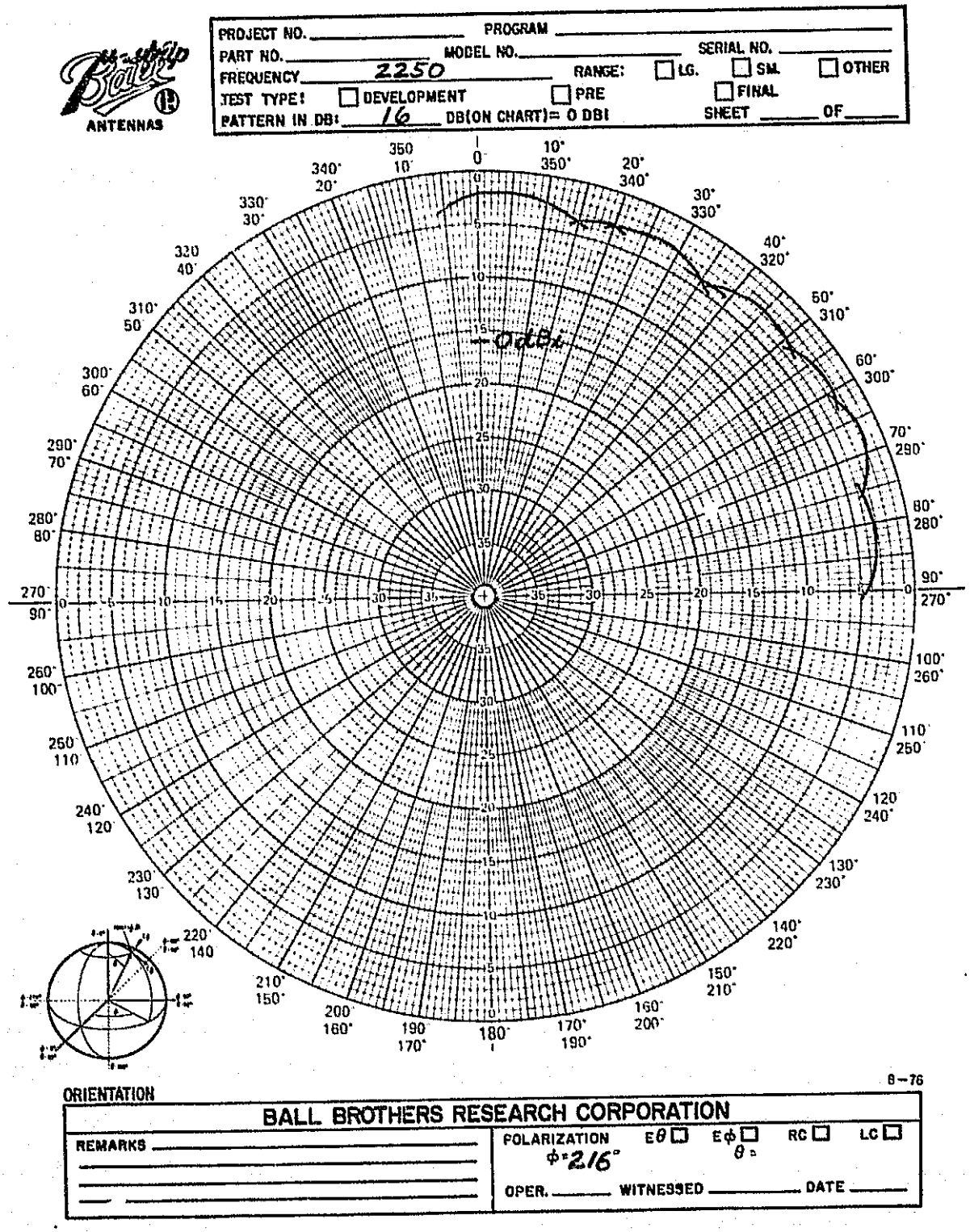

Figure 1-30 Composite Pattern for $\phi = 216^{o}$

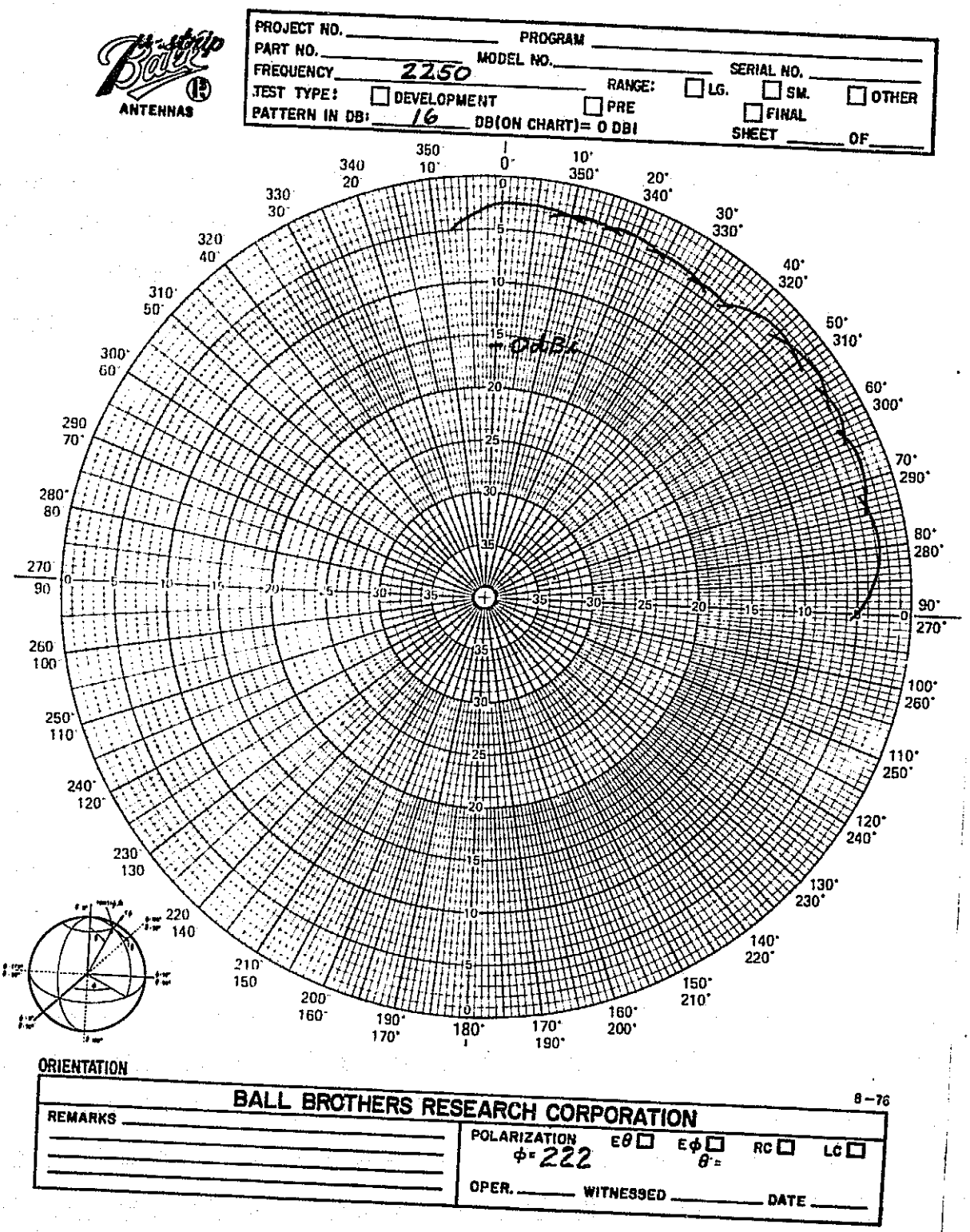

Figure 1-31 Composite Pattern for $\phi = 222^{o}$

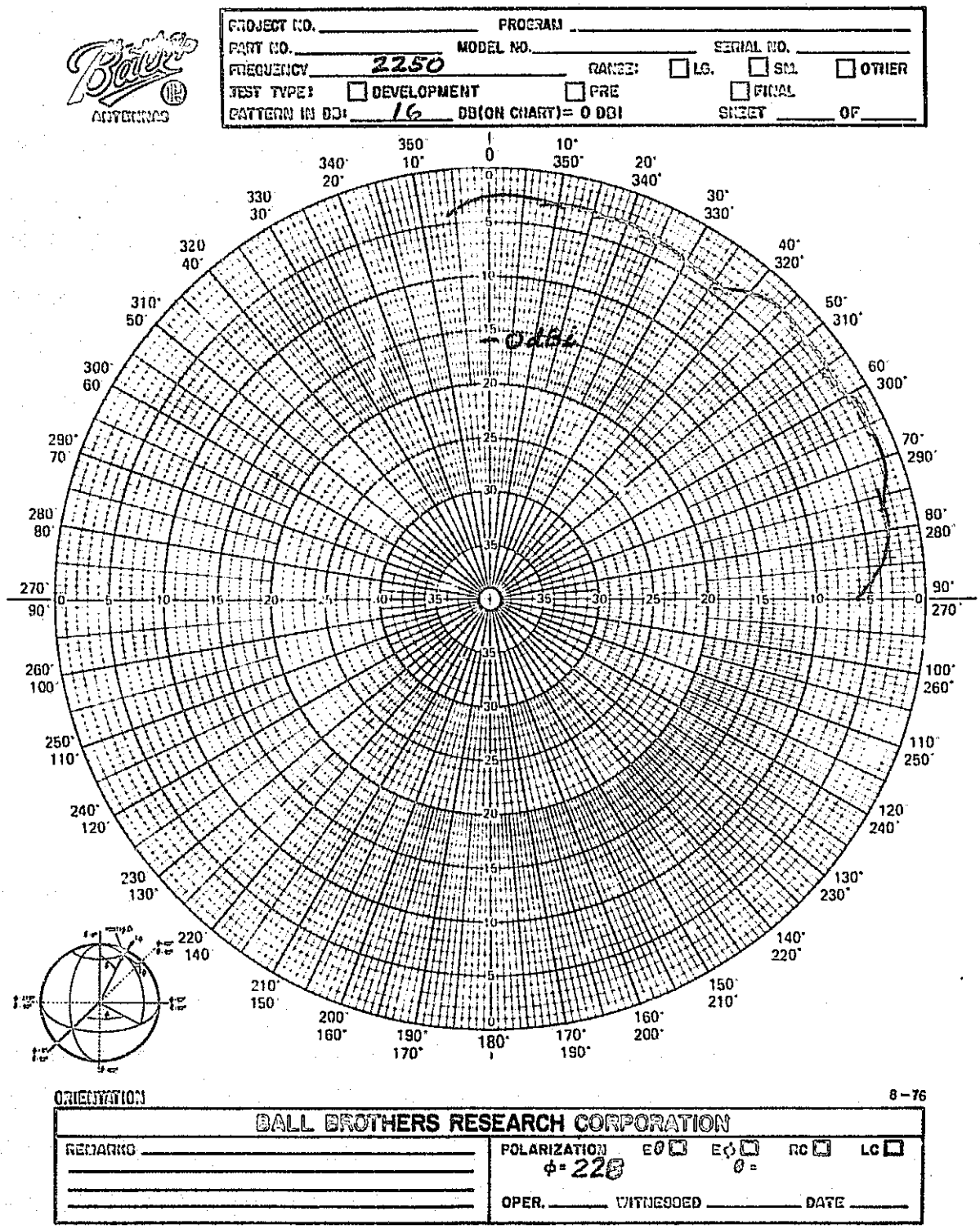

Figure 1-32 Composite Pattern for $\phi = 228^{o}$

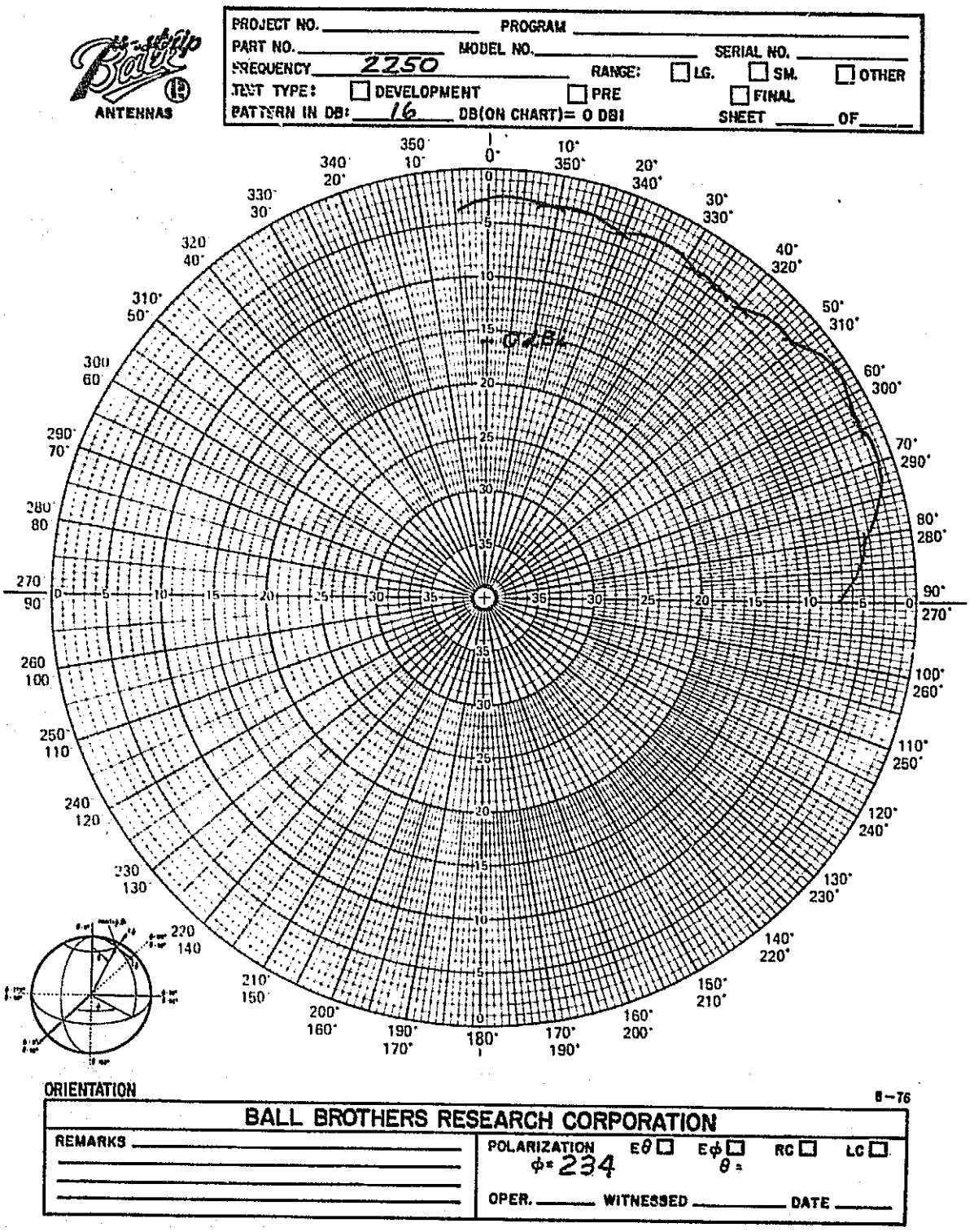

Figure 1-33 Composite Pattern for $\phi = 234^{o}$

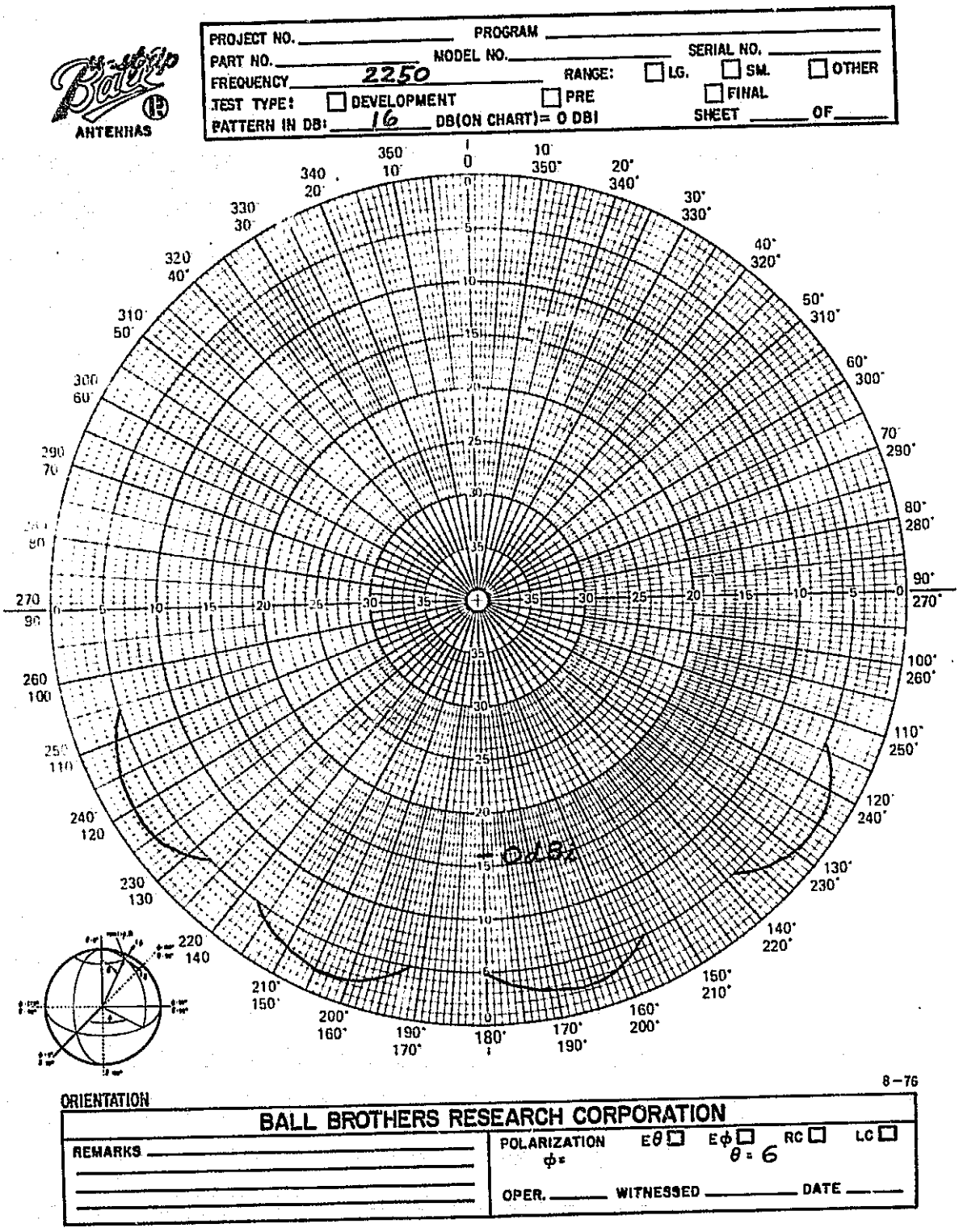

Figure 1-34 Composite Pattern for $\theta = 6^{o}$

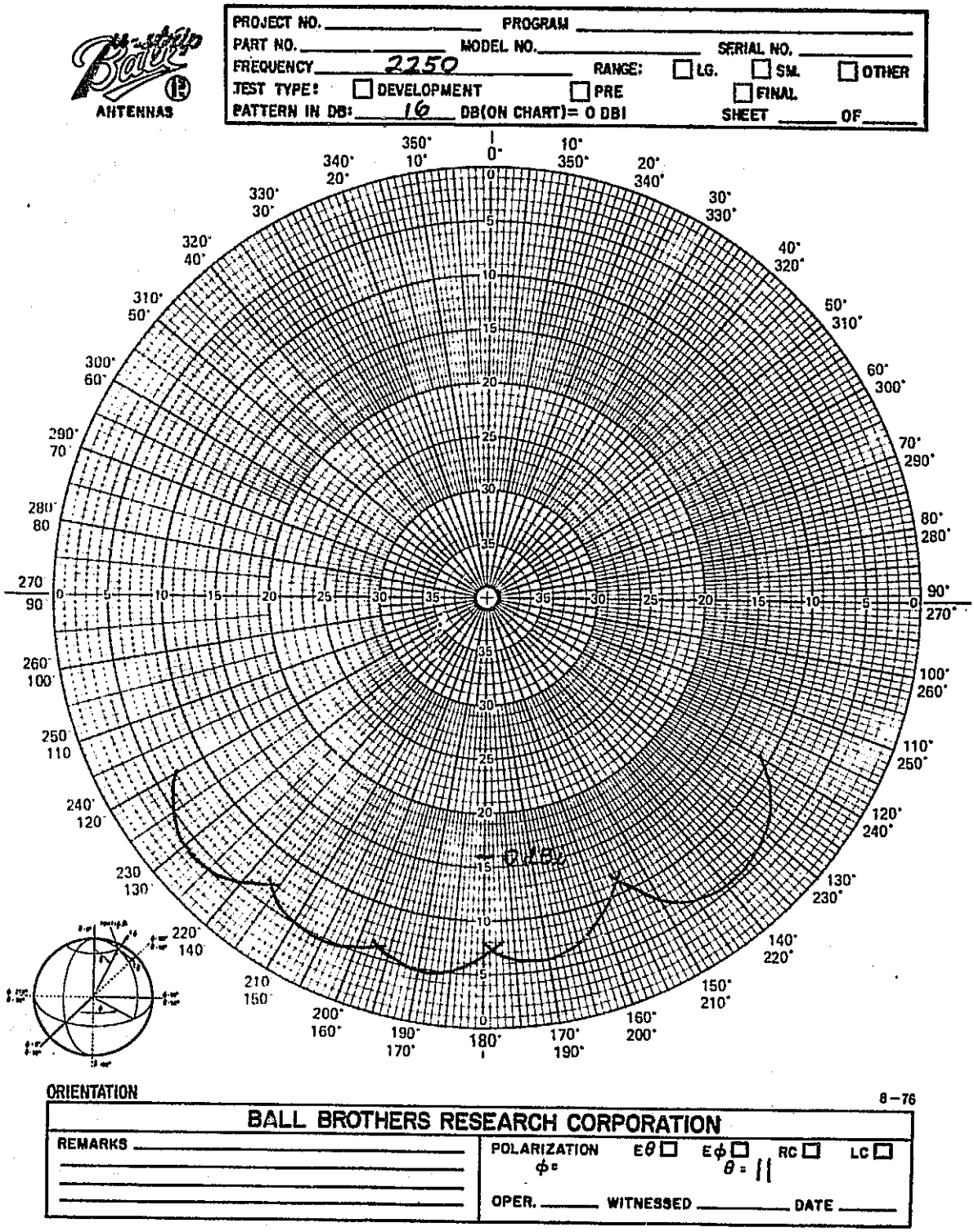

Figure 1-35 Composite Pattern for $\theta = 11^{o}$

REPRODUCIBILITY OF THE
ORIGINAL PAGE IS POOR

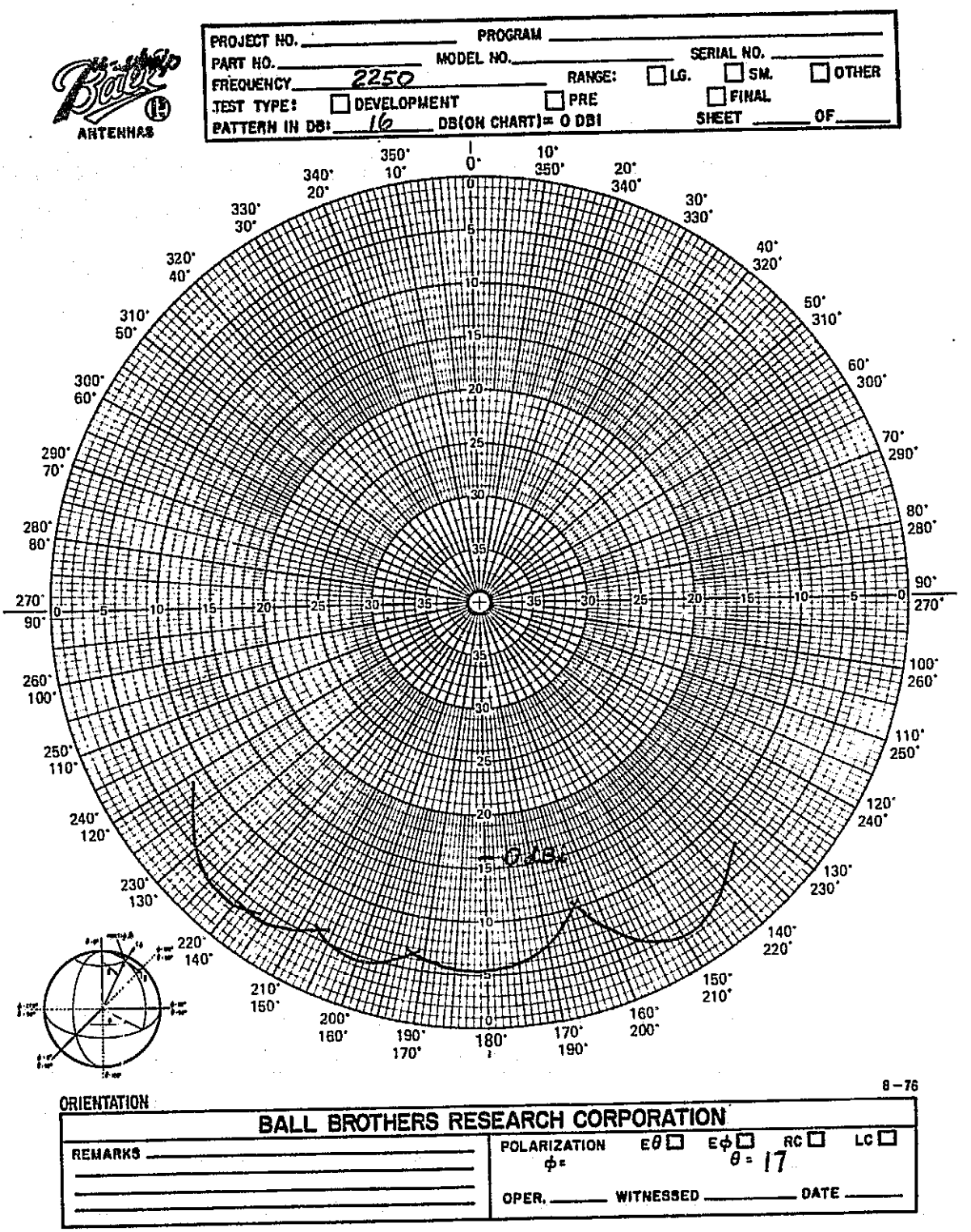

Figure 1-36 Composite Pattern for $\theta = 17^{o}$

REPRODUCIBILITY OF THE
ORIGINAL [illegible] IS POOR

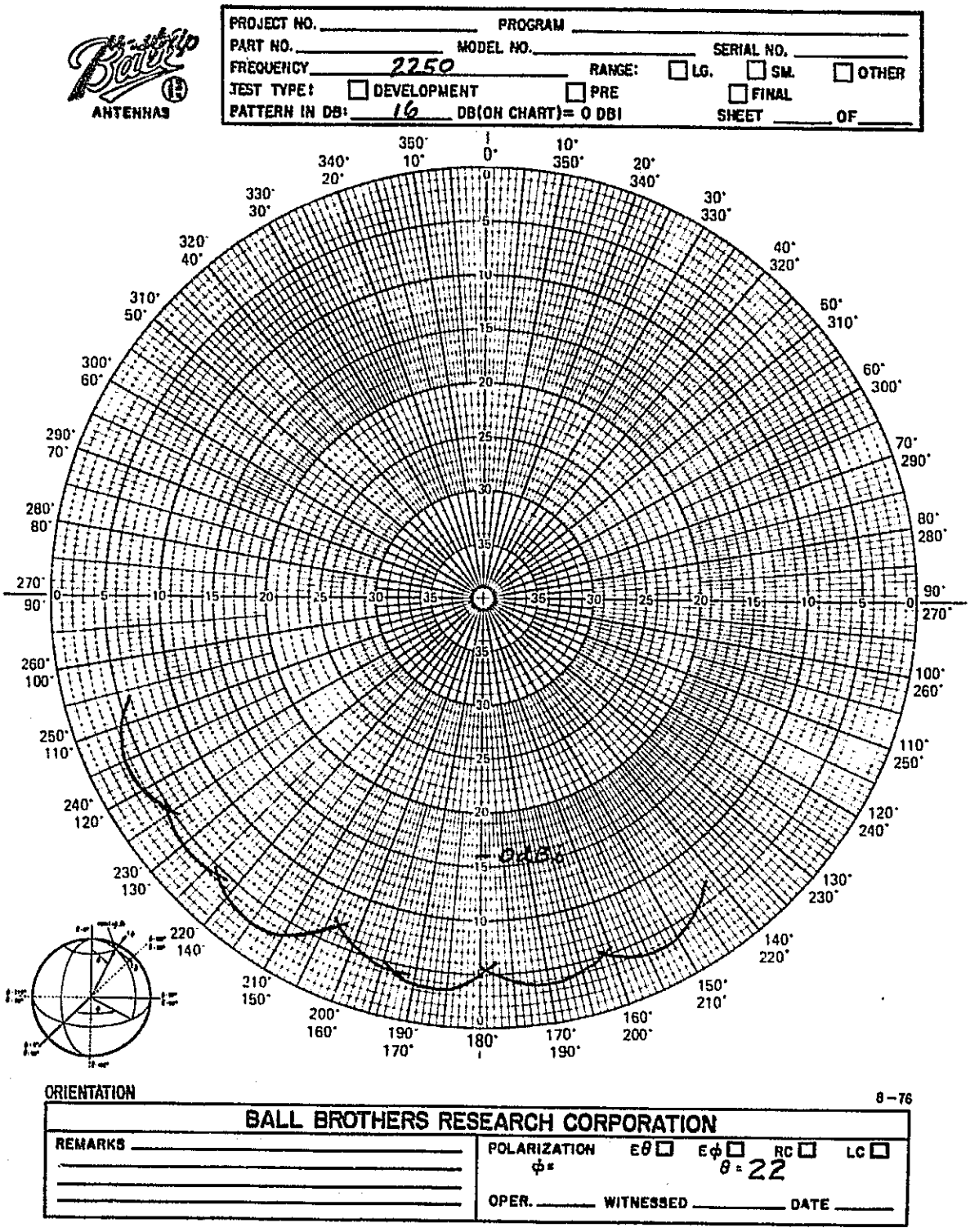

Figure 1-37 Composite Pattern for $\theta = 22^{o}$

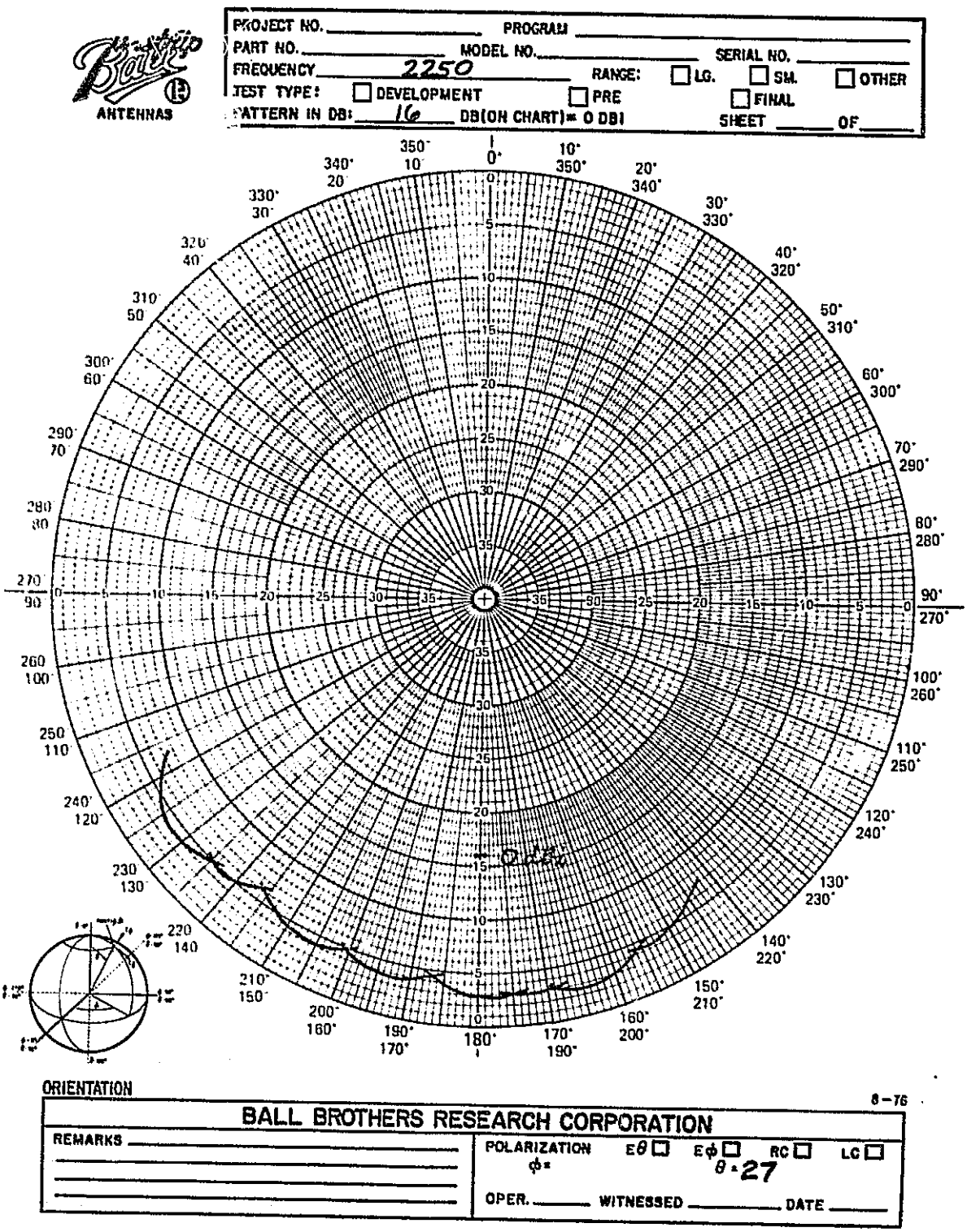

Figure 1-38 Composite Pattern for $\theta = 27^{o}$

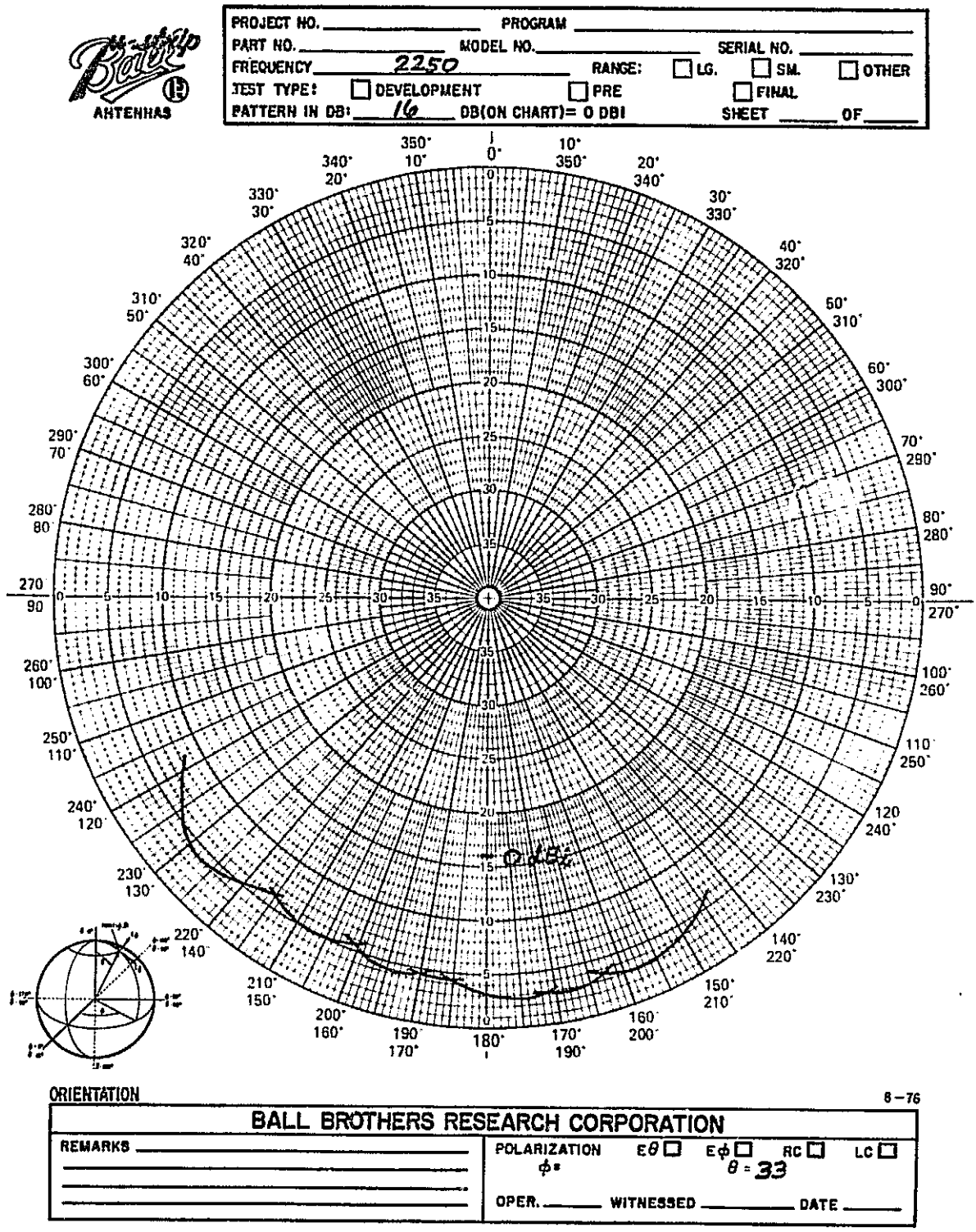

Figure 1-39 Composite Pattern for $\theta = 33^{o}$

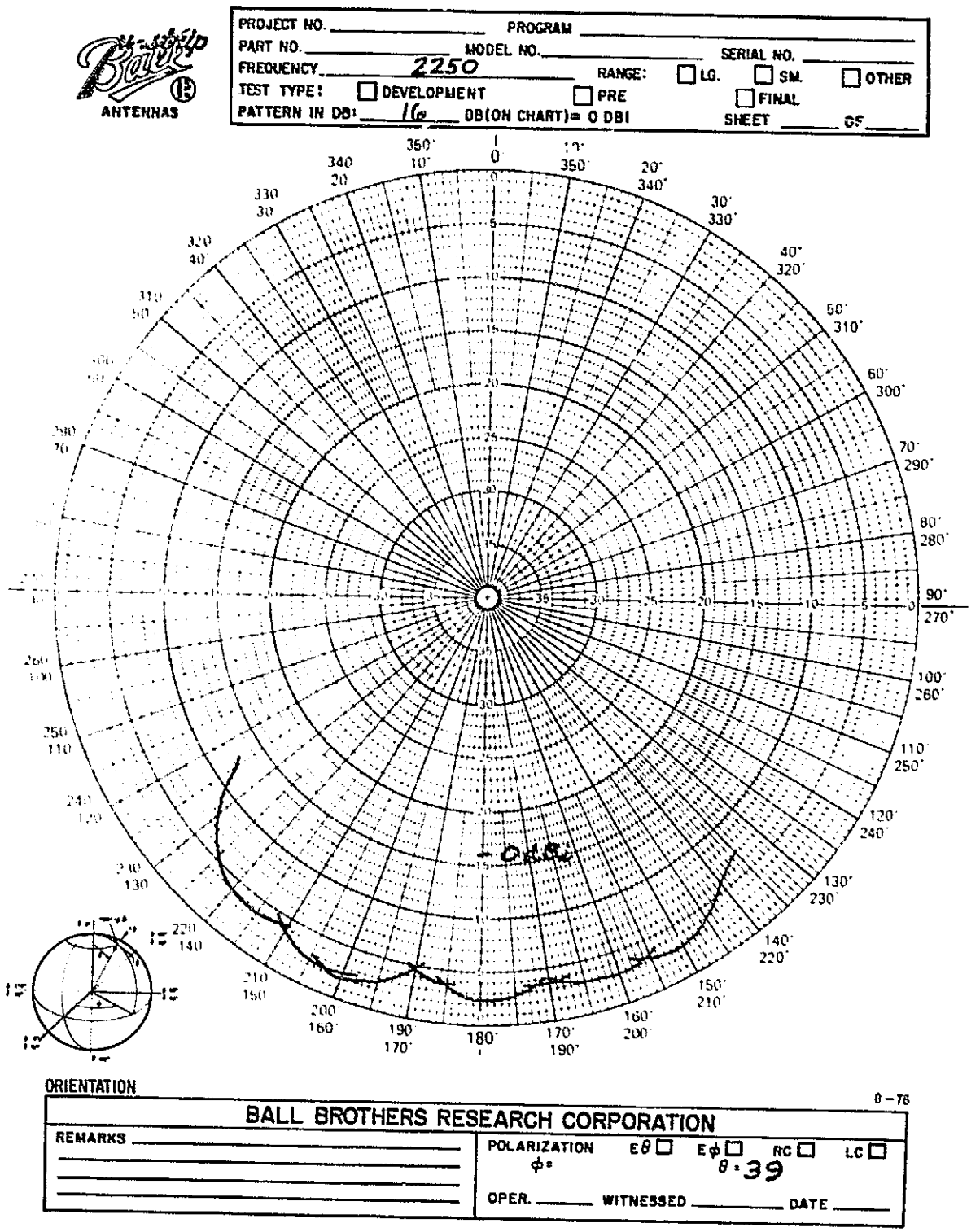

Figure 1-40 Composite Pattern for $\theta = 39^{o}$

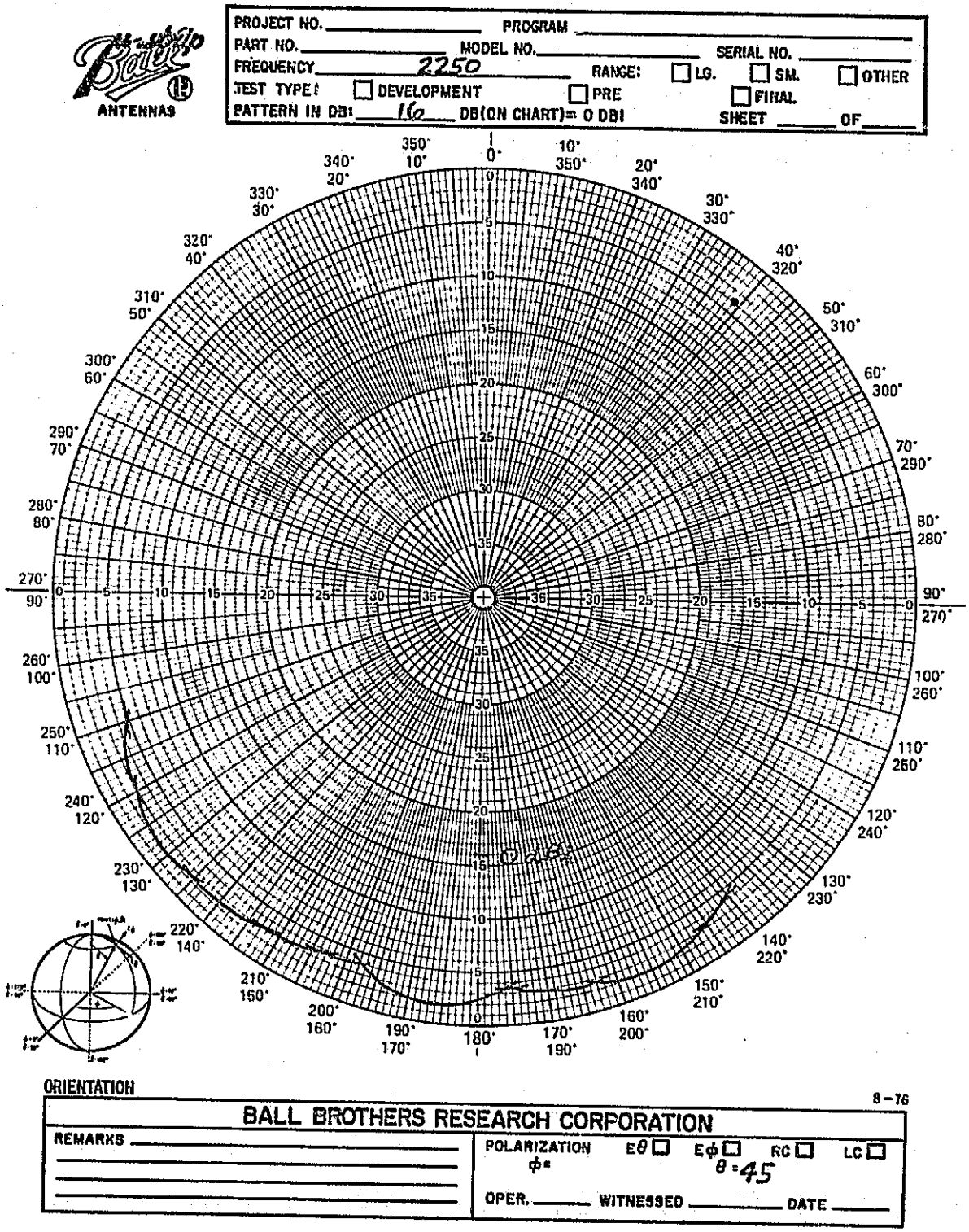

Figure 1-41 Composite Pattern for $\theta = 45^{o}$

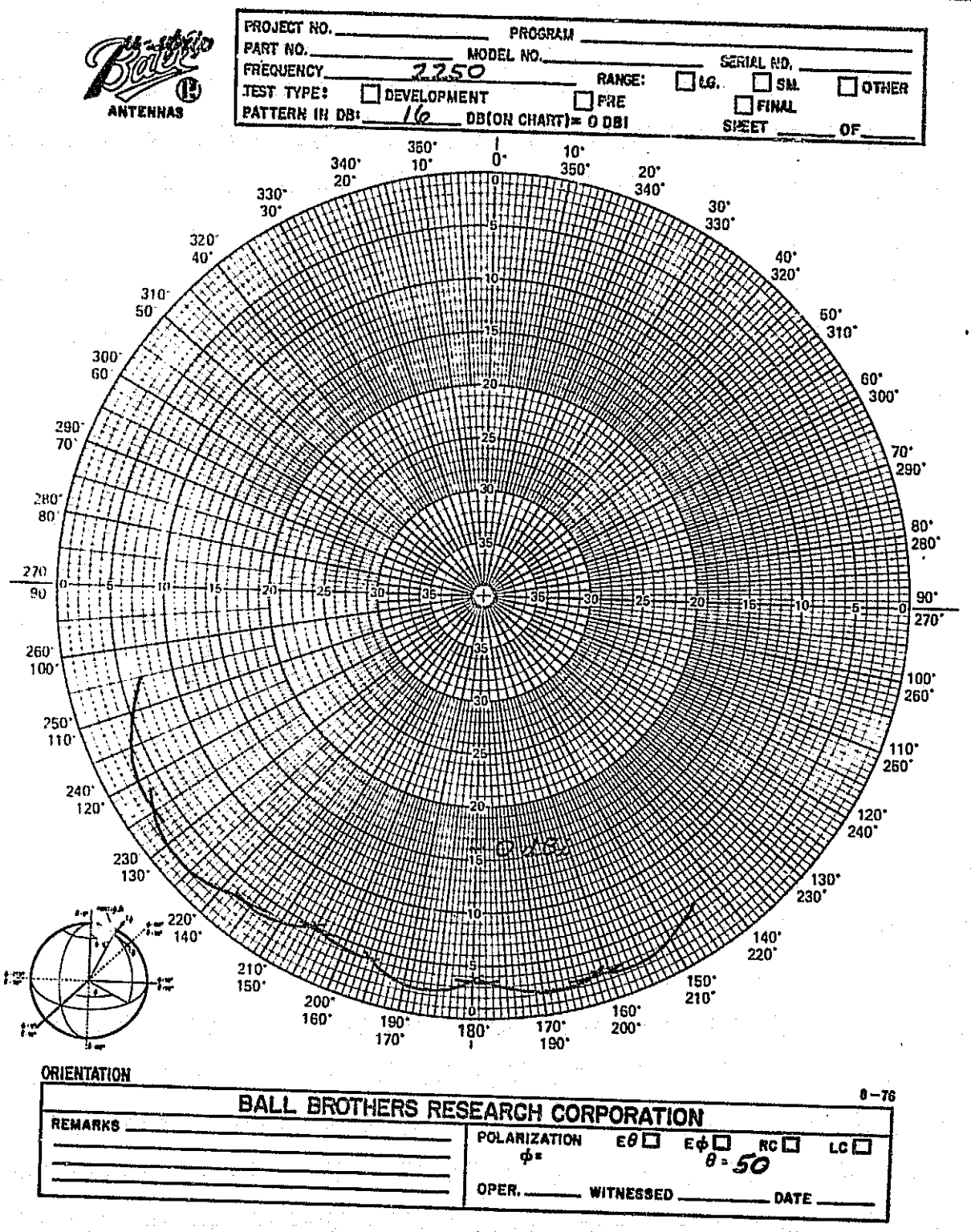

Figure 1-42 Composite Pattern for $\theta = 50^{o}$

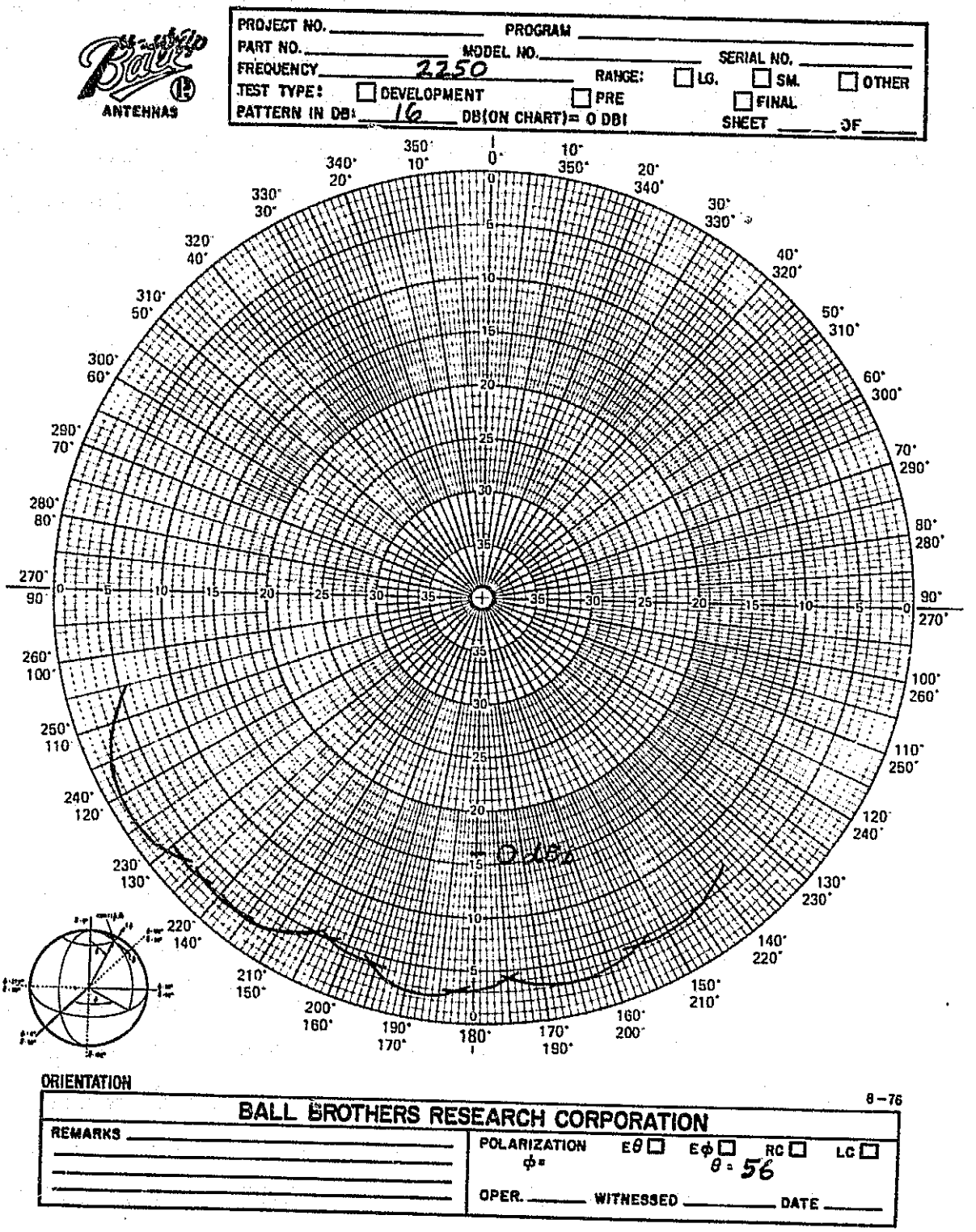

Figure 1-43 Composite Pattern for $\theta = 56^{\circ}$

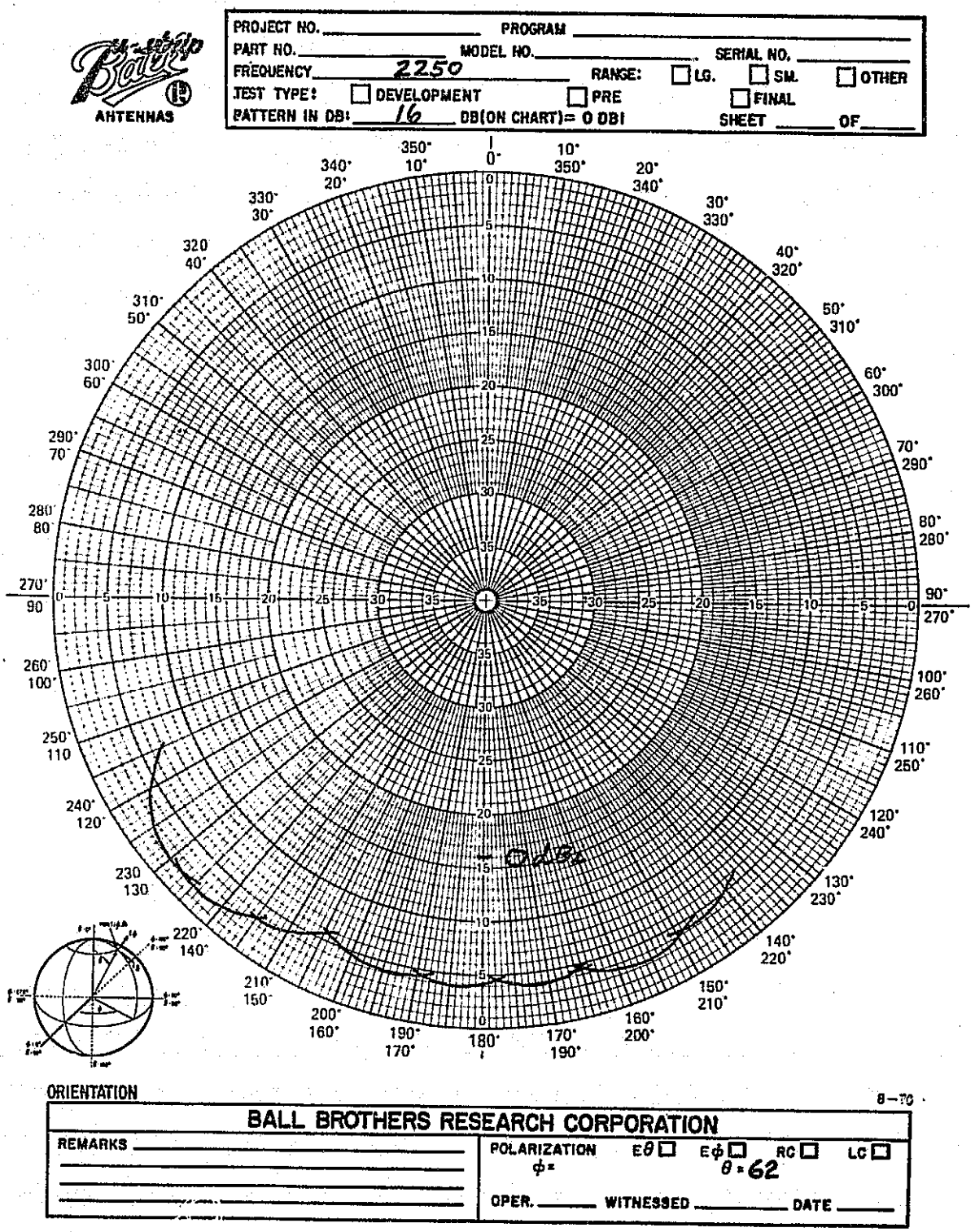

Figure 1-44 Composite Pattern for $\theta = 62^{o}$

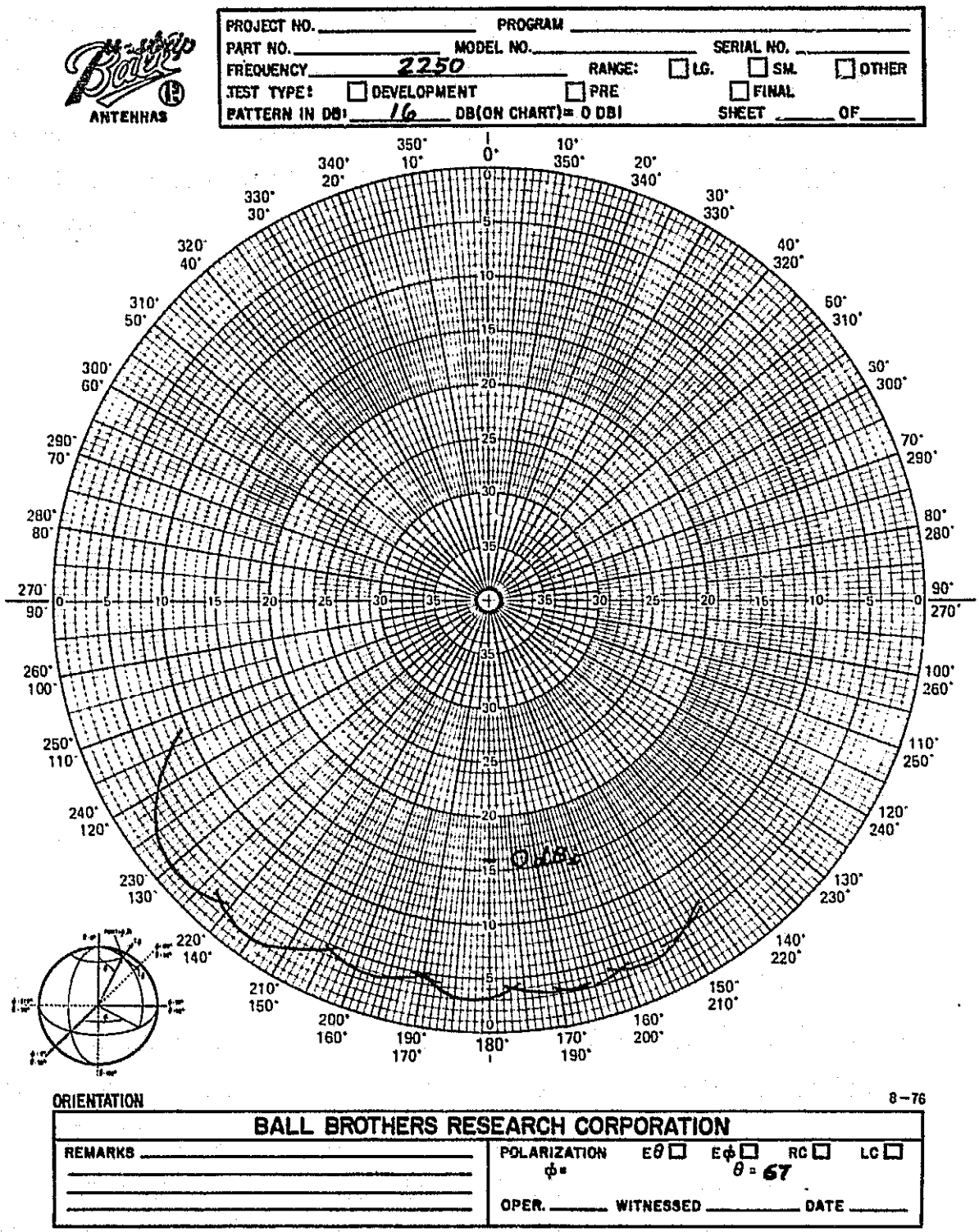

Figure 1-45 Composite Pattern for $\theta = 67^{o}$

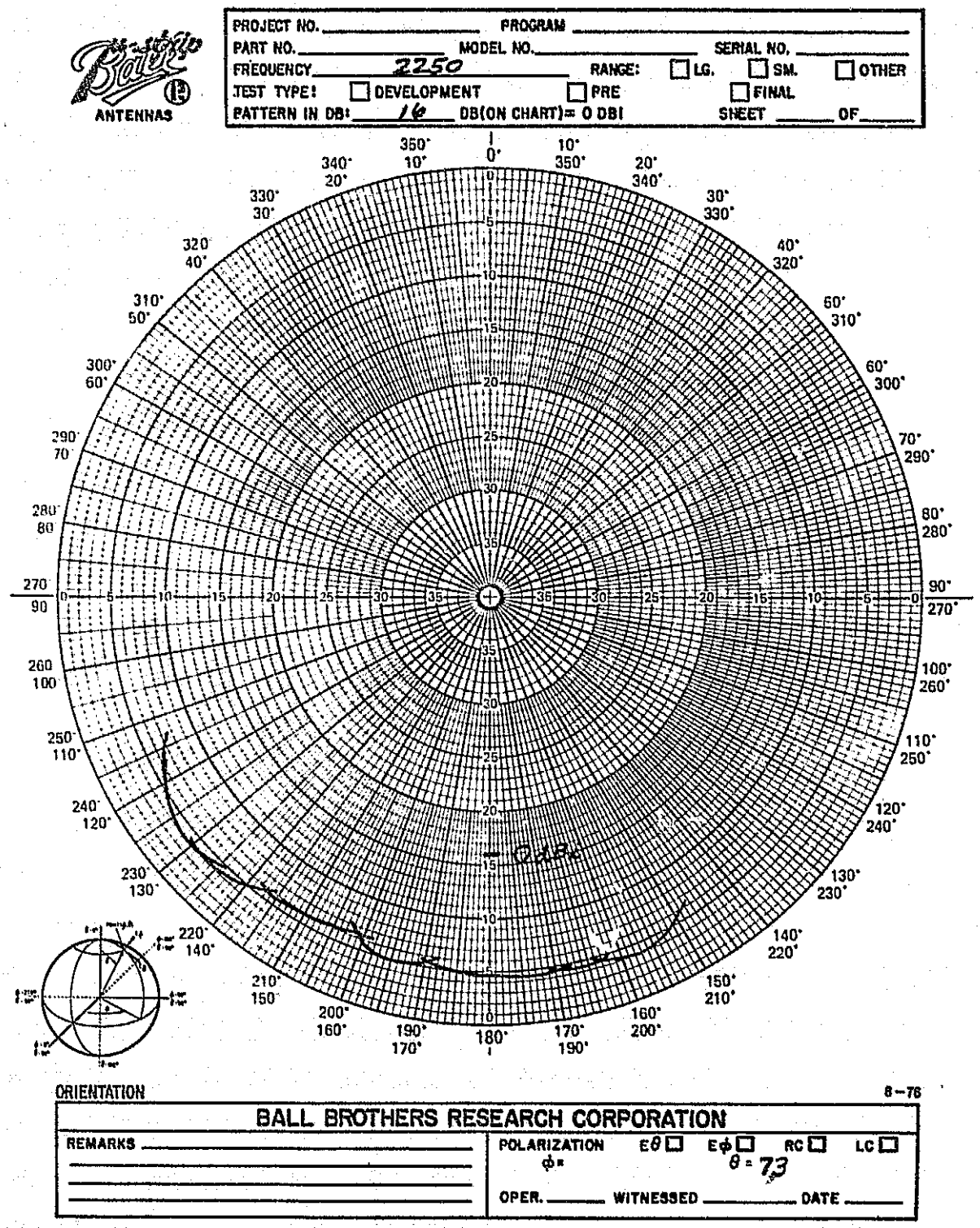

Figure 1-46 Composite Pattern for $\theta = 73^{\circ}$

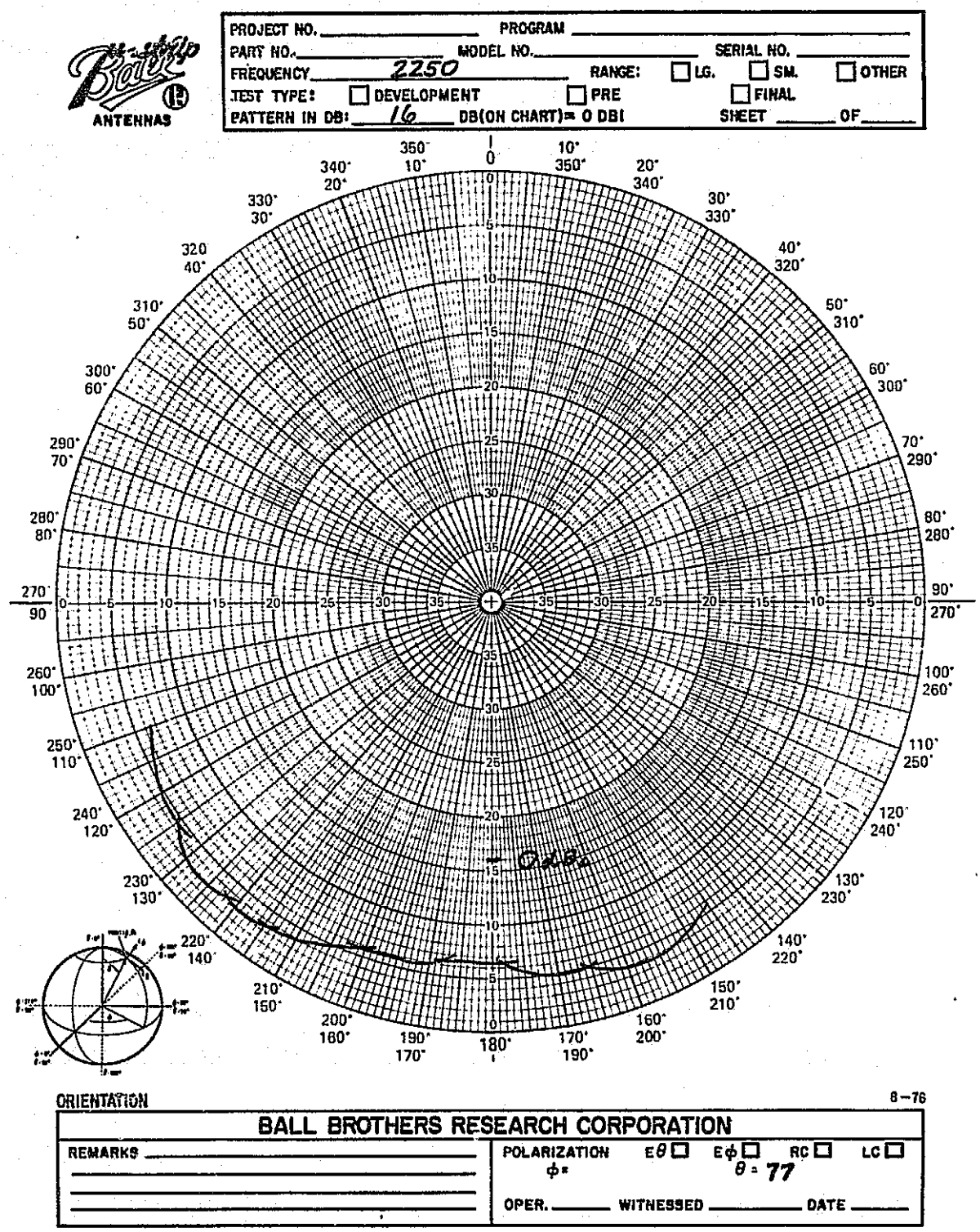

Figure 1-47 Composite Pattern for $\theta = 77^{\circ}$

1.6.2 Ellipticity

Axial ratio was measured for ten beams at 2.0, 2.1, 2.2 and 2.3 GHz. The maximum measured axial ratio over the 3 dB beamwidth is 3.5 dB. The average value is 2.0 dB at the band center. In general, minimum ellipticity occurs at the design center frequency 2150 MHz and increases slightly at the band edges. The axial ratio remains constant over the 3 dB beamwidth. A typical pattern is shown in Figure 1-48.

1.6.3. VSWR

Swept input VSWR was measured for ten beams between 2.0 - 2.3 GHz. The maximum VSWR is 1.5:1 as shown in Figure 1-49. Since the switching power divider is the antenna input, there is little change in VSWR from beam to beam.

1.6.4 Phase Variation

A typical beam to beam phase variation measurement is shown in Figure 1-50. The polar coordinate is ϕ or azimuth and the radial coordinate is phase with each small division equal to 2^{o} of phase change. The continuous lines represent the phase change across the beams and the discontinuities are the phase variations between beams at the crossover points. The maximum jump is 7^{o} between beams 125 and 124. The average phase change is 3^{o}.

1.6.5 Switching Power Divider

Preliminary data was taken on the 120 port switching power divider prior to array assembly. The amplitude and phase of twelve symmetrically spaced "on" ports is shown in Figure 1-51. For ideal twelve-way power division each output is at -10.9 dB. Taking input VSWR and diode loss into account the expected output amplitude is -11.6 dB which is very close to measurement average. The dip at 2125 MHz is due to the unterminated condition of the 108 "off" ports and is a function of the coax length. It does not occur when these outputs are terminated with 50 ohms when used in the array. Phase variations between outputs are less than 18^{o}.

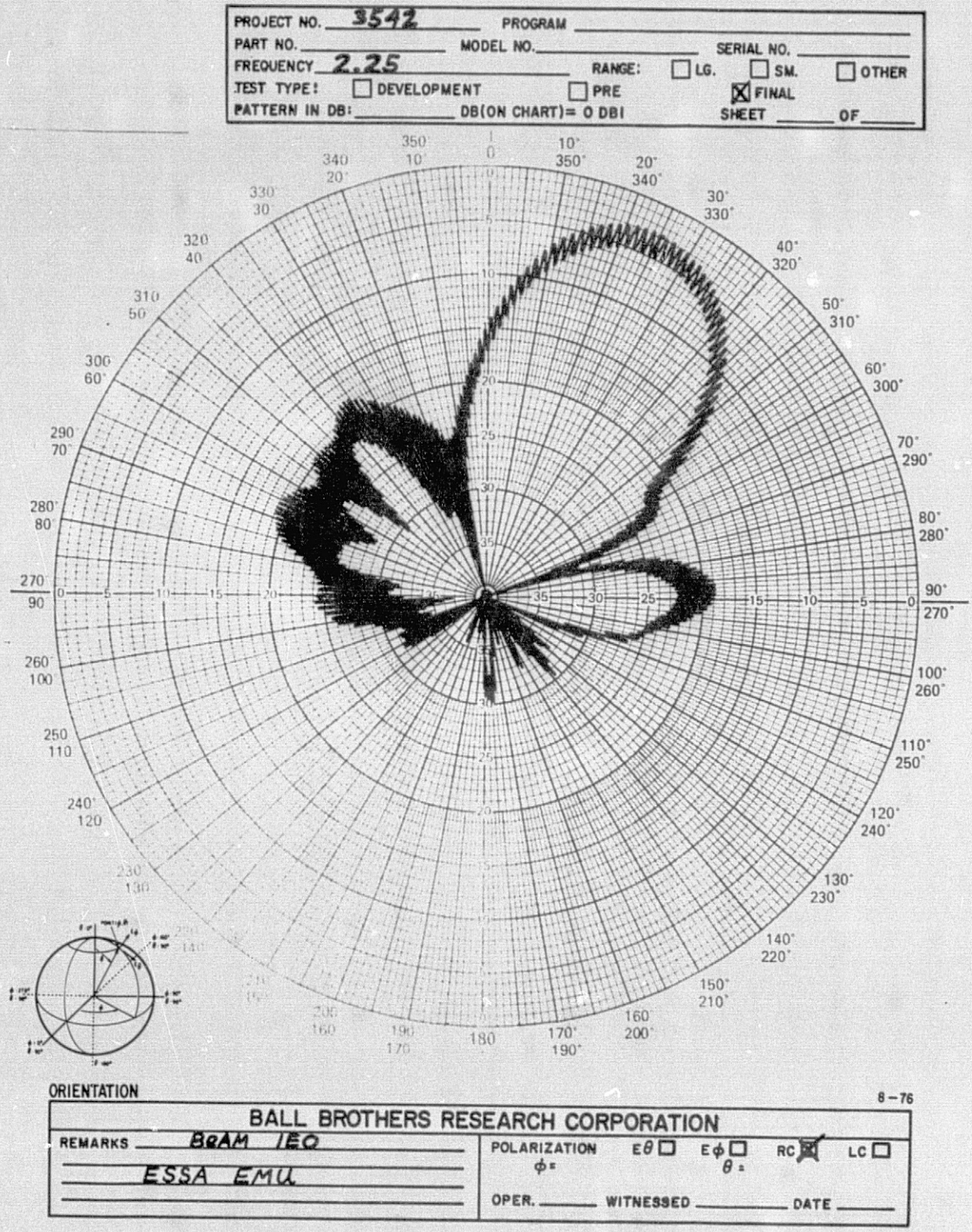

Figure 1-48 Typical Beam Ellipticity

REPRODUCIBILITY OF THE
ORIGINAL PAGE IS POOR

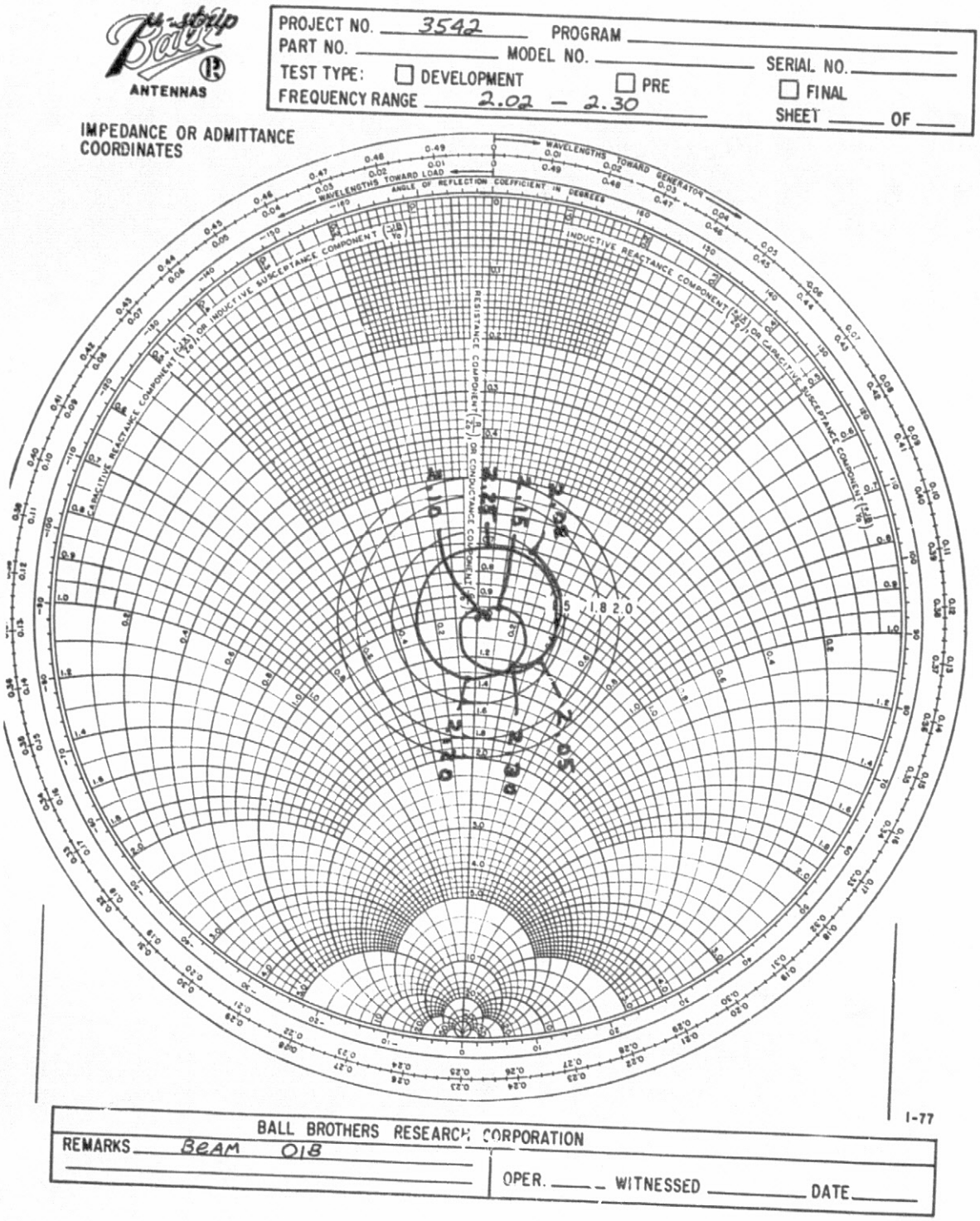

Figure 1-49 Typical Input VSWR

REPRODUCIBILITY OF THE
ORIGINAL PAGE IS POOR

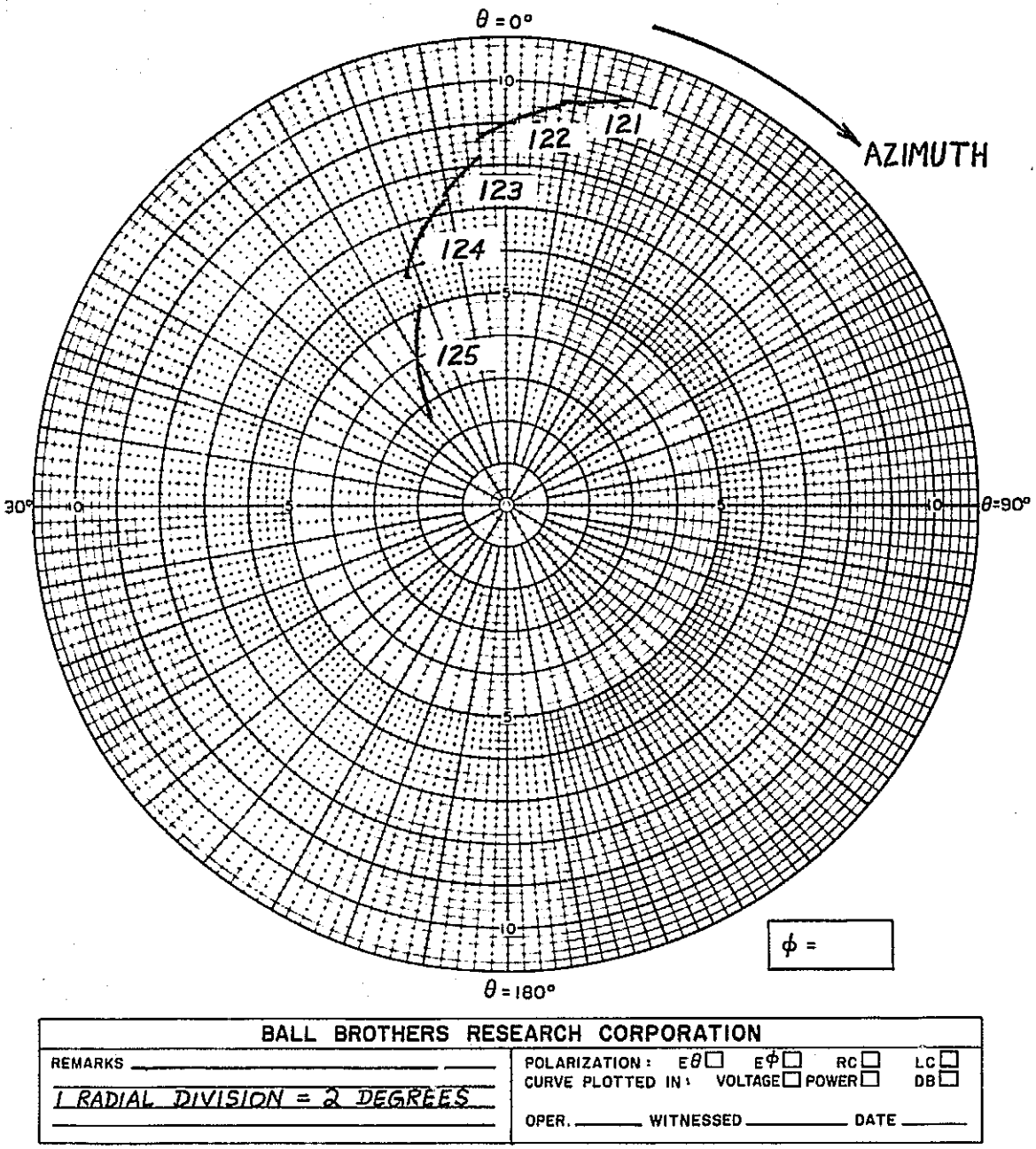

Figure 1-50 Typical Beam to Beam Phase Variations

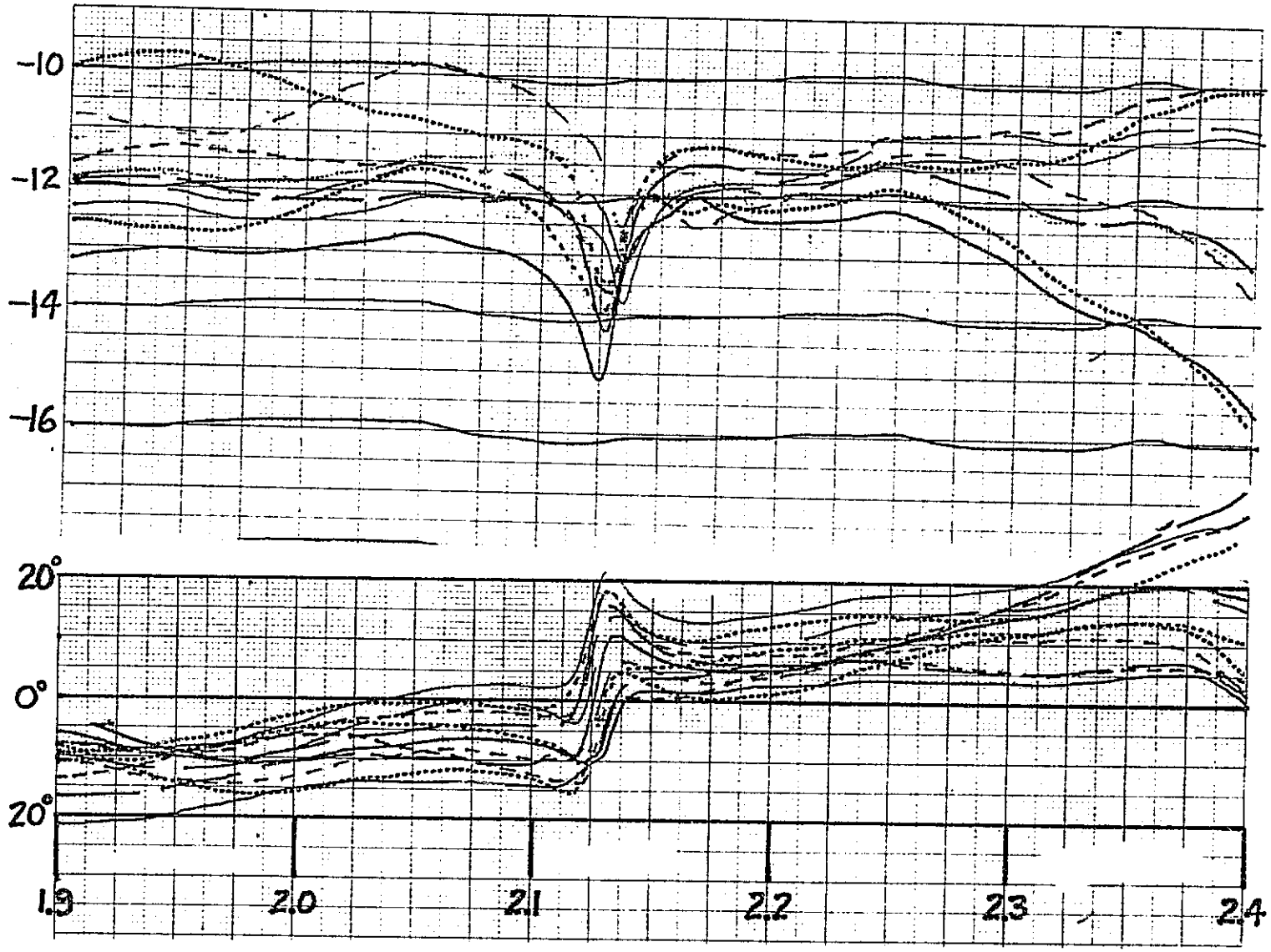

Figure 1-51 Switching Power Divider Amplitude and Phase Data

2.0 SUPPLEMENTARY TESTS

2.1 ESSA/GPS Performance Degradation Tests

In order to extend the capabilities of ESSA and make it a comprehensive solution to the TDRSS acquisition and tracking problem, the beam steering data must be determined by the antenna system. The computations necessary to keep the ESSA beam directed at a particular TDRS are straightforward if the user spacecraft position and orientation are known. Position information can be obtained accurately and conveniently on a real-time basis from the Global Positioning Satellites (GPS) system.

The fact that this position information is available independent of any spacecraft system means that a general purpose TDRSS antenna system with full acquisition and track capability can be implemented.

The key consideration regarding the practicality of an integrated TDRSS/GPS antenna system is that the performance, weight, volume and cost are compatible with scientific spacecraft. As an initial step in assessing the performance of such an integrated antenna system, a series of degradation tests were performed with the two types of antennas described below.

2.1.1 Description of Tests

The EMU ESSA Antenna was configured with two dual-frequency, circularly polarized GPS antenna arrays. The first array consisted of three turnstile antennas and the second array used three GPS microstrip antennas which had been developed previously at Ball Brothers Research Corporation (BBRC).

2.1.1.1 Turnstile Array

Three dual-frequency turnstile antennas were designed and fabricated for operation at the two GPS frequencies, 1227.6 MHz and 1575.4 MHz. The

feed networks employed folded baluns to obtain a 50 ohm balanced transmission line. Separate coaxial phasing lines provided quadrature components at each GPS frequency. The three antennas were mounted 9.6 cm above a smooth 73 cm diameter hemispherical surface at $\theta = 60^{o}$ and $\phi = 95^{o}$, 215^{o} and 335^{o} in order to obtain nearly omnidirectional coverage. The antennas were fed in phase with equal amplitudes by means of a three-way power divider. Radiation distribution patterns (RDPs) and VSWR measurements were taken at both 1227.6 MHz and 1575.4 MHz to obtain a complete record of the coverage characteristics. These patterns are included in Appendix F.

The turnstile antennas were then removed from the smooth hemispherical surface and reconfigured on the ESSA surface. The locations varied slightly from the nominal value of θ and ϕ so that the turnstiles could be mounted in between the ESSA elements. A typical installation is shown in Figure 2-1. Radiation distribution patterns and VSWR measurements were again taken at both GPS frequencies. In addition the ESSA antenna performance was evaluated in the vicinity of one of the turnstile antennas. The principle plane patterns and gain were measured for the 50 beam positions closest to the location of the turnstile. Ellipticity and VSWR were measured for ten adjacent beam positions on a great circle which passed through the turnstile location.

A comparative analysis of both the GPS turnstile antenna system and the ESSA antenna were performed for the pre- and post-integration tests. The RDPs provided the basis of comparison for the GPS system. The integrated GPS/ESSA test data was compared to the ESSA final acceptance test data which was taken prior to integration.

2.1.1.2 Microstrip Array

The tests involving the GPS microstrip antennas are identical to those with the turnstile array except for the following: 1) the dual-frequency circularly polarized microstrip antennas had been previously designed, 2) the three microstrip antennas are mounted directly to the hemispherical ground plane

REPRODUCIBILITY OF THE
ORIGINAL PAGE IS POOR

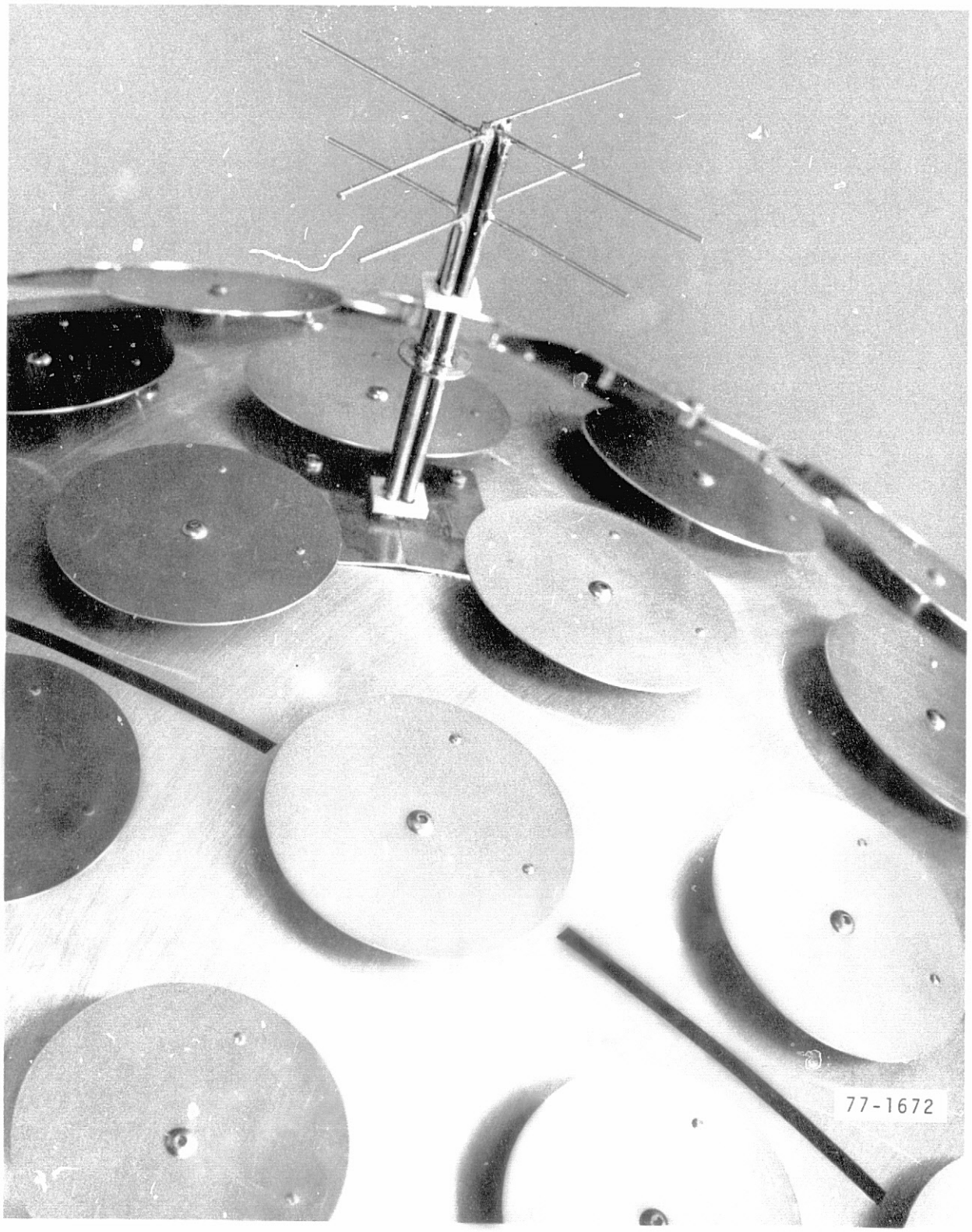

Figure 2-1 GPS Turnstile Element on ESSA

and protrude less than 1 cm above it, 3) two ESSA elements were removed during integration to accommodate each GPS microstrip antenna.

A photograph of a typical GPS microstrip antenna on the ESSA antenna is shown in Figure 2-2.

Radiation distribution patterns for the three element GPS microstrip array are included in Appendix F.

2.1.2 Test Results

The Effect of ESSA on Turnstile Performance

The GPS turnstile array consisted of three antennas located at $\theta = 60^{o}$ and $\phi = 95^{o}$, 215^{o} and 335^{o}. The array was configured on a smooth hemispherical ground plane and performance was measured at both GPS frequencies, 1227.6 MHz and 1575.4 MHz. The RDPs were analyzed using a Xerox 530 computer. The results are presented in Table 2-1.

Table 2-1

TURNSTILE ARRAY PERFORMANCE ON SMOOTH HEMISPHERE

Level (dB)	HEMISPHERICAL COVERAGE (%) ≥ LEVEL	
	@ 1227.6 MHz	@ 1575.4 MHz
0.0	36.7	25.7
-1.0	44.8	33.7
-2.0	52.9	42.1
-3.0	60.3	49.9
-4.0	66.4	57.4
-5.0	72.0	64.8
-6.0	76.6	70.5
-7.0	80.9	75.0
-8.0	84.6	79.4
-9.0	87.5	83.3
-10.0	89.7	86.3
-11.0	91.6	89.2
-12.0	93.3	91.4
-13.0	94.5	93.0
-14.0	95.5	94.5
-15.0	96.3	95.6
-16.0	97.1	96.7
-17.0	97.8	97.5
-18.0	98.2	98.1
-19.0	98.6	98.4
-20.0	98.9	98.7

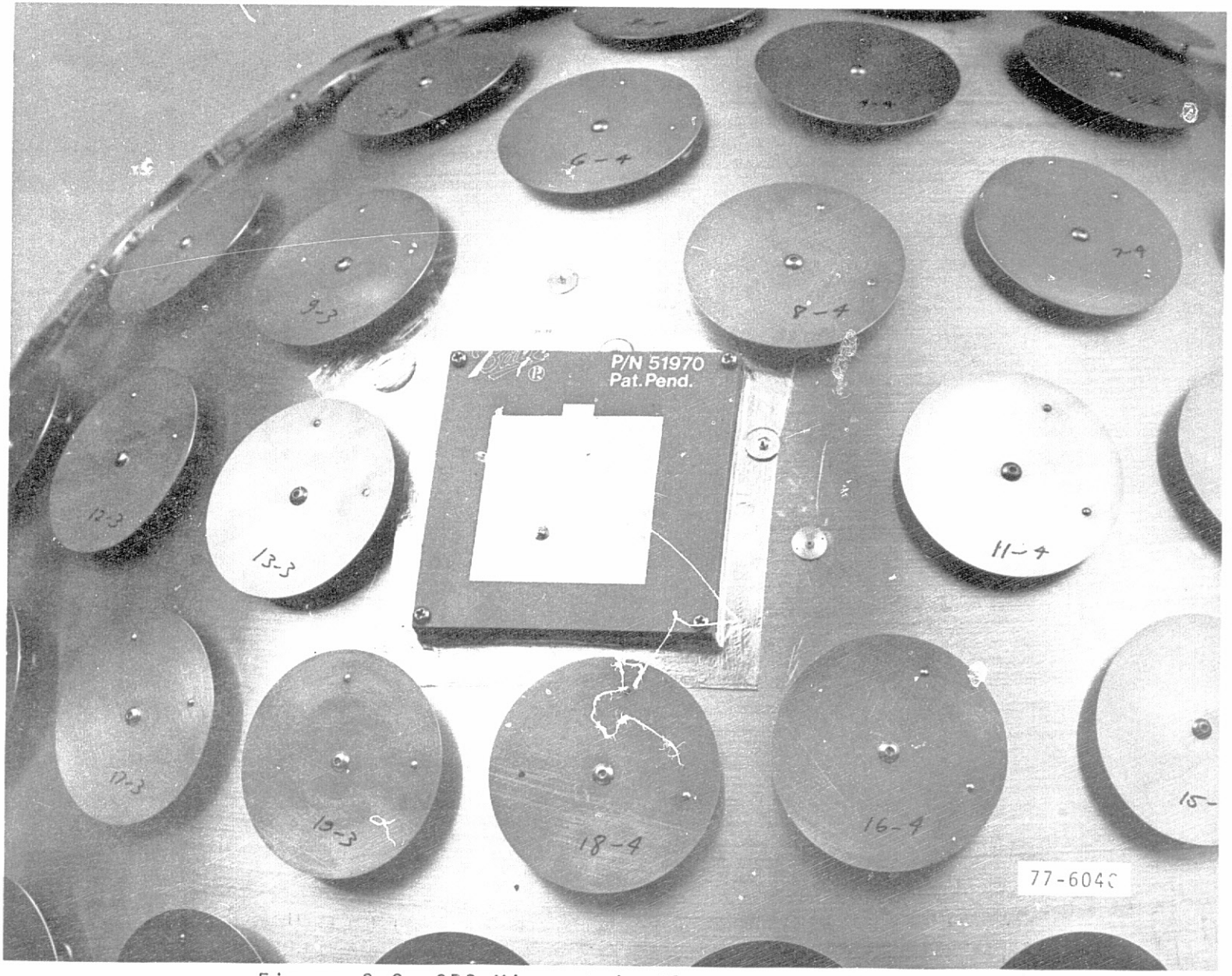

Figure 2-2 GPS Microstrip Element on ESSA

ORIGINAL PAGE IS POOR

The turnstile array was then removed from the smooth hemisphere and reconfigured on the ESSA antenna. RDPs were again taken and analyzed at both GPS frequencies. The results are given in Table 2-2.

Table 2-2
TURNSTILE ARRAY PERFORMANCE ON ESSA ANTENNA

Level (dB)	HEMISPHERICAL COVERAGE (%) ≥ LEVEL	
	@ 1227.6 MHz	@ 1575.4 MHz
0.0	26.5	44.5
-1.0	35.8	53.0
-2.0	43.7	61.3
-3.0	53.1	67.4
-4.0	60.1	74.2
-5.0	66.4	79.1
-6.0	72.6	83.1
-7.0	77.4	86.0
-8.0	80.7	88.4
-9.0	84.1	90.6
-10.0	87.2	92.6
-11.0	89.6	93.9
-12.0	91.4	95.1
-13.0	92.9	96.2
-14.0	93.9	96.8
-15.0	94.9	97.4
-16.0	95.8	97.9
-17.0	96.7	98.4
-18.0	97.3	98.7
-19.0	98.1	99.0
-20.0	98.5	99.2

The performance of the three element GPS turnstile array degraded slightly at 1227.6 MHz when it was integrated with the ESSA antenna. However, a slight performance improvement is apparent at 1575.4 MHz. The -2.0 dB gain level is used for quantitative comparisons of pre- and post-integration performance. Antenna gains below this level will provide marginal signal levels to the GPS receiver/processor. At this level (-2 dB) the coverage percentage decreased at the low frequency and increased at the high frequency. This behavior is reasonable if the physical aspects are considered.

The radiation pattern of a dipole over a ground plane is very dependent upon the height above the conducting surface. At a quarter-wavelength spacing the radiation is primarily vertical or 90^{o} (perpendicular to the ground plane). At half-wavelength spacing, however, the angle of maximum radiation is 30^{o} above the ground plane. For three antennas configured on a hemispherical ground plane, half-wavelength spacing and the associated low angle of radiation is preferred for omnidirectional coverage.

The construction of the turnstiles is such that the low frequency dipoles are further above the ground plane than the high-frequency set. This was done so that each set of dipoles would have half-wavelength spacing at their respective frequencies. This arrangement could not be implemented exactly due to impedance matching considerations, so a compromise spacing was chosen. The low frequency dipoles were spaced slightly less than half-wave and the high frequency set were spaced somewhat over half-wave. This spacing was maintained when the turnstile array was reconfigured on the ESSA antenna. The ground plane, however, was no longer defined by a smooth hemispherical surface. The ESSA S-band radiating elements which protrude 0.635 cm above the hemispherical surface represent a periodic, reactive surface. Although the exact effect is difficult to determine analytically,the presence of this irregular, raised surface has reduced the effective height of the turnstile dipole arrays.

Coverage for the 1227.6 MHz array degraded due to the further departure from half-wave spacing and the associated higher angle of radiation. The 1575.4 MHz array, on the other hand, exhibited improved coverage because the spacing is closer to half-wave and the radiation angle is lower. This prediction was verified by the test data. When the GPS turnstile array was moved from the smooth hemisphere to the ESSA antenna, coverage at the -2.0 dB level decreased from 53% to 44% at 1227.6 MHz and increased from 42% to 61% at 1575.4 MHz. No change in VSWR was observed between the two configurations.

The Effect of GPS Turnstiles on ESSA Antenna Performance

One of the turnstile array antennas was located on the ESSA antenna at $\theta = 60^{o}$, $\phi = 215^{o}$. Forty-nine of the ESSA antenna beams in the range $45^{o} \leq \theta \leq 78^{o}$ and $185^{o} \leq \phi \leq 240^{o}$ were evaluated in terms of gain. These post-integration values were compared to the gains measured for the same beams during the ESSA antenna final acceptance tests. The fiftieth beam was used as a reference beam for a gain standard. This was the zenith beam which was unperturbed by the addition of the GPS array.

In order to reduce systematic errors between the two series of measurements, the gain levels of the post-integration, ESSA antenna beams were compensated by the difference between the reference beam levels. Specifically, 0.3 dB was subtracted from each of post-integration ESSA antenna beam gains. After this adjustment the average change in gain between the two series of measurements was 0.1 dB with the higher gain levels associated with the integrated GPS/ESSA configuration. This difference is well within measurement accuracy limits. This comparison was based on 42 beams which were unaffected by the presence of the GPS turnstile. The other seven beams in the immediate vicinity of the turnstile ($\theta = 61^{o}$) experienced a considerable reduction in gain. The average decrease in gain was 3.3 dB with a maximum change of 8.0 dB. Scattering of the S-band signal from both the horizontal and vertical elements of the turnstile degraded the integrity of the ESSA antenna beams adjacent to the turnstile. In general, as the beams approached the turnstile location, the beamwidths broadened and the gain fell off due to the "flat-topping" characteristics, as shown in Figure 2-3.

This degraded performance was only observed for those seven beams with $\theta = 61^{o}$ that intercepted some portion of the turnstile antenna. A summary of the change in performance level for the affected beams is given in Table 2-3.

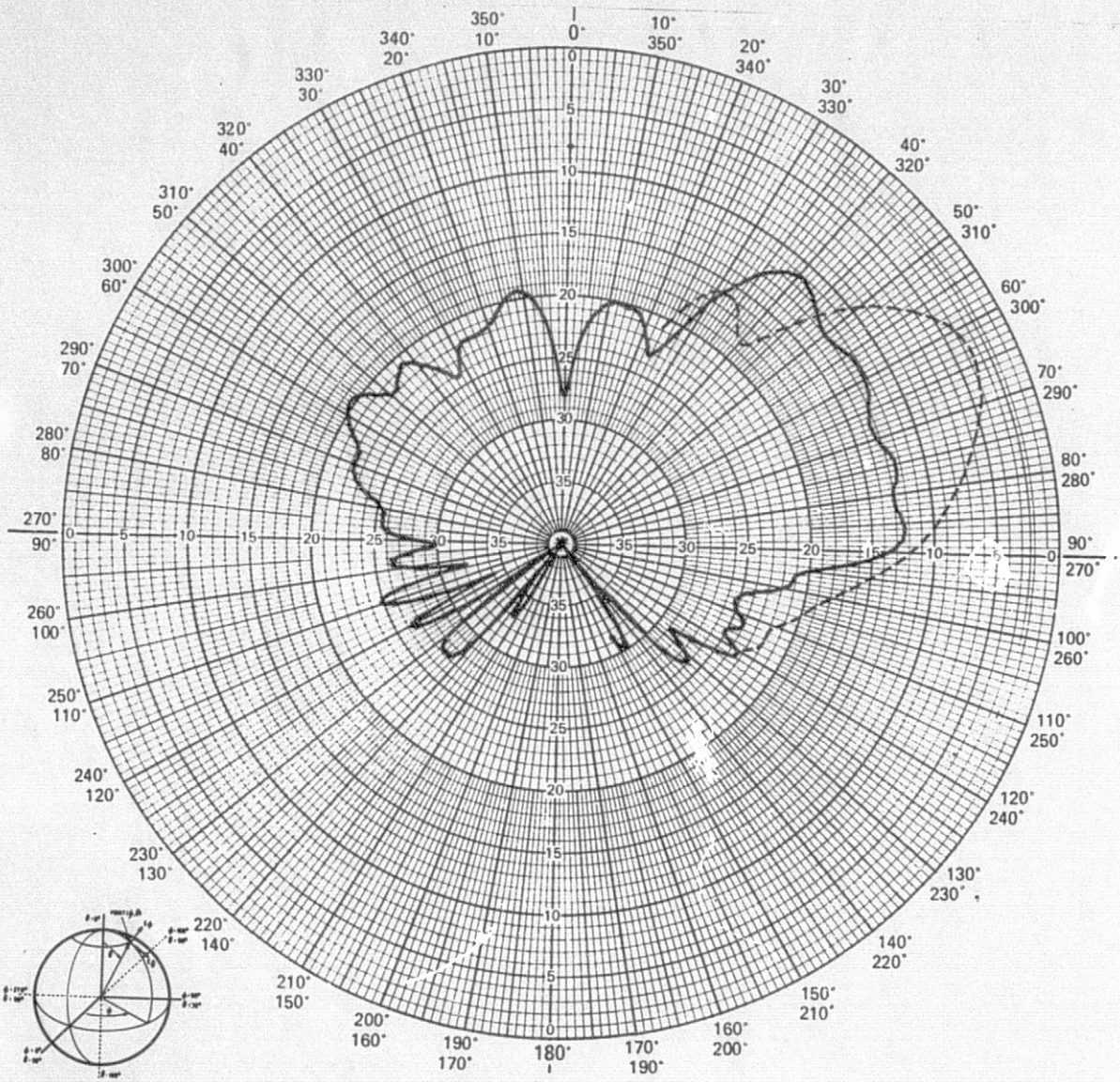

Solid Line : With Turnstile

Dotted Line: Without Turnstile

Figure 2-3 ESSA Degradation Due to GPS Turnstile

Table 2-3

ESSA/GPS Turnstile Performance Summary

Beam Number	Position (deg) θ	Position (deg) φ	ESSA Gain Level (dB) Without GPS Turnstiles	ESSA Gain Level (dB) With GPS Turnstiles
OC0	61	187	12.7	12.0
OC1	61	193	12.9	4.9
OC2	61	198	13.0	12.7
OC3	61	212	12.9	7.2
OC4	61	214	12.8	6.8
OC5	61	223	12.8	10.6
OC6	61	229	13.5	13.3

Turnstile positioned at $\theta = 60^{o}$, $\phi = 215^{o}$

The other 42 beams tested were unaffected by the presence of the turnstile.

The Effect of ESSA on Microstrip Patch Performance

The GPS microstrip array consisted of three antennas located at $\theta = 60^{o}$ and $\phi = 95^{o}$, 215^{o} and 335^{o}. The array was configured on a smooth hemispherical ground plane and performance was measured at both GPS frequencies. The RDPs were analyzed and the results are presented in Table 2-4.

Table 2-4

MICROSTRIP ARRAY PERFORMANCE ON SMOOTH HEMISPHERE

Level (dB)	HEMISPHERICAL COVERAGE (%) ≥ LEVEL @ 1227.6 MHz	@ 1575.4 MHz
0.0	55.1	58.7
-1.0	64.1	67.8
-2.0	72.1	75.1
-3.0	77.7	81.2
-4.0	82.4	85.4
-5.0	85.9	88.5
-6.0	89.1	90.8
-7.0	91.3	92.6
-8.0	93.2	93.8

Table 2-4 (Cont'd)

MICROSTRIP ARRAY PERFORMANCE ON SMOOTH HEMISPHERE

Level (dB)	HEMISPHERICAL COVERAGE (%) ≥ LEVEL	
	@ 1227.6 MHz	@ 1575.4 MHz
-9.0	94.6	95.1
-10.0	95.7	96.1
-11.0	96.8	96.8
-12.0	97.6	97.7
-13.0	98.0	98.2
-14.0	98.6	98.8
-15.0	98.9	99.2
-16.0	99.1	99.3
-17.0	99.3	99.4
-18.0	99.5	99.5
-19.0	99.6	99.7
-20.0	99.6	99.7

The microstrip patch array was removed from the smooth hemisphere and reconfigured on the ESSA antenna. In order to accommodate the patch two ESSA radiating elements were removed at each of the three mounting locations. RDPs were again taken and analyzed at both GPS frequencies. The results are given in Table 2-5.

Table 2-5

MICROSTRIP ARRAY PERFORMANCE ON ESSA ANTENNA

Level (dB)	HEMISPHERICAL COVERAGE (%) ≥ LEVEL	
	@ 1227.6 MHz	@ 1575.4 MHz
0.0	31.5	26.3
-1.0	46.8	42.4
-2.0	60.8	55.8
-3.0	70.6	65.6
-4.0	77.4	73.7
-5.0	82.3	79.5
-6.0	86.5	84.7
-7.0	89.5	87.6
-8.0	91.9	90.4
-9.0	93.7	92.5
-10.0	95.2	94.2
-11.0	96.3	95.4
-12.0	97.4	96.4
-13.0	98.2	97.2
-14.0	98.6	97.8
-15.0	99.0	98.3
-16.0	99.2	98.6
-17.0	99.4	98.9
-18.0	99.5	99.1
-19.0	99.6	99.3
-20.0	99.8	99.4

As with the turnstile array the performance of the three element GPS microstrip antenna degraded slightly when configured on the ESSA antenna. At the -2 dB level the coverage dropped from 72% to 61% at 1227.6 MHz and from 75% to 56% at 1575.4 MHz. The reason for this change in performance level is due to aperture blockage by the ESSA antenna radiating element. Since the height of the microstrip patch and the ESSA elements are nearly equal (Figure 2-2), their close lateral proximity will distort the radiated field. With this particular geometry it is likely that a portion of the radiated field from the GPS antenna is attenuated under the adjacent ESSA radiating elements.

The Effect of GPS Microstrip Patches on ESSA Performance

After the three microstrip patch antennas had been reconfigured on the ESSA antenna, forty-nine ESSA beams in the vicinity of one of the patches were measured. Since the patch was located at $\theta = 60^{o}$, $\phi = 215^{o}$, the ESSA antenna beams included the same beams as before in the range, $45^{o} \leq \theta \leq 78^{o}$ and $185 \leq \phi \leq 240^{o}$. Compensation was unnecessary. The gain of the reference beam was identical to that measured during final acceptance tests, 12.9 dB. Since there were no singular deviations between the two sets of gain data outside the range of measurement error, ±0.25 dB, the average change in gain computation included all forty-nine beams. The average difference was 0.1 dB with the higher values associated with the integrated configuration.

Although two ESSA elements were removed to accommodate each L-band microstrip patch, the gain of the ESSA subarray without these elements was not affected. This does not represent typical ESSA performance, but is related to the fact that the 12-element subarray exceeded the optimum aperture size (see Section 1.3.1). Therefore, when the subarray was reduced to 10-elements for certain beams because of the missing elements, the aperture size was slightly below optimum and had roughly the same gain as the original 12-element subarray. The input VSWR for the 10-element subarray beams increased from 1.5:1 to 2.0:1 at the high end of the band.

The ellipticity measured at 2250 MHz for ten beams on a great circle passing through the location of the patch was between 2.0 and 3.0 dB which is typical for this frequency.

2.1.3 Conclusions

The limited testing described in the previous sections provides an adequate base for generalized projections regarding the performance of an integrated GPS/ESSA antenna system. This concept should be pursued so that a complete package for a user satellite or shuttle payload consisting of an S-band transponder, ESSA antenna, GPS antenna, receiver and processor assembly is developed. The RF performance for specific configurations could be determined at that time.

The test results of the two GPS arrays indicate that either the turnstile or the microstrip patch 3-element arrays will provide adequate hemispherical coverage at the required frequencies. The performance of both arrays can be improved over the level measured for the integrated configuration. The height of the turnstiles can be adjusted for optimum coverage when configured on the ESSA antenna. Similarly the coverage using the microstrip patches can be restored to the original level (75% at -2 dB) by increasing the separation between the patches and the ESSA radiating elements, thereby reducing aperture blockage. There are other factors to consider, however, regarding the two approaches. Table 2-6 points out the major advantages and disadvantages of each configuration.

Table 2-6

GPS ARRAY TRADE-OFFS

Consideration	Turnstiles Excel	Microstrip Patches Excel	Comments
Effect on ESSA	•	•	See text
Ruggedncss		•	Microstrip patches are low profile, laminated dielectric.
Simplicity		•	Turnstile requires phasing network for circular polarization. Patches do not.

Table 2-6 (Cont'd)
GPS ARRAY TRADE-OFFS

Consideration	Turnstiles Excel	Microstrip Patches Excel	Comments
Weight	•	•	About the same when turnstile phasing network is included.
Volume Require		•	Turnstiles protrude 10 cm above ESSA surface. Patches are only 0.5 cm above.

The estimated weight for a 3-element GPS array including input power divider, cabling and radiating elements is 500 gm.

The test data indicated that presence of the turnstile substantially reduced the gain of several adjacent ESSA beams, yet a quantitative projection for future systems cannot be made until a final configuration is established. The degradation in gain due the turnstile can be minimized for those ESSA beams which look through it, however, the elimination of such adverse effects is not possible since the physical dimensions of the turnstile are large compared to a wavelength at S-band. The advantage of the turnstiles is that they can be mounted between the ESSA elements.

Although the addition of the microstrip patches and the deletion of two ESSA elements at each patch location had a negligible effect on the ESSA beam gains, it does not represent typical performance. As mentioned previously the EMU 12-element subarray exceeded the optimum aperture size and has an associated gain reduction. When the two elements were removed to accommodate the microstrip patch, those ESSA beams using only 10-element subarrays also exhibited reduced gain since the aperture was now less than optimum. The presence of the microstrip patch did not perturb the gain since neither subarray had optimum gain.

In general, the addition of the microstrip patch and the deletion of ESSA elements will degrade ESSA performance somewhat. For the ideal 12-element subarray the elimination of two elements would cause a worst case gain reduction of 0.6 dB for the peak of the beam. Of equal importance, however, is the fact that these missing elements will affect the beam steering increments in the vicinity of the patch. An additional worst case 0.3 dB of beam crossover loss should be expected for a few beams in this region.

2.2 Volumetric Coverage Tests

In a practical application the ESSA antenna will be deployed from the spacecraft in order to reduce blockage and attain nearly spherical coverage. The task of predicting antenna performance at very large coverage angles close to the blockage angle becomes extremely complex. This is because the conducting surfaces of the deployment boom and the spacecraft affect performance. The RF currents induced on these surfaces re-radiate and alter the original pattern.

The engineering model was used in a simulation of a deployed antenna to determine actual coverage angle limits. The ESSA antenna was inverted to simulate the lower hemisphere of a full spherical array.

2.2.1 Description of Tests

Spacecraft blockage was simulated by configuring an aluminum hexagon plate above the zenith of the hemisphere as shown in Figure 2-4. The plate was 86.4 cm across its maximum point to point dimension. A 5.1 cm O.D. aluminum tube was used to support the plate as shown. Spacecraft blockage was simulated for two deployment distances: 144.8 cm and 53.3 cm.

Coverage gain and axial ratio data was taken at each distance and compared to the reference data which represented the unblocked or normal configura-

ORIGINAL PAGE IS
OF POOR QUALITY

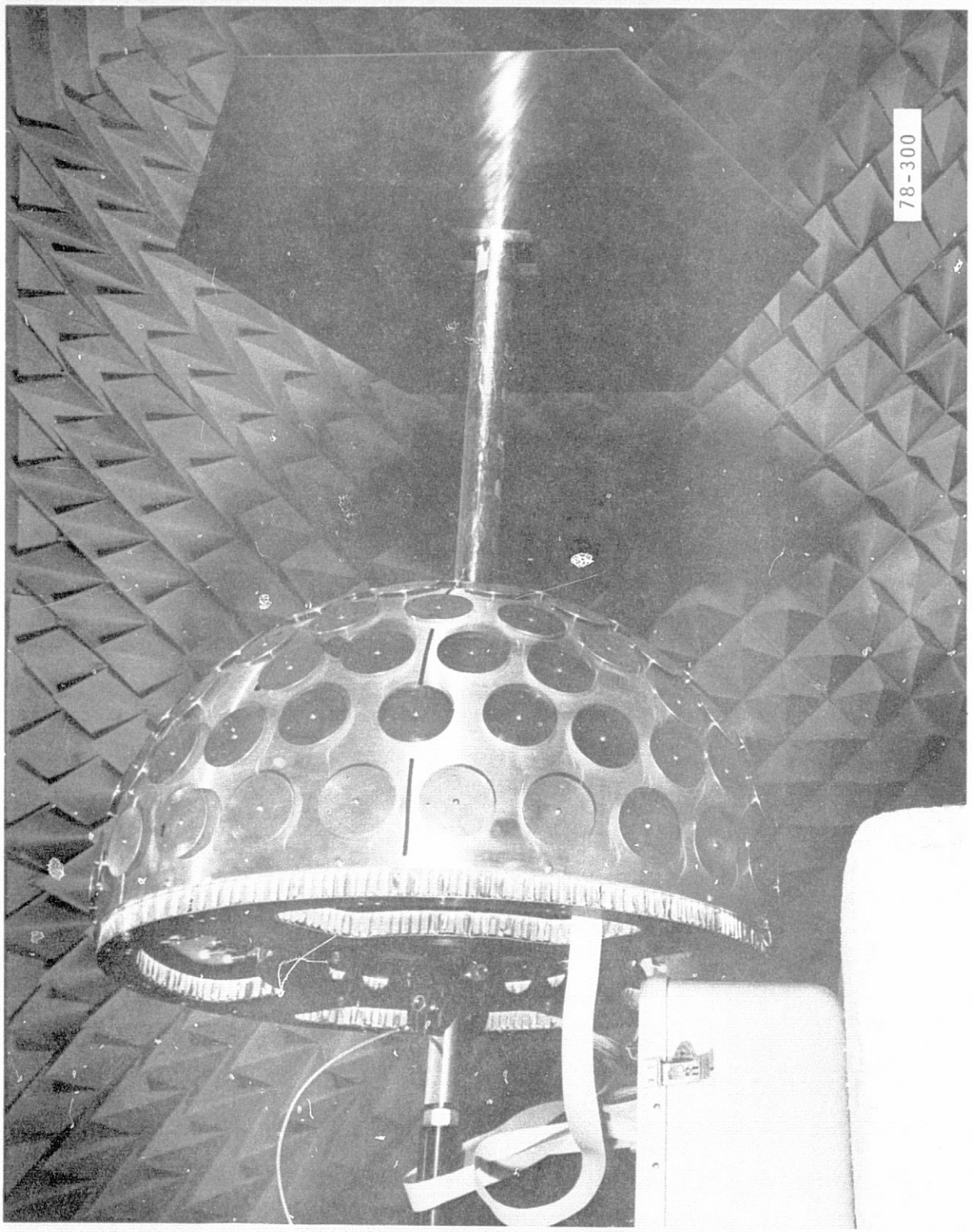

Figure 2-4 ESSA Configuration for Coverage Limit Tests

tion. The reference data was obtained by scanning the ESSA beam from $\theta = 73^0$ to 6.5^0 along three fixed values of ϕ; 150^0, 192^0 and 228^0. This data was repeated with the hexagon plate simulating an AEM type spacecraft at each spacing. The coverage angle limit was defined as the angle from the zenith ($\theta = 0$) at which the coverage gain degraded 1.0 dB below the reference level. This angle was determined independently for each deployment distance.

2.2.2 Test Results

Typical coverage gain data for the 53.3 cm and 144.8 cm deployment distances are shown respectively in Figure 2-5 and 2-6. The solid lines represent the unblocked or reference data and the dotted lines are a repeat of the reference data with the simulated spacecraft present. The coverage angle limit is 39^0 and 22^0 for the respective deployment spacings of 53.3 cm and 144.8 cm. A summary of all the measured coverage gain data is presented in Table 2-7.

Table 2-7
COVERAGE LIMITS DATA SUMMARY

ϕ Angle	53.3 cm Deployment Spacing	144.8 cm Deployment Spacing
150^0	39^0	22^0
192^0	36^0*	22^0
228^0	36^0	25^0 - 35^0**

* See Text
** Constant 1.0 dB gain reduction over this range

As expected the data confirms that the coverage is greater when the antenna is deployed further from the spacecraft. On the average the coverage angle limits are 37^0 and 25^0 respectively for the 53 cm and 145 cm spacings. Some anomalies were observed, however. At the closer spacing (53 cm) a 2 dB coverage gain reduction was observed when the beam was pointed at $\theta = 55^0$,

REPRODUCIBILITY OF THE
ORIGINAL PAGE IS POOR

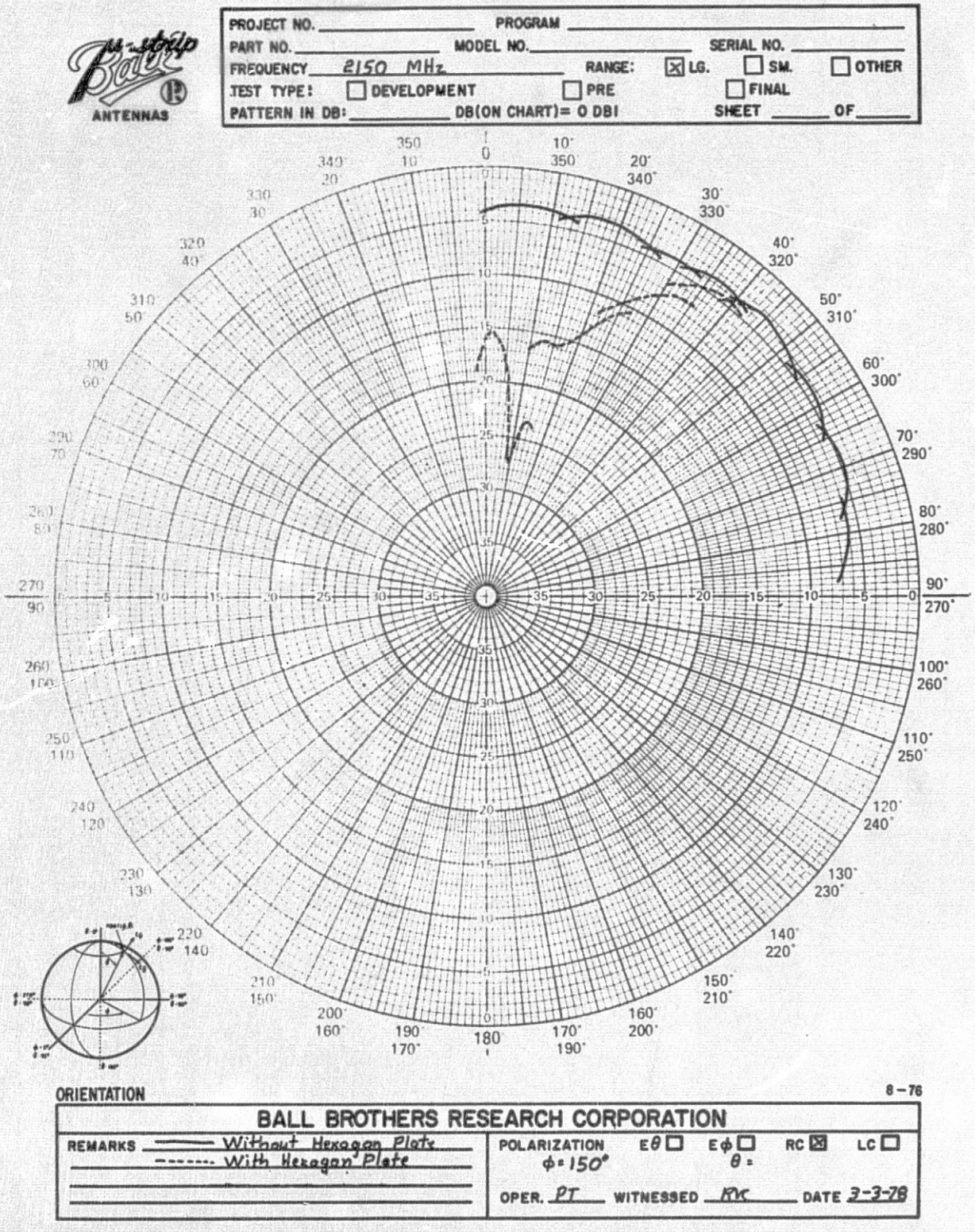

Figure 2-5 Coverage Gain Limit for 53 cm Spacing

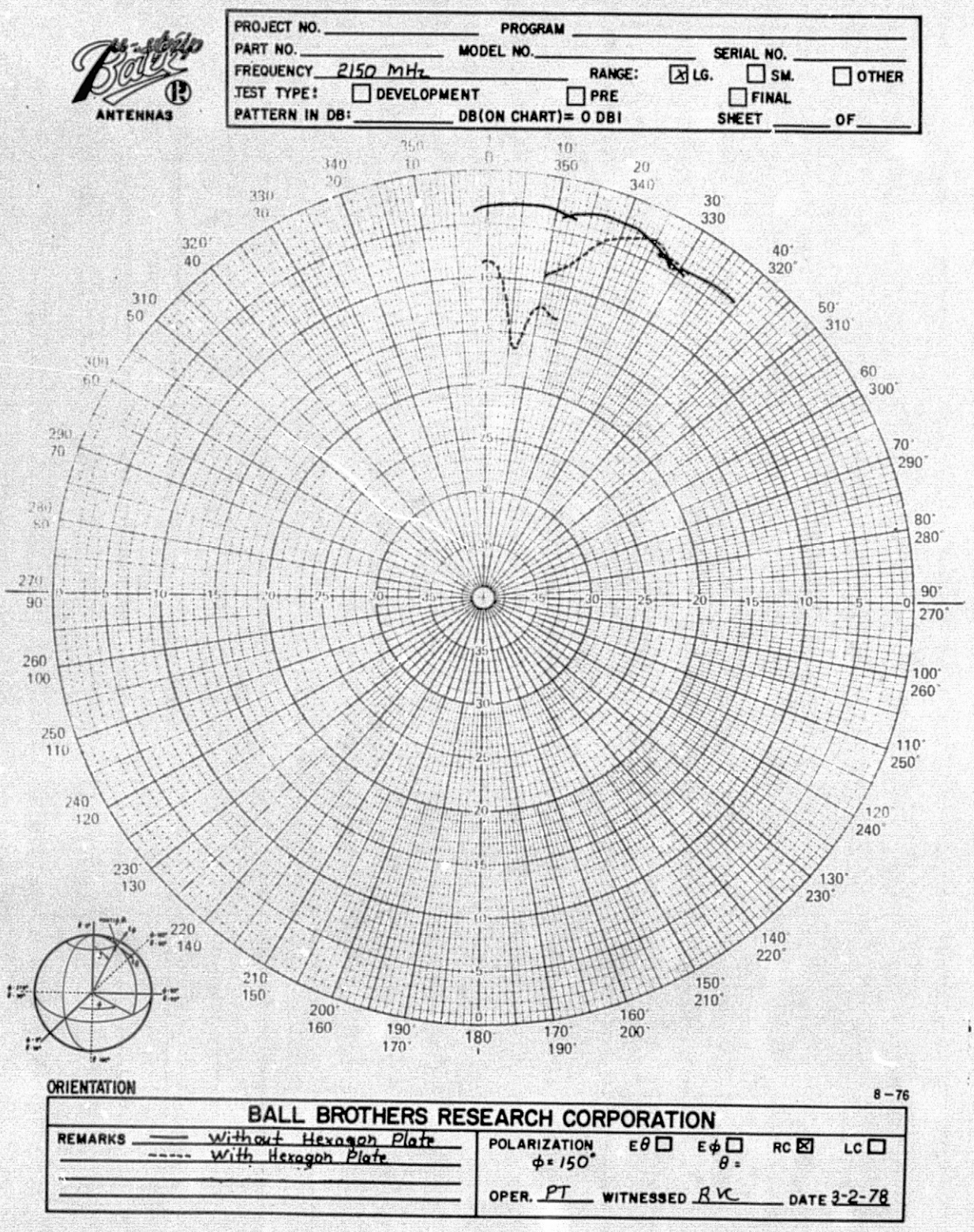

Figure 2-6 Coverage Gain Limit for 145 cm Spacing

$\phi = 192^{o}$, and a 0.75 dB improvement in gain occurred for the direction $\theta = 43^{o}$, $\phi = 192^{o}$ as shown in Figure 2-7. Such behavior is probably best explained by multiple reflections between the flat hexagon plate and the curved hemispherical surface and subsequent phase shifted re-radiation. This reflected energy can come from several sources such as sidelobes, or the portion of the main beam blocked by the flat plate. The number and degree of such irregularities were significantly less for the 145 cm spacing.

Typical axial ratio data for the two spacings are shown in Figures 2-8 and 2-9. The axial ratio is relatively independent of the degree of blockage for either spacing.

2.2.3 Conclusions

The volumetric coverage tests described in this section provided specific information on the coverage angle limits in the presence of a simulated AEM spacecraft. If a spherical ESSA antenna were deployed on a 53 cm boom, the expected coverage area would be a $\pm 143^{o}$ cone angle or 90% spherical with some variations in the coverage gain.

If the same antenna were deployed 145 cm away from an AEM type spacecraft, the expected coverage area would increase to 95% spherical or $\pm 155^{o}$ cone angle with negligible variations in the coverage gain. It is important to note, however, that the actual coverage limits may vary somewhat in the presence of a real spacecraft with additional appendages.

Tests at several frequencies within the 2.0 - 2.3 GHz band indicate that the coverage area is frequency independent.

The axial ratio is relatively unaffected by spacecraft blockage.

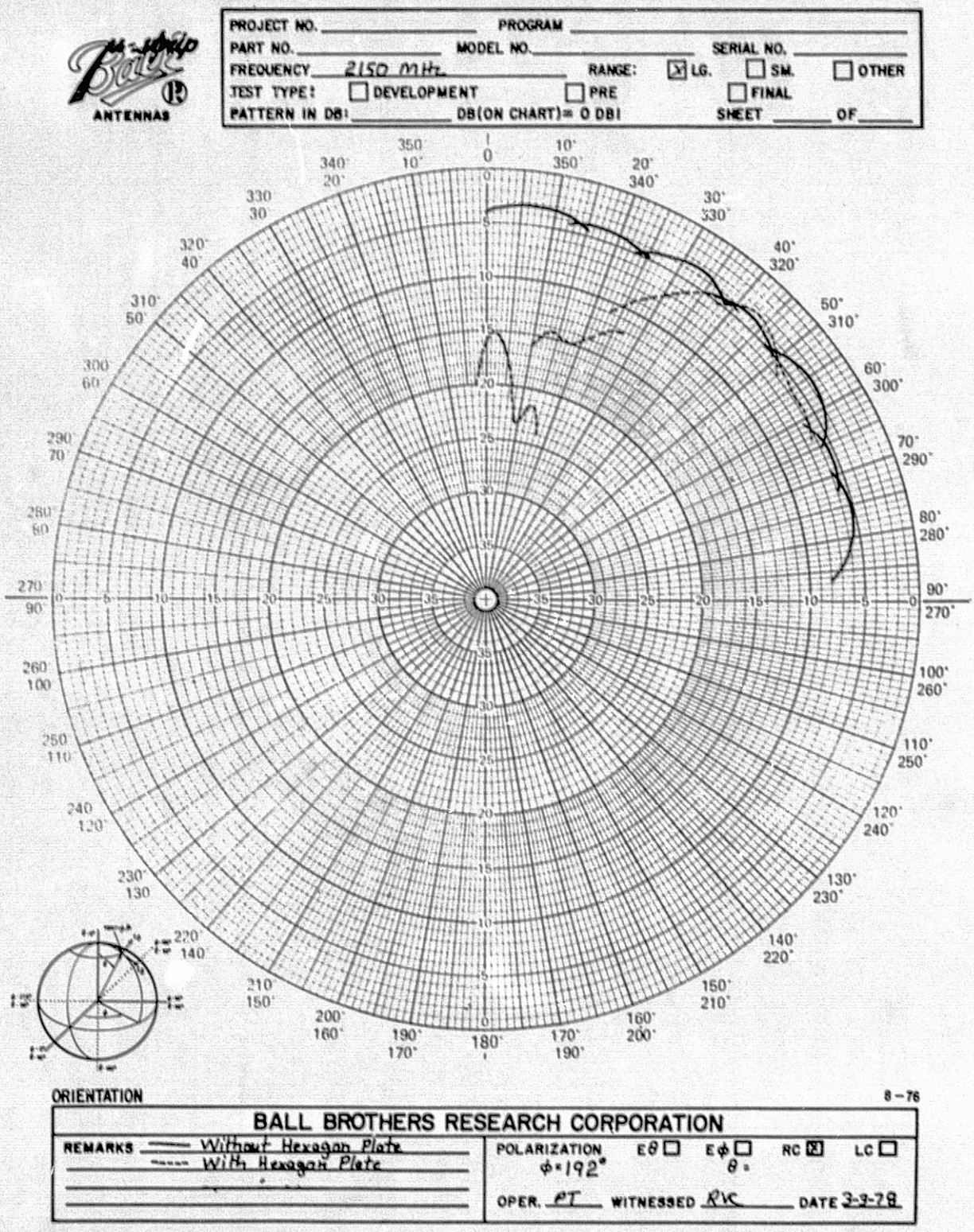

Figure 2-7 Coverage Gain Anomaly at 53 cm Spacing

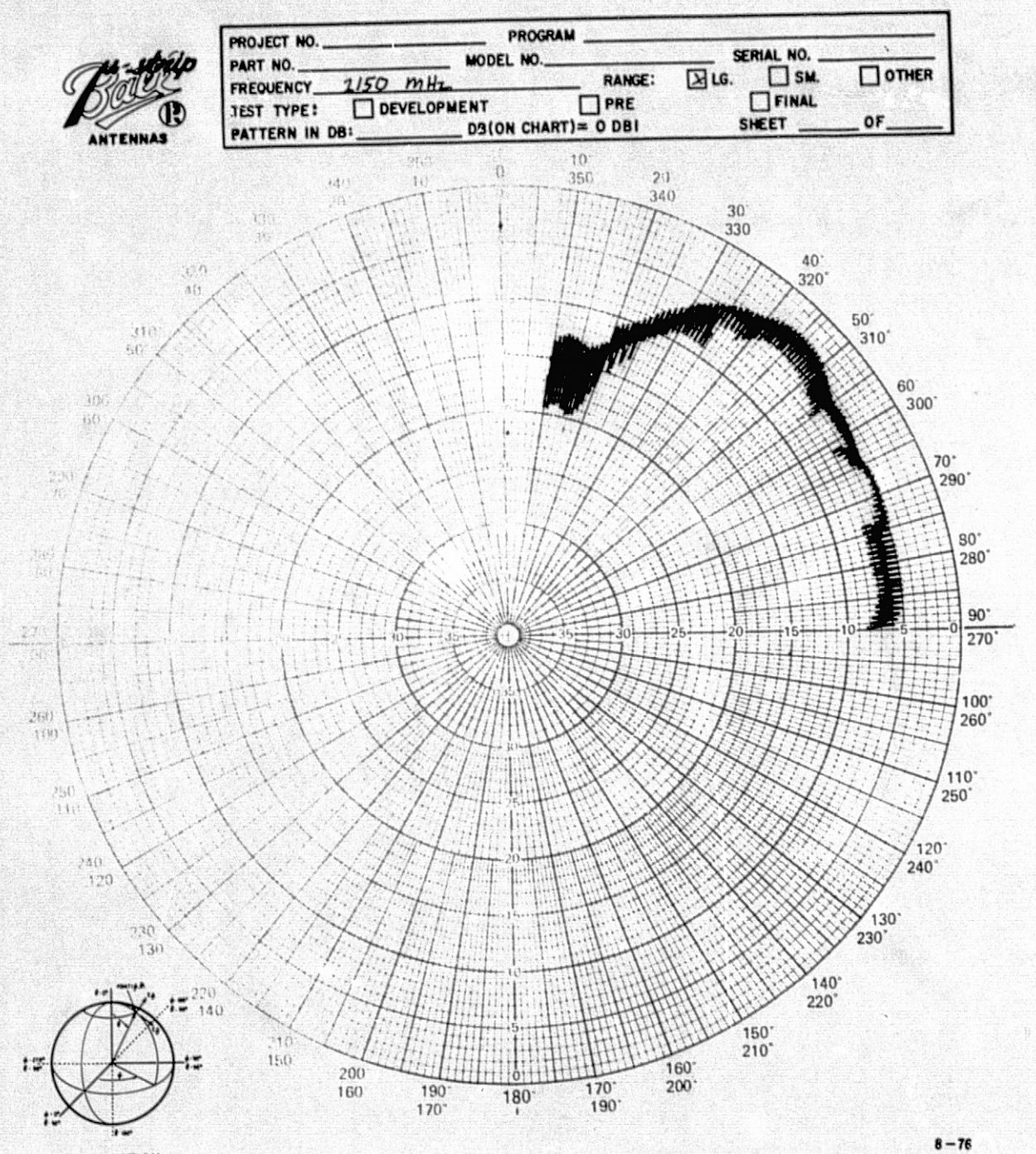

Figure 2-8 Axial Ratio at 53 cm Spacing

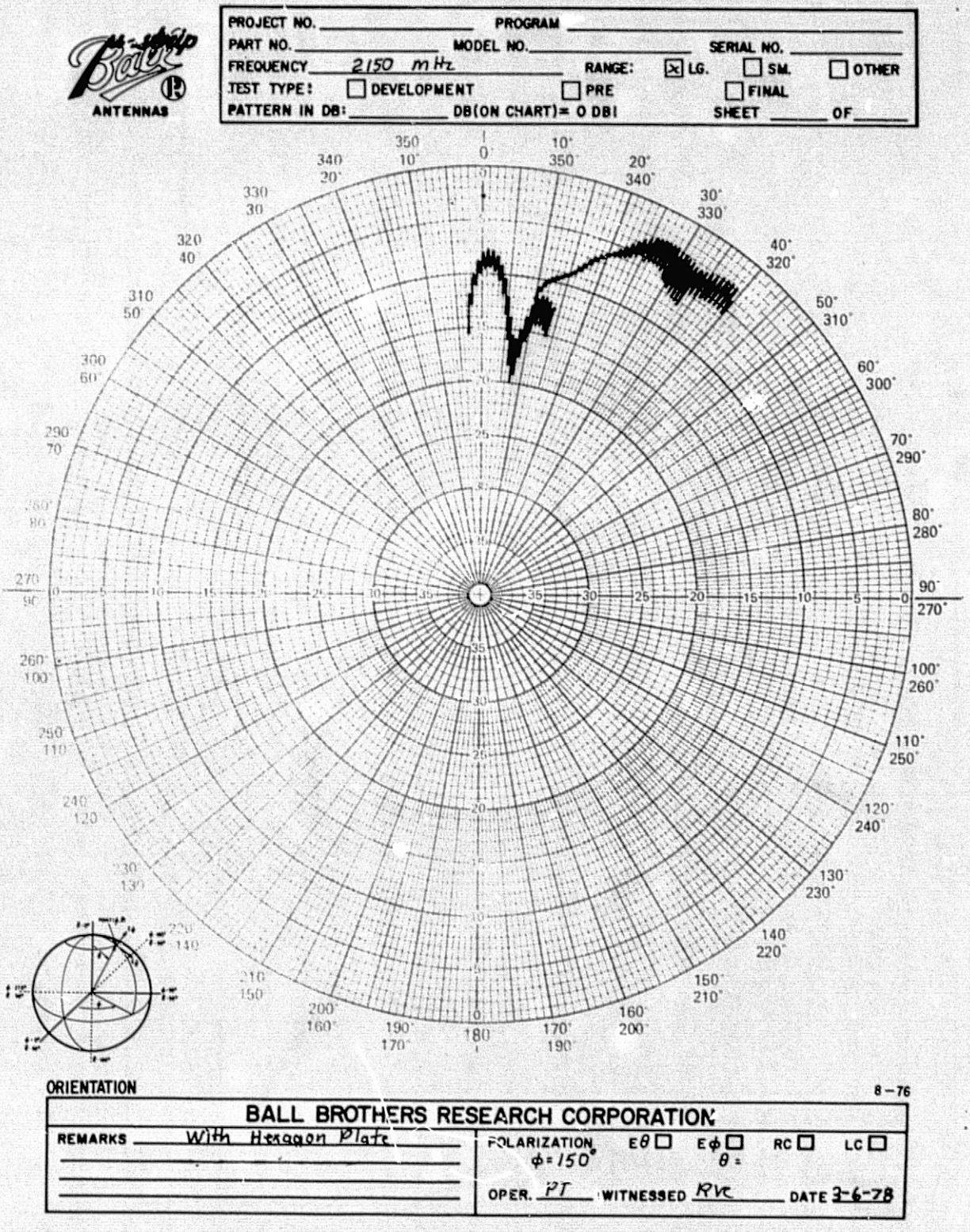

Figure 2-9 Axial Ratio at 145 cm Spacing

REFERENCES:

(1) R. E. Munson, "Conformal Microstrip Antennas and Microstrip Phased Arrays," IEEE Trans., Vol. AP-22, pp. 74-78, January 1974.

(2) D. L. Sengupta, T. M. Smith, and R. W. Larson, "Radiation Characteristics of a Spherical Array of Circularly Polarized Elements," IEEE Trans., Vol. AP-16, pp. 2-7, January 1968.

(3) R. B. Fuller, Comprehensive Thinking: World Design Science Decade 1965-1975. Carbondale, Ill.: Southern Illinois University, 1965, pp. 14-22.

(4) J. D. Clinton, "Structural Design Concepts for Future Space Missions" Progress Report NASA Contract 606-607 (Nov 1965).

Appendix A

SPHERICAL ARRAY COMPUTER PROGRAM

A computer program was written to calculate the theoretical directivity of an aperture on a spherical surface. The size and shape of the aperture are defined by the element locations. The required input data consists of the amplitude, phase and θ, ϕ location of each element and the radius of the sphere.

The aperture directivity calculation is based on the radiation pattern and directivity of a single element which is included as part of the program. The procedure simply sums the contribution of each element at every far-field observation point. The points are every degree along a desired value of constant θ and ϕ. The directivity, therefore, is the peak amplitude value divided by the average value for the specified pattern cut. This computation represents a true aperture directivity if 1) the cut includes the peak of the beam, and 2) the beam is symmetrical about the peak. These conditions are not limitations, however, since both are easily met. The location of the peak of the beam coincides with the θ, ϕ values for the center of the aperture. Beam symmetry is inherent with the circular apertures being considered.

In addition to the computed directivity an X-Y plot of the far-field pattern is available as an optional output.

A listing of the program is given on the following pages.

REPRODUCIBILITY OF THE
ORIGINAL PAGE IS POOR

```
C*** HEMISPHERICAL ARRAY   13 JULY 197
C
      COMMON/ARRY/A(260),P(260),X(3,260),X1(260),X2(260),E(180),
     1  PHID(360),AMP(360),EA(180),IPAM(14),CPHIN(100)
        DIMENSION IHS1(2), IHS2(2)
        DIMENSION ISCALE(2,5),ISCRIB(2),IDEG(3)
        DIMENSION IHSCAL(2,7)
      DIMENSION PTHETA (3)
      REAL  LAMB
C
C
C
        DATA RAD/57.2957795131/
        DATA ISCALE/' -','90',' -','45','  ','0.','  ','45',' ','90'/
        DATA IDB/'DB'/
        DATA IHS1/'-9','0.'/
        DATA IDEG/'-D','EG','- '/
        DATA IHSCAL/' -','90',
     2  ' -','60',
     3  ' -','30',
     4  '  ','0 ',
     5  ' +','30',
     6  ' +','60',
     7  ' +','90'/
C
        DATA F/0.,0.,0.,0.,0.,-.04,-.05,-.06,-.07,-.08,
     1  -.1,-.15,-.16,-.17,-.18,-.24,-.27,-.31,-.38,-.43,
     2  -.5,-.55,-.6,-.68,-.75,-.82,-.9,-1.0,-1.1,-1.2,
     3  -1.3,-1.4,-1.5,-1.6,-1.75,-1.9,-2.04,-2.15,-2.3,-2.5,
     4  -2.6,-2.8,-2.95,-3.15,-3.35,-3.62,-3.84,-4.06,-4.28,-4.5,
     5  -4.76,-4.97,-5.17,-5.38,-5.55,-5.8,-6.,-6.2,-6.4,-6.6,
     6  -6.8,-7.0,-7.2,-7.4,-7.6,-7.8,-8.,-8.2,-8.4,-8.6,
     7  -8.8,-8.98,-9.16,-9.32,-9.5,-9.64,-9.8,-9.96,-10.1,-10.25,
     8-10.4,-10.6,-10.75,-10.9,-11.06,-11.25,-11.5,-11.65,-11.85,-12.0,
     9-12.2,-12.4,-12.6,-12.8,-13.0,-13.2,-13.4,-13.6,-13.8,-14.0,
     X-14.5,-14.7,-14.9,-15.1,-15.3,-15.9,-16.5,-17.1,-17.7,-18.3,
     1-18.7,-19.1,-19.4,-19.8,-20.2,-20.3,-20.4,-20.5,-20.6,-20.6,
     2-20.6,-20.6,-20.7,-20.7,-20.7,-20.8,-20.8,-20.9,-20.9,-21.0,
     3-21.2,-21.4,-21.6,-21.8,-22.0,-21.6,-21.2,-20.7,-20.3,-19.9,
     4-19.8,-19.7,-19.6,-19.5,-19.5,-20.1,-20.7,-21.3,-21.9,-22.5,
     5-22.5,-22.6,-22.6,-22.5,-22.5,-22.4,-22.3,-22.2,-22.1,-22.0,
     6-22.2,-22.4,-22.6,-22.8,-23.0,-23.6,-24.2,-24.8,-25.4,-26.0,
     7-25.1,-24.1,-23.2,-22.2,-21.3,-21.1,-20.9,-20.7,-20.5,-20.3/
      IFIXY=950
C
      DO 500 IJ=1,180
500   EA(IJ)=10.**((E(IJ)+7.)/20.)
        WRITE(102,9000)
9000  FORMAT(' SET DATA SWITCHES D'/'    15 ON FOR PATERN PRINT'/
     1 '    14 ON TO DEFEAT PLOTTING')
      PAUSE
C
41    CONTINUE
      READ(105,90,END=788)NEE,NARY,THETA1,THETA2,THETAD,RP,PHI,F
90    FORMAT(2I5,6F10.0)
      READ(105,290) ICUT
```

```
      IF(NEE.NE.3 .OR. NEE.NE.4) GOTO 555

      DO 550 IDG=1,179
      DEGR=(FLOAT(IDG))/RAD
550   EA(IDG)=((1.+(COS(DEGR))*.5))**(2.8*COS(DEGR/ 2.225))
         EA(180)=EA(179)

      GO TO 640
C**** OPTION TO REPLACE THE E  ARRAY
555   IF(NEE.EQ.5 .OR. NEE.EQ.6) READ(105,197)EA
197      FORMAT(10F8.0)
C
C
640   NE=IAND(NFE,1)
      IF(NE.EQ.1) GO TO 777
      CALL IPLOT(0,0,3)
      CALL IPLOT(0,1000,4)
         DO 700 IEI=1,90
         IX=IEI*10
         Y=(20.+E(IEI))*50.
         IY=IFIX(Y+.51)
700   CALL IPLOT(IX,IY,4)
      CALL IPLOT(IX,IY,3)
        CALL IPLOT(IX,0,3)
         IX=IX+100)
      CALL IPLOT(IX,0,3)
      CALL IPLOT(0,0,5)
      CALL IPLOT(0,0,2)
777      CONTINUE
C
C
666   J=1
10    READ(105,91,END=100)A(J),P(J),X(1,J),X(2,J),X(3,J)
91    FORMAT(5F12.0)
         J=J+1
         GO TO 10
C
C***     THE INPUT DATA IS NOW IN MEMORY AS PRINTED BELOW
100      J=J-1
      IF(J.LT.1) GO TO 788
      WRITE(108,95)NEE,J,THETA1,THETA2,THETAD,RP,PHI,F
95    FORMAT(1H1,1X,' RUN',T11,'NO.DATA',T22,'THETA  THETA  DELTA'/
     X 1X,'OPTIONS',T11,'ENTRIES',T22,'START  STOP   THETA',T45,
     1 '     RP       PHI       F     '/1X,I3,T14,I3,T19,3F7.1,
     2 4X,2F8.1,F10.3///
     3  T5,'ELEMENT',T20,'AMPLITTUDE',T35,'PHASE',T50,'R',T65,'THETA',
     4  T82,'PHI')
         DO 200 I=1,J
  200 WRITE(108,96)I,A(I),P(I),X(1,I),X(2,I),X(3,I)
96    FORMAT(T8,I3,T20,F10.3,T30,F10.3,T46,F10.3,T60,F12.6,T75,F12.6)
      AMAVG=0.
      DO 16  I=1,J
      AMAVA=A(I)**2
       AMAVG=AMAVG+AMAVA
16    CONTINUE
C
      LAMB=11.811/F
         SAM=0
      NSAM=0
```

REPRODUCIBILITY OF THE
ORIGINAL PAGE IS POOR

```
      PAMP=-100.
         ITHR=IFIX((THETA2-THETA1)/THETAD)
      IF(ITHR.GT.360) ITHR=360
C***     START
      DO 22 I=1,J
      X1(I)=X(2,I)/RAD
      X2(I)=X(3,I)/RAD
   22 CONTINUE
C
      CALL DATSW(15,ISET)
      IF(ISET.EQ.1) GO TO 2
      GO TO 3
2     IF(ICUT.EQ.1) WRITE(108,92)
      IF(ICUT.EQ.2) WRITE(108,93)
3     CONTINUE
         DO 2000 IT=1,ITHR
         DTHETA=(IT-1)*THETAD+THETA1
         THETA=DTHETA/RAD
      SUMJ=0.
      SUMK=0.
C
      PHIP=PHI
      IF(ICUT.EQ.2) GO TO 17
      IF(THETA.LT.0.)  GO TO 17
      PHIP=PHI+180.
   17 PHIR=PHIP/RAD
      IF(ICUT.EQ.1) GO TO 4
      DUM=PHIR
      PHIR=THETA
      THETA=DUM
4     CONTINUE
C
C
      DO 1000 I=1,J
      X1(I)=X(2,I)/RAD
      X2(I)=X(3,I)/RAD
      THETE=THETA
      IF(THETA.LT.0.)     THETE=-THETA
C
      DM=SQRT(2.*X(1,I)**2*(1.-SIN(THETE)*SIN(X1(I))*(COS(PHIR)*
     1COS(X2(I))+SIN(PHIR)*SIN(X2(I)))-COS(THETE)*COS(X1(I))))
      AC=2.*ASIN(DM/(2.*X(1,I)))
      AD=X(1,I)*SIN(AC)
      AE=SQRT(DM**2-AD**2)
      AF=AE*360./LAMB
      DX=2.*X(1,I)**2
      DY=(DX-DM**2)/DX
      THETAN=ACOS(DY)*RAD
      IF(THETAN.LT.1.)  THETAN=1.
C
      SB=(6.283185*AE/LAMB)+P(I)/RAD
      SJ=EA(THETAN)*A(I)*COS(SB)
      SK=EA(THETAN)*A(I)*SIN(SB)
      SUMJ=SUMJ+SJ
      SUMK=SUMK+SK
C
1000     CONTINUE
      IF(NEE.NE.3.OR.NEE.NE.4) GO TO 1010
         WRITE(108,98) SUMJ,SUMK
98       FORMAT(23X,'----------',5X,'----------'/
```

```
177         1 18X,'SUMJ=',F10.2,' SUMK=',F10.2/
178         2  )
179   92     FORMAT(
180         2 1H1,5X,'THETA',5X,'AM',6X,'AMP(I)')
181   93     FORMAT(
182         2 1H1,5X,' PHI ',5X,'AM',6X,'AMP(I)')
183   1010      CONTINUE
184   C
185   C                                                    REPRODUCIBILITY OF THE
186           AM=SQRT(SUMJ**2+SUMK**2)                     ORIGINAL PAGE IS POOR
187   C
188           NSAM=NSAM+1
189              ARG1=20.**ALOG10(AM)
190              AMP (IT)=ARG1
191              IF(AMP(IT).GT.PAMP) PPHAS=DTHETA
192              IF(AMP(IT).GT.PAMP)PAMP=AMP(IT)
193
194           CALL DATSW(15,ISET)
195           IF(ISET.EQ.2) GO TO 2000
196           WRITE(108,99)DTHETA,AM,AMP(IT)
197   2000       CONTINUE
198      99 FORMAT(3X,F6.0,2F10.2)
199
200           WRITE(108,95)NEE,J,THETA1,THETA2,THETAD,RP,PHI,F
201              DO 209 I=1,J
202     209   WRITE(108,96)I,A(I),P(I),X(1,I),X(2,I),X(3,I)
203           AMPK=10.**(PAMP/10.)
204           PG=AMPK/AMAVG
205           PLANAR=10.*ALOG10(PG)
206           WRITE(108,193) PLANAR,PPHAS
207   193     FORMAT(//10X,'****PLANAR DIRECTIVITY=',F10.2/
208         1 10X,'**** PHASE AT PEAK AMP.',F8.2)
209           CALL DATSW(14,ISET)
210           IF(ISET.EQ.1) GO TO 666
211   C**   DRAW THE SCALE
212              CALL MARGIN(5,0.,-50.)
213           CALL LETTER(-100,985,IDB,2)
214           CALL IPLOT(0,0,3)
215           CALL IPLOT(10,900,0)
216   C*** PLOT THE AMPLITUDE FUNCTION
217           ENCODE(28,199,IPAM) PLANAR
218   199     FORMAT('  PLANAR DIRECTIVTTY',F8.2)
219           CALL LETTER(10,IFIXY,IPAM,28,2)
220           IFIXY=IFIXY-50
221           CALL IPLOT(IX,0,3)
222              DO 4000 IP=1,5
223              IHS=(IP-1)*450
224           CALL IPLOT(IHS,0,4)
225           CALL IPLOT(IHS,10,4)
226           CALL IPLOT(IHS,10,3)
227           DTX=(FLOAT(IP-1)/4.)*        (THETA2-THETA1)+THETA1
228           ENCODE(6,192,KXD)DTX
229   192     FORMAT(F6.1)
230           CALL LETTER(IHS-20,15,KXD,6,1)
231              IF(IP.EQ.3)CALL LETTER (IHS,50,IDEG,6,3)
232           CALL IPLOT(IHS,0,3)
233   4000       CONTINUE
234           CALL IPLOT(0,0,3)
235   C
236   C
```

```
C************   PLOT THE 1ST FUNCTION
          IY=(AMP(1)-PAMP+50.)*20
          IF(IY.LT.0)IY=0
          IF(IY.GT.1000)IY=1000
       CALL IPLOT(0,IY,3)
       DTXX=1800./FLOAT(ITHR+1)
          DO 3000 IT=1,ITHR
          DTHETA=(IT-1)*THETAD
       XX=(IT-1)*DTXX
          IX=(XX+.51)
          Y=(AMP(IT)-PAMP+50.)*20.
          IY=(Y+.51)
          IF(IY.LT.0) IY=0
          IF(IY.GT.1000) IY=1000
          YA=AMP(IT)-PAMP
C         WRITE(108,198)IT,IX,IY,PHID(IT),YA
3000   CALL IPLOT(IX,IY,4)
       IX=IX+600
       CALL IPLOT(IX,0,3)
       CALL IPLOT(0,0,2)
       CALL IPLOT(0,0,5)
C
          GO TO 666

788    CONTINUE
       IF(ISET.EQ.1) GO TO 8000
C
198       FORMAT(3I5,2F10.2)
       CALL IPLOT(0,0,5)
       CALL IPLOT(0,0,6)
8000   STOP
          END
       SUBROUTINE IPLOT(IX,IY,IZ)
C
C      IXC,IYC = CURRENT ABSOLUTE PEN POSITION
C      IX0,IY0 = OFFSET TO CONVERT USER PEN POSITION TO ABSOLUTE
C
       DATA IFIRST/0/
C
       DATA IXC,IYX,IX0,IY0/0,0,0,0/
C
       IF(IFIRST.NE.0) GO TO 5
       CALL CLRPLT
       IFIRST=1
     5 GO TO (10,20,30,40,50,50,10),IZ
    10 RETURN
C
C        COMPUTE NEW OFFSET VALUES
C
    20 IX0=IXC-IX
       IY0=IYC-IY
       GO TO 10
C
C      PEN UP TO IX,IY
C
    30 IPEN=3
       GO TO 45
C
C      PEN DOWN TO IX,IY
```

REPRODUCIBILITY OF THE
ORIGINAL PAGE IS POOR

```
C
   40 IPEN=2
C
   45 IXC=IX+IX0
      IYC=IY+IY0
      X=FLOAT(IXC)/100.0
      Y=FLOAT(IYC)/100.0
      CALL PLOT(X,Y,IPEN)
      GO TO 10
C
C     END OF PLOT


C
   50 IX0=0
      IY0=0
      CALL CLRPLT
      GO TO 10
      END
```

Appendix B

HEMISPHERE FABRICATION TECHNIQUES

SYSTEM ENGINEERING REPORT

REPORT NO

7-19-76

PROJECT
Hemispherical Coverage Medium Gain Antenna

TITLE Array Study - Structural Configuration

PREPARED BY	DATE	APPROVED BY	DATE
R. W. Loomis	7-16-76		

SCOPE/TEXT: (ATTACH ADDITIONAL SHEETS AS REQUIRED)

Introduction:

The study was undertaken to determine the most feasible method of fabricating a light weight 30" diameter hemisphere to provide support and ground plane for the 120 element array. The study was limited to existing technology and methods requiring process experimentation and developments were not considered to be within the limits of the study.

Conclusion:

A shear spun aluminum (6061-0) solution treated to T6 condition after forming appears to best meet the majority of requirements. Chemical milling after forming will be required if weight target is to be met. The final configuration from a cost consideration should be a hemisphere with a skirt extension of constant diameter at the major diameter.

DISTRIBUTION

I. Structural Analysis

The purpose of the analysis was simply to 'ball park' the general hemisphere structural requirements to assure that the fabrication techniques studies would be compatible with the environmental requirements. To meet the weight goal, a thickness of .020 inch was selected as a minimum practical value for a uniform thickness hemisphere skin.

Two stress conditions, using the Scout environment, were evaluated:

1. Acoustic loading.
2. Single element/hemisphere interface loading using an existing BBRC computer program for thin shells.

The results of the caluclations are attached. The acoustic load is of no concern, however, the element mounting technique to the hemisphere skin does require attention as to the standout footprint area. With a standoff foot diameter of 0.5 inch, the skin stress is 25820 psi which is satisfactory for an aluminum fabrication, but marginal for magnesium.

II. Fabrication Techniques

A. Shear Spinning

Based on information from three metal forming houses, no significant problems would be encountered in spinning the hemisphere and meeting a minimum thickness of .02 inch. However, the thickness at the pole would be anywhere from .035 to .06 with .050 most likely. This imposes a considerable weight penalty for this method of fabrication.

LOADS ON THE 0.05 LB WEIGHT FROM LAUNCH

SCOUT LAUNCH

MAX g LOAD = 7.5 g INPUT

ASSUME ① = 20

$g_{TOTAL} = 7.5 \times 20 = 150$

LOAD $P = .05 \times 150 = 7.5$ LB

STRESS SUMMARY

t IN	-P LB	H LB	M IN-LB	MERIDIONAL STRESS PSI	TANGENTIAL STRESS PSI
.02	7.5	0	0	10559	3168
.02	0	7.5	0	91	27
.02	0	0	3.75	38822	11647
.03	7.5	0	0	5737	1721
.03	0	7.5	0	43	13
.03	0	0	3.75	18292	5488

FOR D = 0.5 IN

.02	7.5	0	0	7678	2303
.02	0	7.5	0	25820	7746
.02	0	0	3.75	107	32

REPRODUCIBILITY OF THE
ORIGINAL PAGE IS POOR

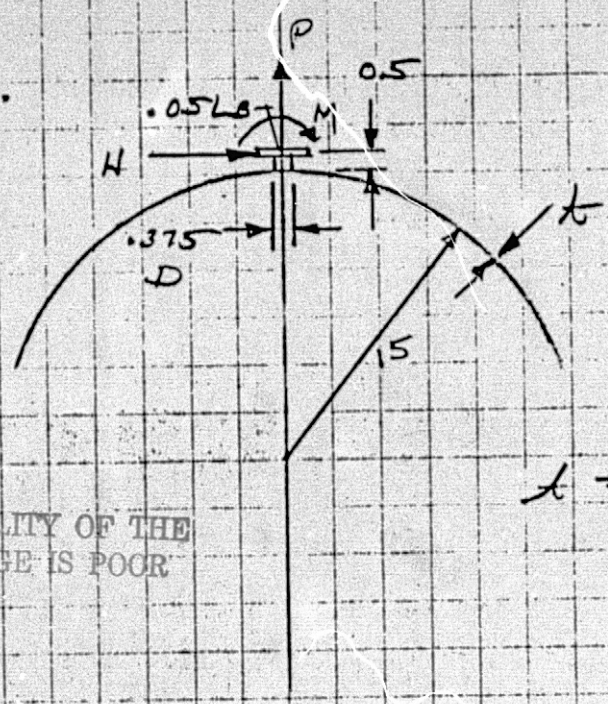

ALUM SPHERE SEGMENT

$t = 0.02$ IN

REPRODUCIBILITY OF THE ORIGINAL PAGE IS POOR

MAX ACOUSTIC SPL = 130 db @ 250 Hz

$$SP = 2.9\times10^{-9}\times10^{\frac{db}{20}}$$

$$= 2.9\times10^{-9}\times10^{\frac{130}{20}} = .00917$$

$$P_{max} = SP \times Q = .00917 \times 20 = .183 \text{ PSI}$$

CONSIDER A TOTAL SPHERE ACTED UPON BY THIS CRUSHING PRESSURE

$$P' = \frac{2Et^2}{r^2\sqrt{3(1-\nu^2)}} = \frac{2\times10^7\times.02^2}{15^2\sqrt{3(1-.3^2)}} = 21.5 \text{ PSI}$$

$$M.S. = \frac{21.5}{.183} - 1 = \underline{\text{HIGH}}$$

The proposed configuration was a 5/8 sphere. Simple fiberwood spin tooling can produce a hemisphere with a straight skirt at a constant diameter (sphere major dia.). To produce a true 5/8 sphere would require more elaborate tooling which must be disassembled for removal from the finished spinning. An approximate estimate would be a minimum factor of 2 for part cost over the more simple configuration. To reduce the weight caused by non-uniform wall thickness chemical milling is feasible, and has been used previously. The part would be immersed and withdrawn at a controlled rate depending upon the rate of change of the skin thickness caused by spinning operation. If the skin thickness change is non-uniform selective masking would be required, however, the vendor contacted indicated this as a cost problem, not a procedural one.

The obvious extension of chemical milling (depending on cost/weight value) would be to mask-off a grid pattern forming appropriate bosses and interconnecting ribs for element support, and reduce the remaining skin below the .02 thickness.

None of the forming vendors contacted expressed any enthusiasm or encouragement for spinning the hemisphere from magnesium. The concensus was that a spinning of this size from magnesium would become a development program.

B. Flame Spray

The techniques of flame spraying (Metco S.F. Aluminum) on a mandrel treated with a release agent was very briefly pursued. The vendor contacted had experience with the forming technique, but rather positively stated that this size and thickness was out of the question both from fabrication and removal (intact) from the form.

C. Fabricated Structure

Two fabricated structure configurations were considered:

1. Geodesic Dome

The value of a geodesic dome is its substitution of curved elements with straight elements more easily handled in certain materials while maintaining the desirable structural characteristics of a dome. In the proposed application, a three frequency alternate icosahedron would fill the 5/8 sphere requirement. This construction would require 150 joints between individual triangular panels. Since individual triangle size vary, the array element location, ground plane spacing uniformity behind individual elements, and element direction with respect to the hemisphere center will vary from element to element.

No feasible way of construction which would result in a lighter weight structure than a uniform skin dome was invented, and consideration of the form was discontinued as a candidate.

2. Gore and Rib Structure

A built-up electron beam welded umbrella configuration was evaluated, as the configuration was the only one that the benefits of weight reduction by using magnesium was apparent. Discussion with forming vendors was negative with respect to forming a complex curvature gore based on tooling size requirements, and accurate trimming required to assure proper joint fit.

A simple curvature gore can be cut in flat pattern and rolled. Similarily the ribs would be machined prior to bending. The cap piece and major diameter peripheral ring in conjuction with the ribs would form a self jigging structure with mechanical fasteners prior to electron beam welding. The same drawback with respect to array element mounting uniformity exists to a lesser degree with this configuration.

D. Wire Form

Based on the stresses generated at the element standoff to skin interface, the wire form (screen) hemisphere was not pursued. The configuration remains attractive, however, development testing should be performed to determine strength characteristics. From this the required standoff footprint diameter and design configuration could be established.

E. Honeycomb

Awaiting vendor response.

Honeycomb hemispheres have been constructed using a core configuration designated by Hexcel as 'flex-core' which can be formed into complex curves.

R W Loomis

CAP DETAIL (FABRICATED DOME)

½ SIZE

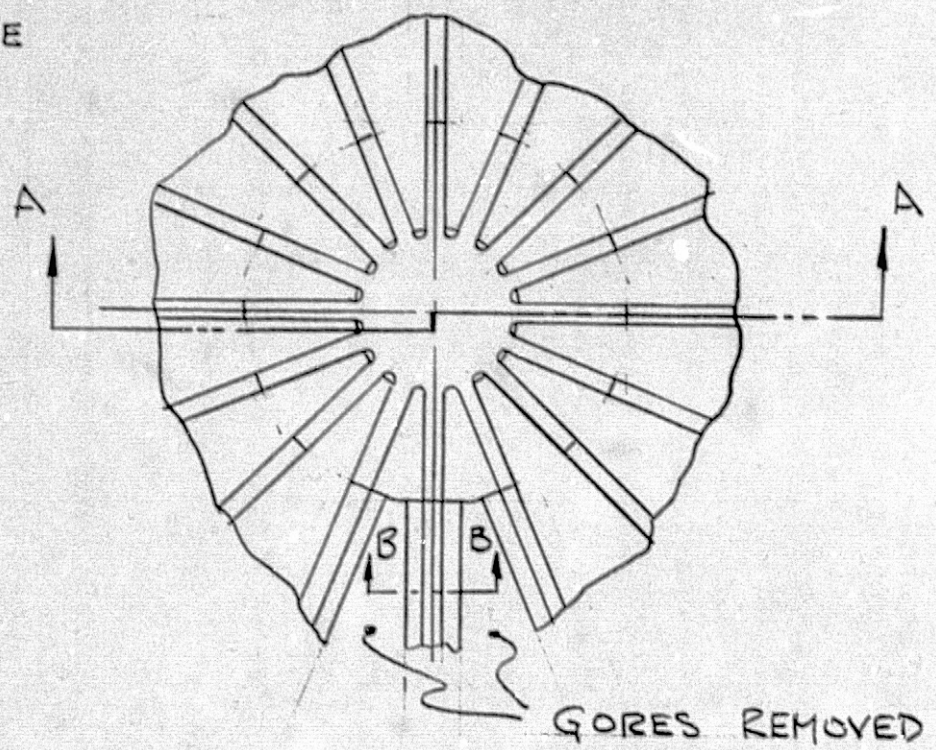

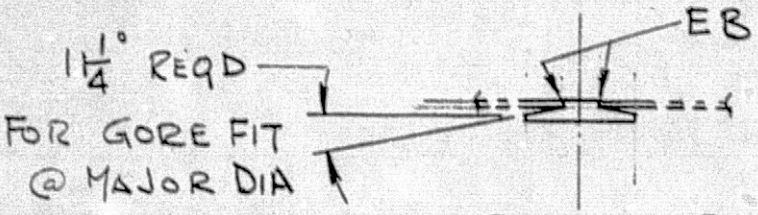

SECTION B-B (FULL SIZE)

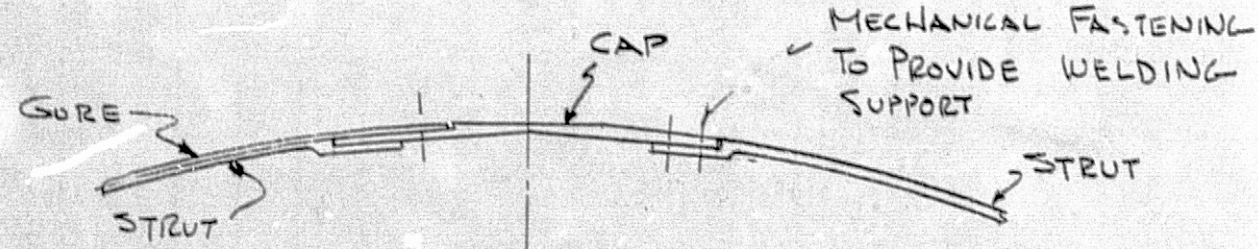

SECTION A-A

EB WELD

FABRICATED DOME.

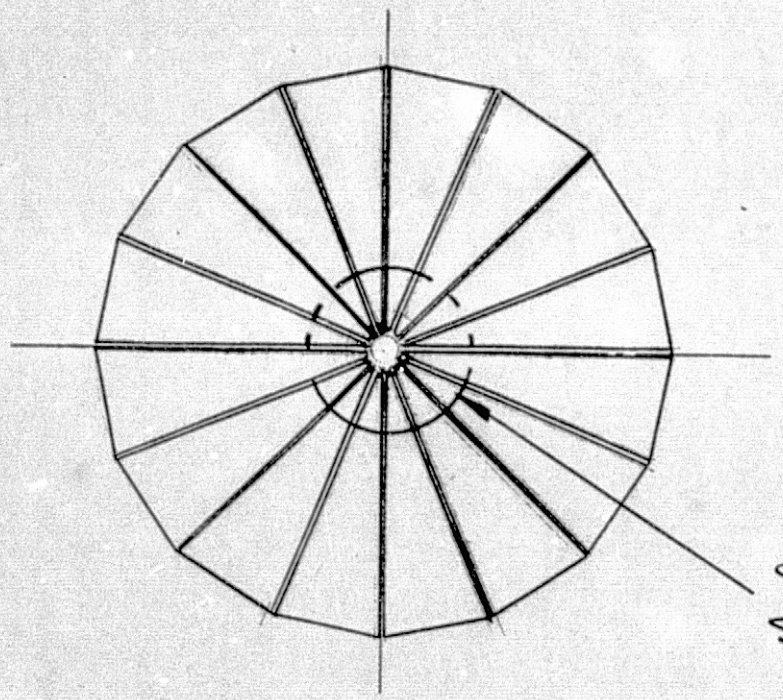

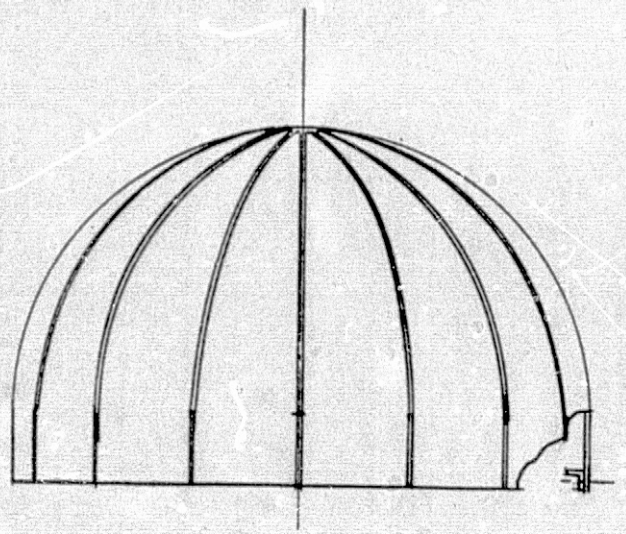

Weight Estimate Comparisons

Configuration* -

Shear Spun	4.1 lb.
Shear Spun and Chem. Milled for uniform thickness (.020/.025)	3.6 lb.
Shear Spun and Chem. Milled to grid pattern (estimate)	2.9 lb.
Umbrella Structure	3.61 lb.
Skin 2.87	
Ribs .66	
Cap .08	

*Major diameter peripheral stiffener ring omitted. It would be magnesium for all configurations.

I.I. Further Study Recommended

- Create sufficiently detailed drawings to secure accurate cost quotes for:

  1. Chem Milled grid pattern spinning.
  2. Umbrella structure.

- Procure and test screen materials for element standoff support pad design.

Appendix C

COMPONENT DIMENSIONS AND MATERIALS

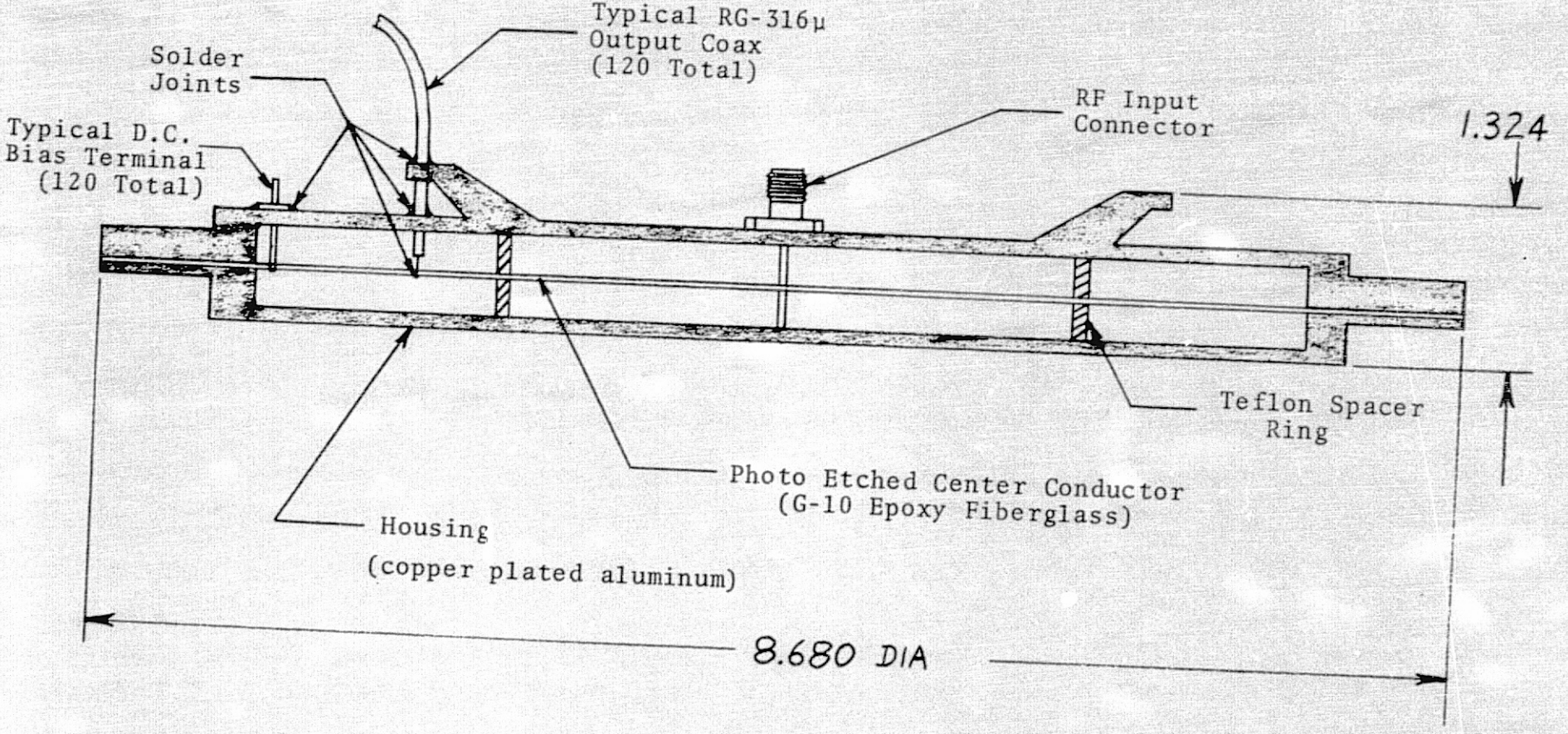

Figure C-1 Switching Power Divider

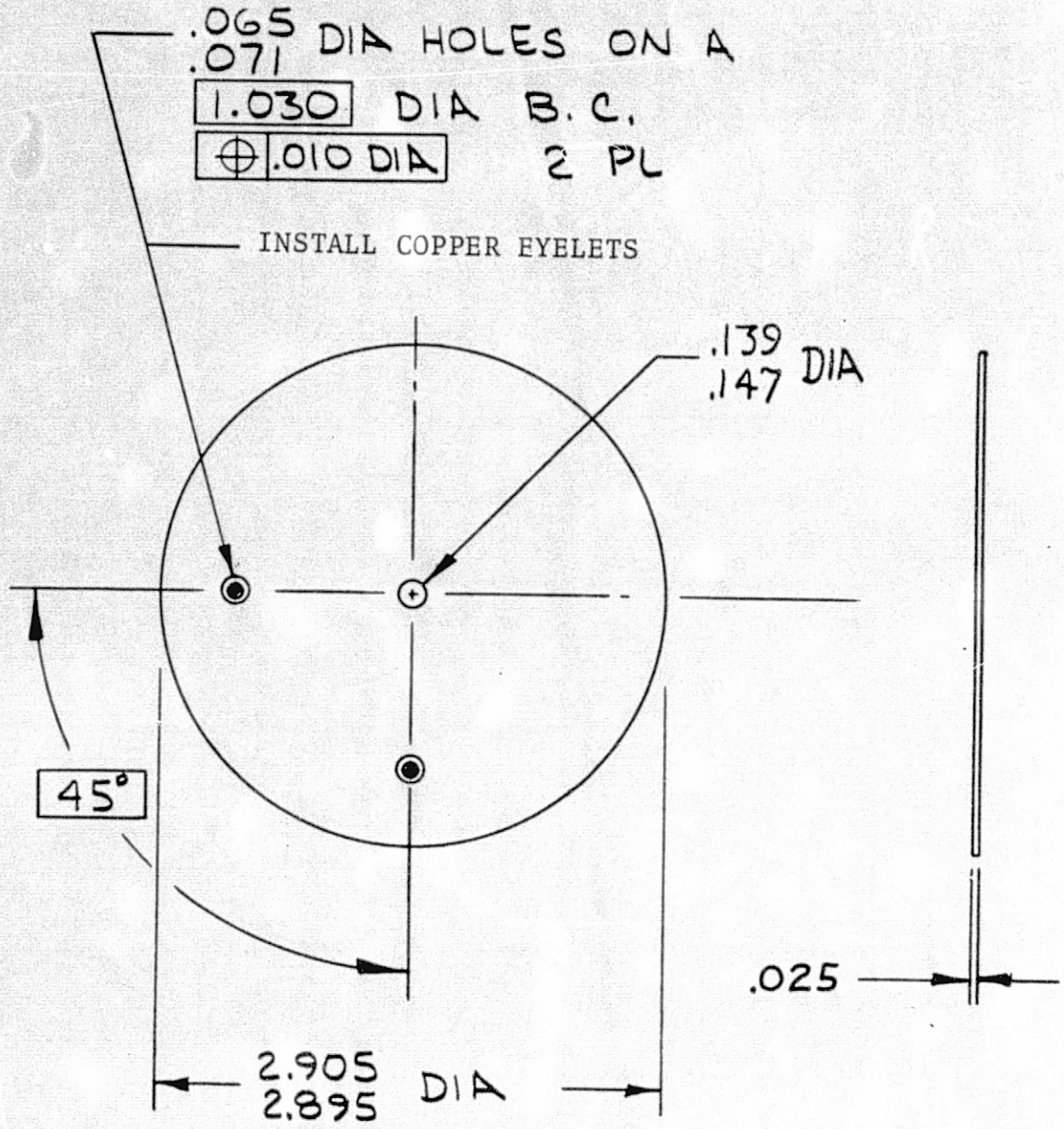

MATERIAL: Aluminum

Figure C-2 Radiating Element

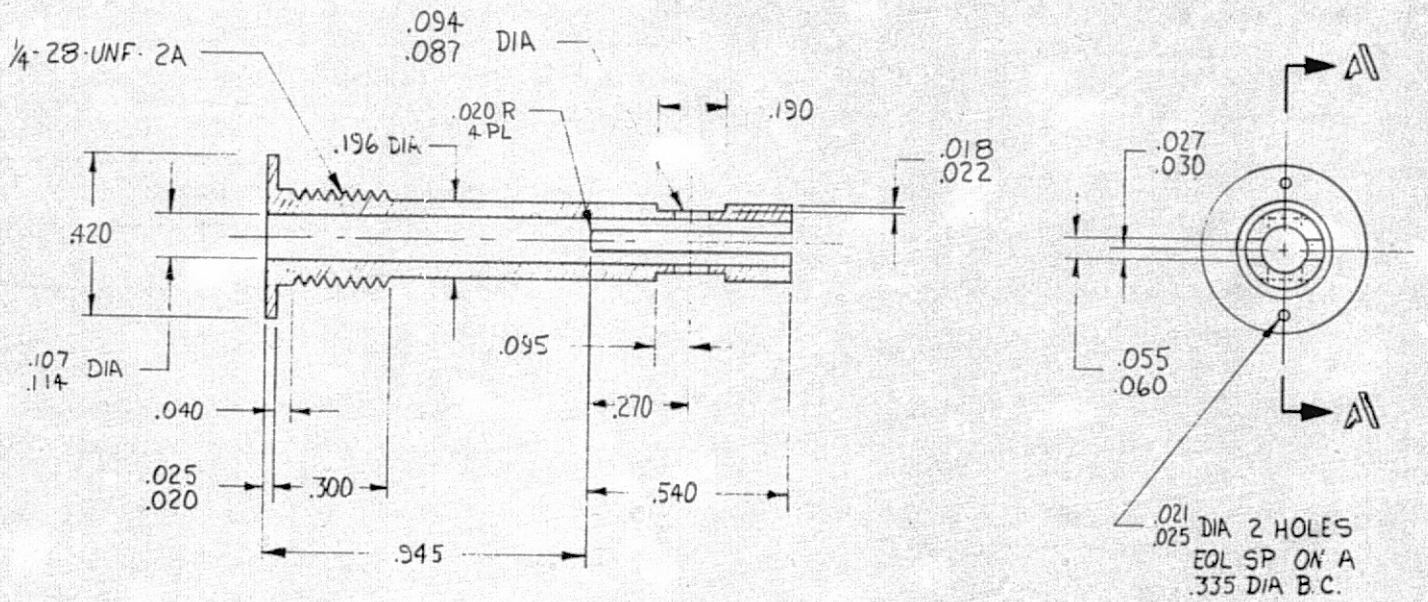

SECTION A-A

MATERIAL: Aluminum

Figure C-3 70Ω Transformer Housing

REPRODUCIBILITY OF THE ORIGINAL PAGE IS POOR

REPRODUCIBILITY OF THE
ORIGINAL PAGE IS POOR

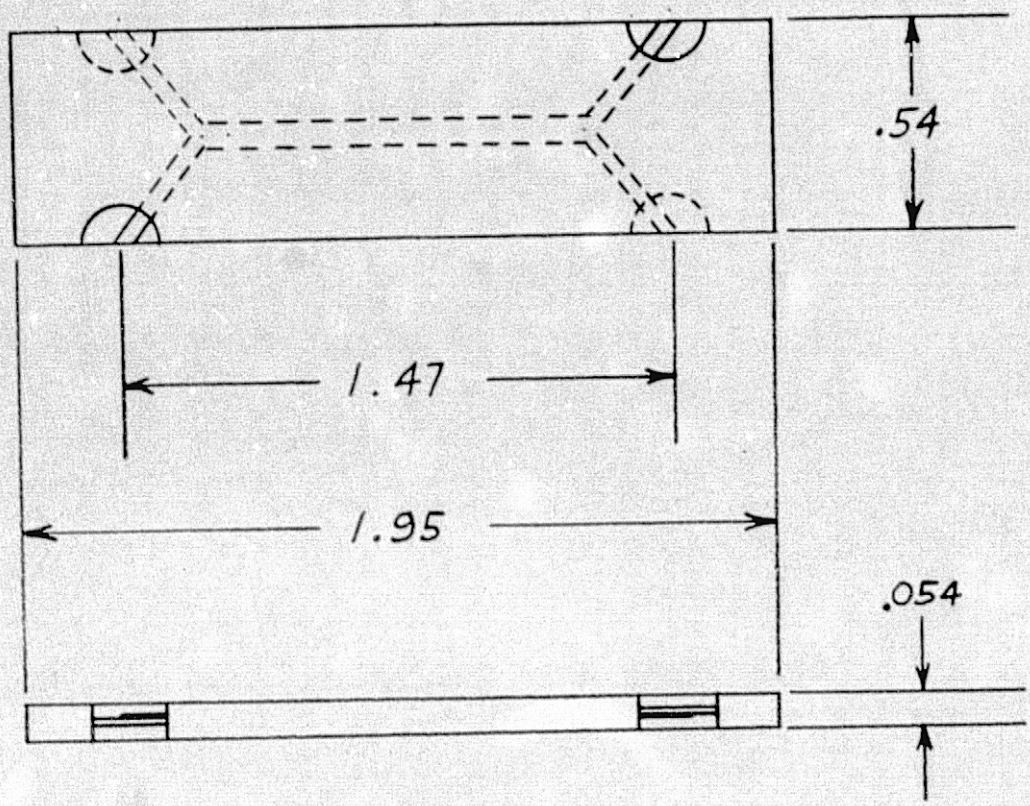

Coupler consists of three dielectric layers (Rogers Duroid 5880) laminated together.

1) .020 thick with ground plane
2) .005 thick photo etched both sides
3) .020 thick with ground plane

Completed assembly is wrapped with embossed copper foil (3M Scotch Brand #1245). Overlap seam is soldered

Figure C-4 3 dB Stripline Quadrature Hybrid

MATERIAL: Magnesium

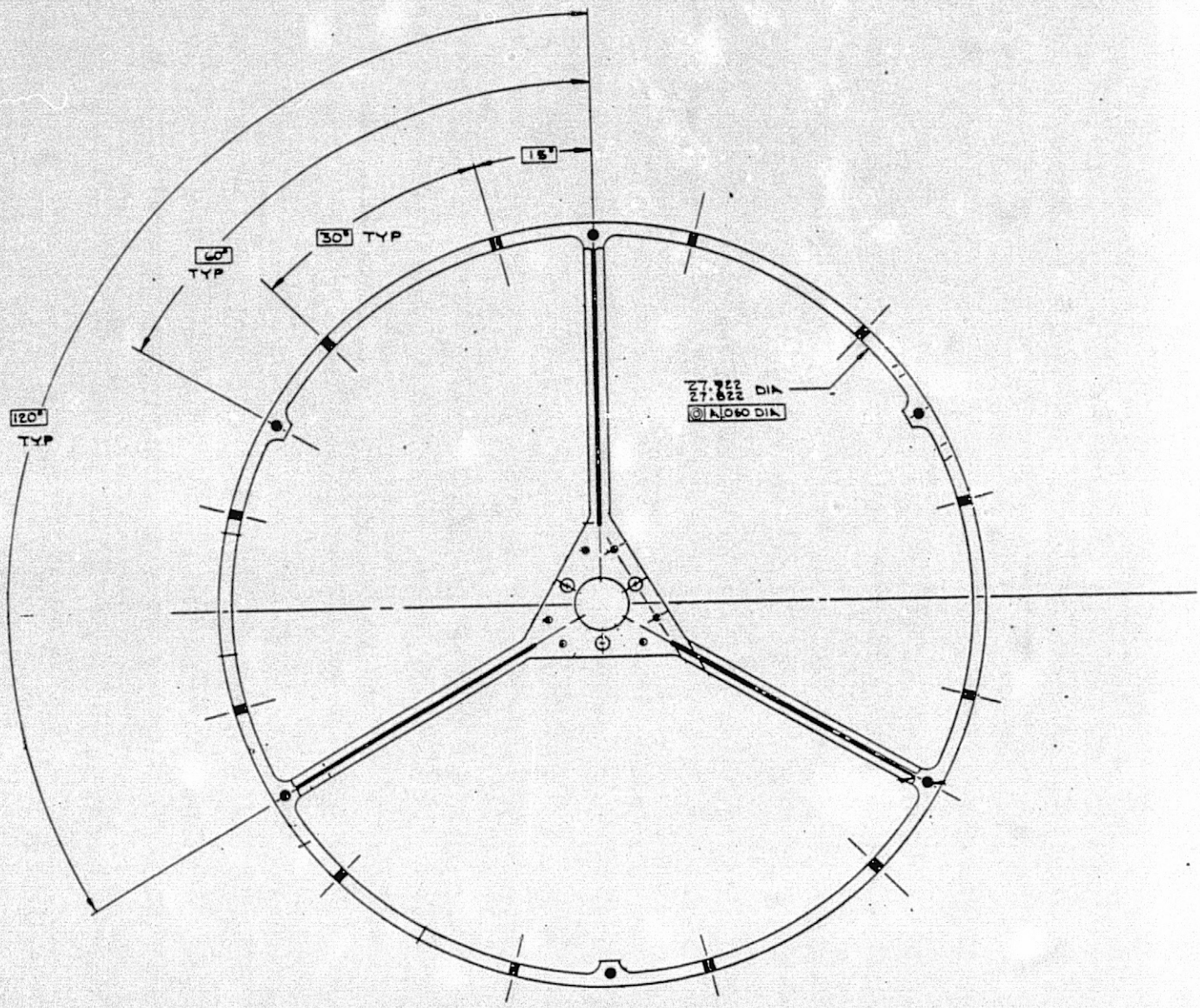

Figure C-5 Peripheral Stiffening Ring

Appendix D

BEAM POSITIONS

BEAM	POSITION θ	(DEGREES) φ	BEAM	POSITION θ	(DEGREES) φ
000	76.5	86	020	76.5	280
001		92	021		286
002		99	022		292
003		106	023		298
004		112	024		302
005		118	025		308
006		124	026		315
007		131	027		322
008		136	028		328
009		142	029		334
00A		148	02A		340
00B		154	02B		347
00C		159	02C		352
00D		164	02D		358
00E		171	02E		4
00F		178	02F		10
010		184	030		14
011		190	031		20
012		196	032		27
013		203	033		34
014		208	034		40
015		214	035		46
016		220	036		52
017		226	037		59
018		230	038		64
019		236	039		70
01A		243	03A		76
01B		250	03B	76.5	82
01C		256	03C	73	86
01D		262	03D	73	92
01E		268	03E	73	99
01F	76.5	275	03F	73	104

BEAM	POSITION (DEGREES) θ	φ	BEAM	POSITION (DEGREES) θ	φ
040	73	111	060	73	302
041		117	061		308
042		123	062		315
043		129	063		320
044		135	064		327
045		141	065		333
046		147	066		339
047		153	067		345
048		158	068		351
049		164	069		357
04A		171	06A		3
04B		176	06B		9
04C		183	06C		14
04D		189	06D		20
04E		195	06E		27
04F		201	06F		32
050		207	070		39
051		213	071		45
052		219	072		51
053		225	073		57
054		230	074		63
055		236	075		69
056		243	076		75
057		248	077	73	81
058		255	078	67	89
059		261	079		96
05A		267	07A		102
05B		273	07B		109
05C		279	07C		115
05D		285	07D		122
05E		291	07E		128
05F	73	297	07F	67	135

BEAM	POSITION (DEGREES) θ	φ	BEAM	POSITION (DEGREES) θ	φ
080	67	141	0A0	67	351
081		148	0A1		357
082		155	0A2		4
083		161	0A3		11
084		168	0A4		17
085		174	0A5		24
086		181	0A6		30
087		187	0A7		37
088		194	0A8		43
089		200	0A9		50
08A		207	0AA		56
08B		213	0AB		63
08C		220	0AC		69
08D		227	0AD		76
08E		233	0AE	67	83
08F		240	0AF	62.5	88
090		246	0B0		94
091		253	0B1		102
092		259	0B2		109
093		266	0B3		113
094		272	0B4		120
095		280	0B5		126
096		285	0B6		134
097		292	0B7		140
098		299	0B8		145
099		305	0B9		153
09A		312	0BA		160
09B		318	0BB		166
09C		325	0BC		174
09D		331	0BD		181
09E		338	0BE		185
09F	67	344	0BF	62.5	191

BEAM	POSITION (DEGREES) θ	φ	BEAM	POSITION (DEGREES) θ	φ
0C0	62.5	198	0E0	62.5	47
0C1		206	0E1		54
0C2		212	0E2		62
0C3		217	0E3		68
0C4		225	0E4		73
0C5		232	0E5	62.5	81
0C6		238	0E6	56	93
0C7		246	0E7		101
0C8		253	0E8		107
0C9		257	0E9		115
0CA		263	0EA		122
0CB		270	0EB		128
0CC		278	0EC		136
0CD		284	0ED		142
0CE		289	0EE		149
0CF		297	0EF		157
0D0		304	0F0		165
0D1		310	0F1		173
0D2		318	0F2		179
0D3		325	0F3		187
0D4		329	0F4		194
0D5		335	0F5		200
0D6		342	0F6		208
0D7		350	0F7		214
0D8		356	0F8		221
0D9		1	0F9		229
0DA		9	0FA		237
0DB		16	0FB		245
0DC		22	0FC		251
0DD		30	0FD		259
0DE		37	0FE		266
0DF	62.5	41	0FF	56	272

BEAM	POSITION θ	(DEGREES) φ	BEAM	POSITION θ	(DEGREES) φ
100	56	280	120	50	149
101		286	121		157
102		293	122		165
103		301	123		171
104		309	124		180
105		317	125		185
106		323	126		194
107		331	127		201
108		338	128		209
109		344	129		215
10A		352	12A		221
10B		358	12B		229
10C		5	12C		237
10D		13	12D		244
10E		21	12E		252
10F		29	12F		257
110		35	130		266
111		43	131		273
112		50	132		281
113		56	133		287
114		64	134		293
115		70	135		301
116		77	136		309
117	56	85	137		315
118	50	93	138		324
119		99	139		329
11A		108	13A		338
11B		113	13B		345
11C		122	13C		353
11D		129	13D		359
11E		137	13E		5
11F	50	143	13F	50	13

BEAM	POSITION θ	(DEGREES) φ
140	50	21
141		27
142		36
143		41
144		50
145		57
146		65
147		71
148		77
149	50	85
14A	45	86
14B		94
14C		101
14D		113
14E		120
14F		126
150		134
151		143
152		150
153		158
154		166
155		173
156		185
157		192
158		198
159		206
15A		215
15B		223
15C		230
15D		238
15E		245
15F	45	257

BEAM	POSITION θ	(DEGREES) φ
160	45	264
161		270
162		278
163		287
164		295
165		302
166		310
167		317
168		329
169		336
16A		343
16B		350
16C		359
16D		6
16E		14
16F		22
170		29
171		41
172		48
173		54
174		62
175		71
176	45	78
177	39	86
178		95
179		103
17A		113
17B		121
17C		131
17D		139
17E		148
17F	39	157

BEAM	POSITION (DEGREES) θ	ϕ	BEAM	POSITION (DEGREES) θ	ϕ
180	39	167	1A0	33	112
181		175	1A1		122
182		185	1A2		132
183		193	1A3		144
184		203	1A4		154
185		211	1A5		163
186		220	1A6		174
187		229	1A7		184
188		239	1A8		194
189		247	1A9		204
18A		257	1AA		216
18B		265	1AB		226
18C		275	1AC		235
18D		283	1AD		246
18E		292	1AE		256
18F		301	1AF		266
190		311	1B0		276
191		320	1B1		288
192		329	1B2		298
193		337	1B3		307
194		347	1B4		318
195		356	1B5		328
196		4	1B6		338
197		13	1B7		348
198		23	1B8		0
199		31	1B9		10
19A		41	1BA		19
19B		49	1BB		30
19C		59	1BC		40
19D		67	1BD		50
19E	39	76	1BE		60
19F	33	102	1BF	33	72

BEAM	POSITION (DEGREES) θ	φ	BEAM	POSITION (DEGREES) θ	φ
1C0	33	82	1E0	22	100
1C1	33	91	1E1		116
1C2	27	100	1E2		128
1C3		112	1E3		145
1C4		125	1E4		156
1C5		134	1E5		172
1C6		149	1E6		188
1C7		160	1E7		200
1C8		172	1E8		217
1C9		184	1E9		228
1CA		197	1EA		244
1CB		206	1EB		260
1CC		221	1EC		272
1CD		232	1ED		289
1CE		244	1EE		300
1CF		256	1EF		316
1D0		269	1F0		332
1D1		278	1F1		344
1D2		293	1F2		1
1D3		304	1F3		12
1D4		316	1F4		28
1D5		328	1F5		44
1D6		341	1F6		56
1D7		351	1F7		73
1D8		5	1F8	22	84
1D9		16	1F9	17	85
1DA		28	1FA		104
1DB		39	1FB		121
1DC		53	1FC		139
1DD		62	1FD		157
1DE		77	1FE		176
1DF	27	88	1FF	17	193

BEAM	POSITION (DEGREES) θ	ϕ	BEAM	POSITION (DEGREES) θ	ϕ
200	17	211	220	6.5	237
201		229	221		272
202		248	222		309
203		265	223		344
204		283	224		21
205		301	225	6.5	56
206		320	226	0	94
207		337			
208		355			
209		13			
20A		32			
20B		49			
20C	17	67			
20D	11	93			
20E		117			
20F		135			
210		165			
211		189			
212		207			
213		237			
214		261			
215		279			
216		309			
217		333			
218		351			
219		21			
21A		45			
21B	11	63			
21C	6.5	93			
21D	6.5	128			
21E	6.5	165			
21F	6.5	200			

APPENDIX E

Controller Schematics

FOLDOUT FRAME

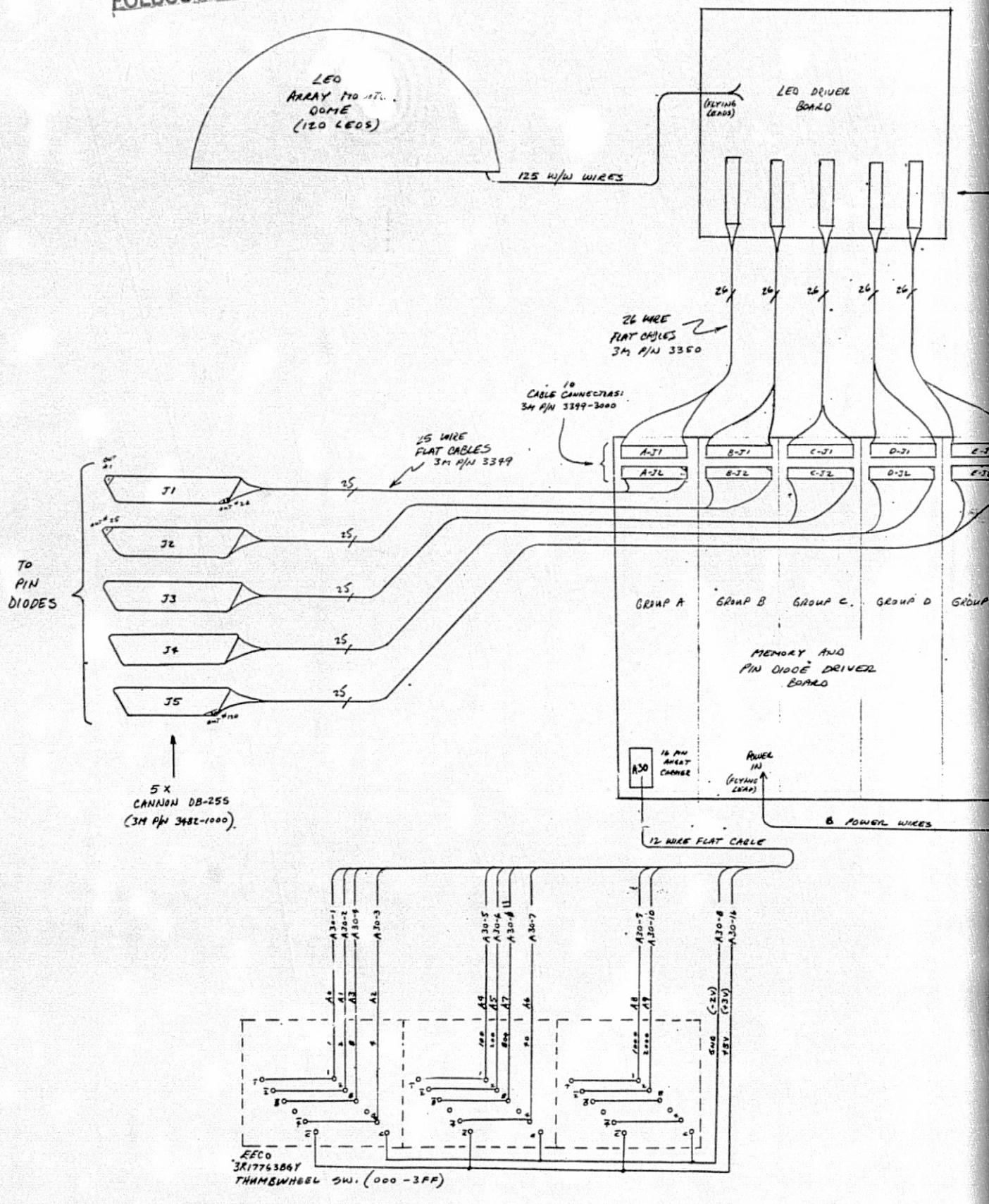

REPRODUCIBILITY OF THE ORIGINAL PAGE IS POOR

EOLDOUT FRAME L

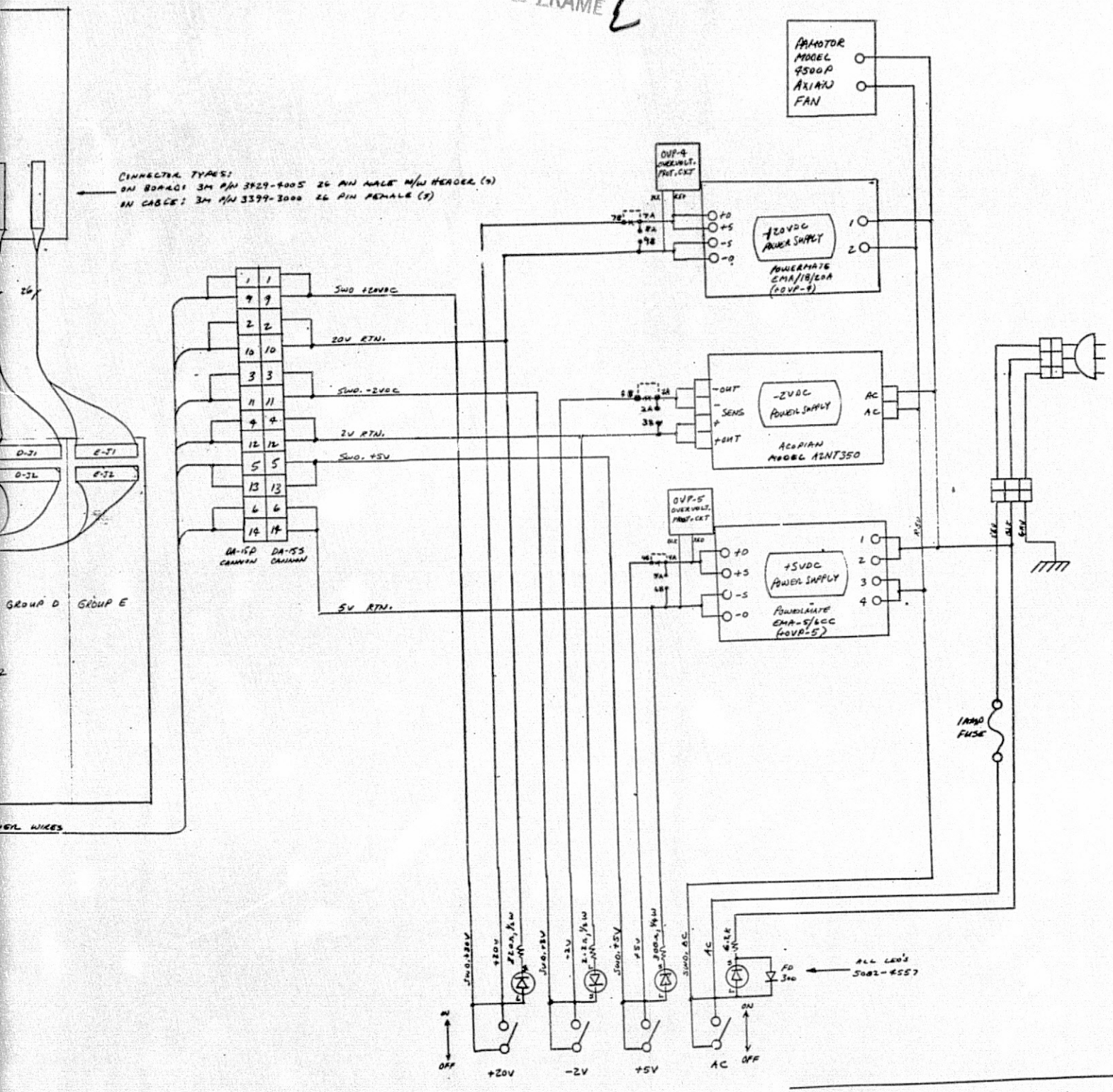

REPRODUCIBILITY OF THE ORIGINAL PAGE IS POOR

Ball

HEMI-SPHERICAL COVERAGE MEDIUM GAIN ANTENNA CONTROLLER DEMONSTRATOR SUITCASE WIRING

L. WEBB

11-3-76

FOLDOUT FRAME

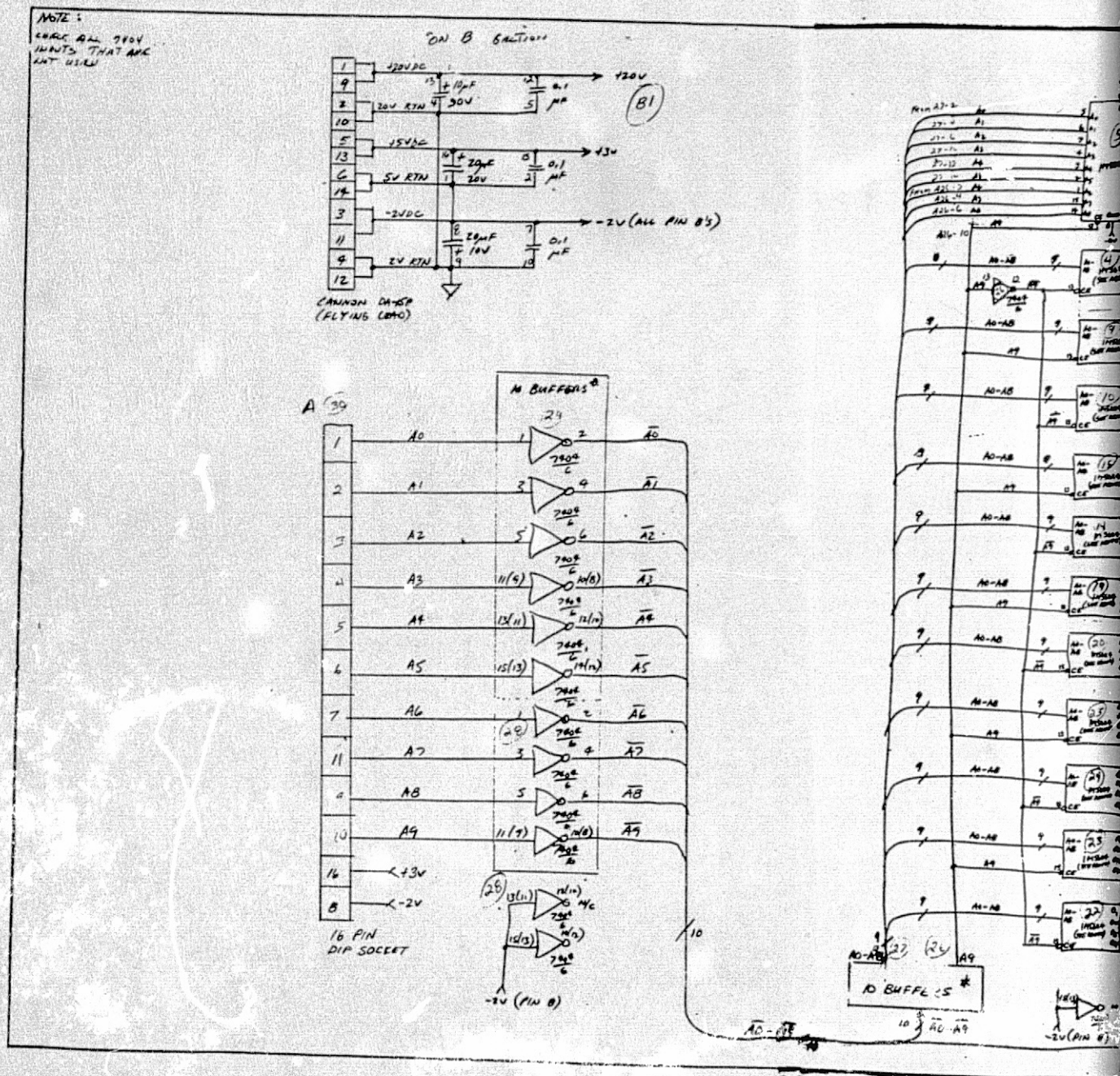

REPRODUCIBILITY OF THE ORIGINAL PAGE IS POOR

FOLDOUT FRAME

2

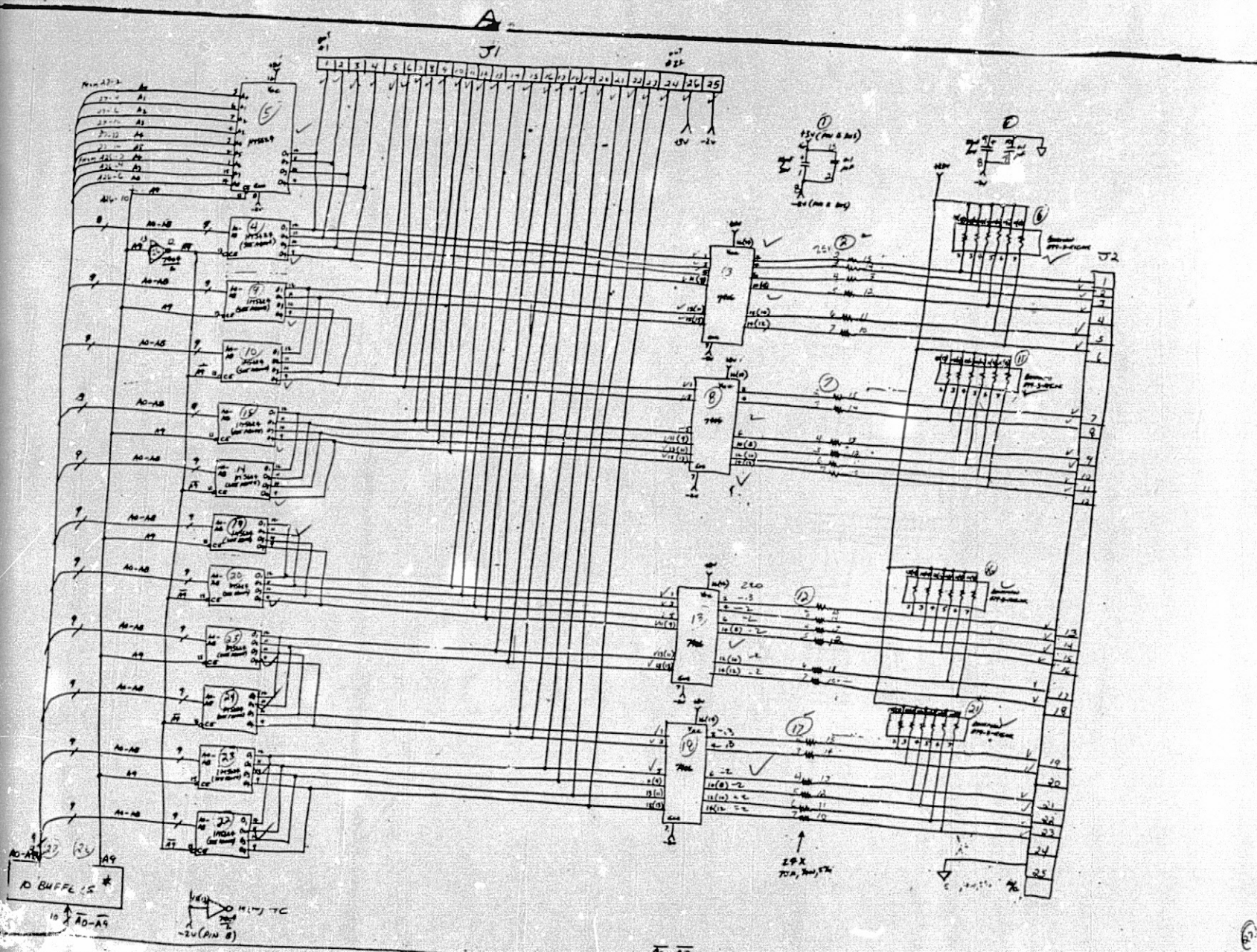

REPRODUCIBILITY OF THE
ORIGINAL PAGE IS POOR

FOLDOUT FRAME 3

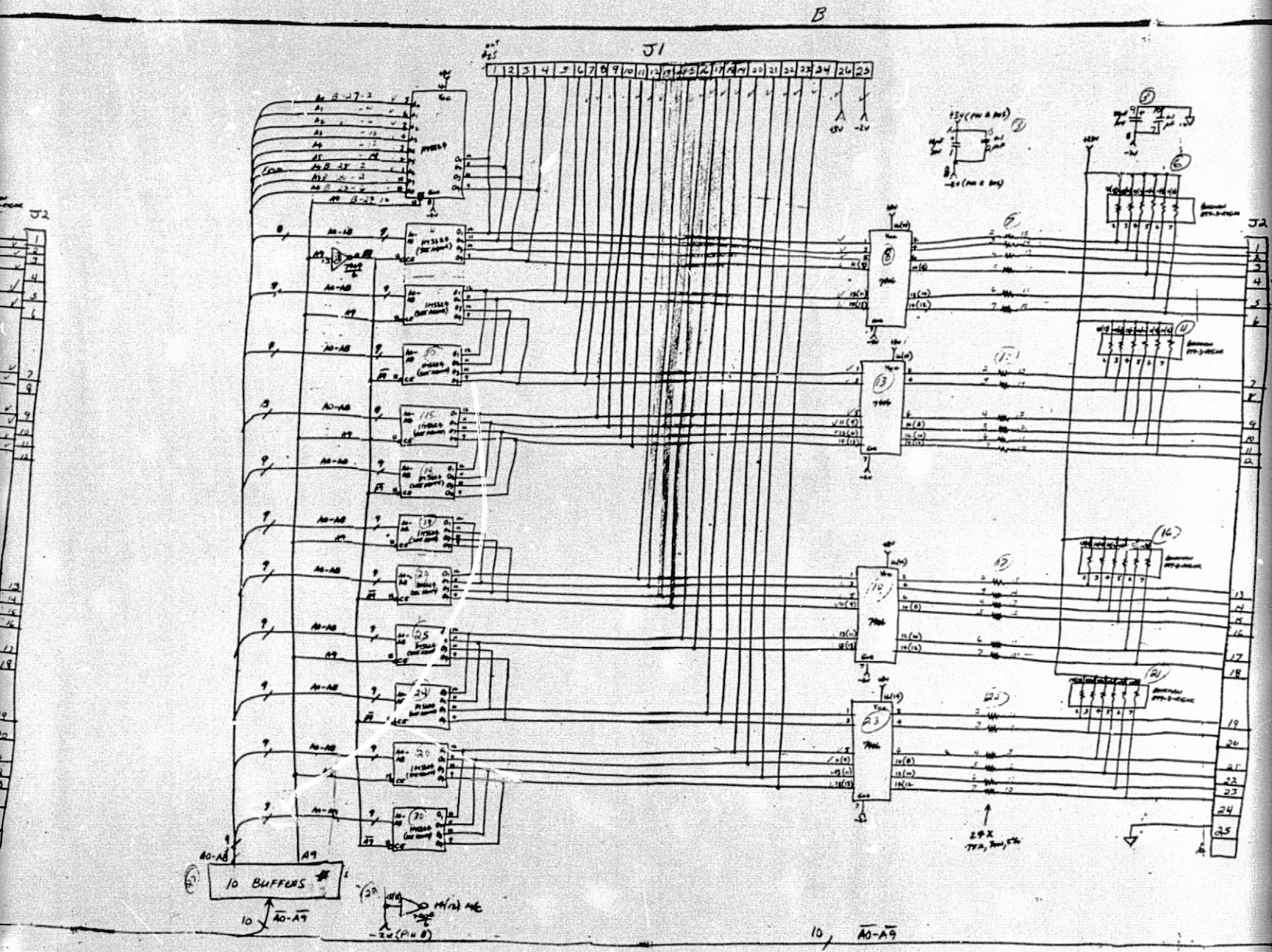

FOLDOUT FRAME 4

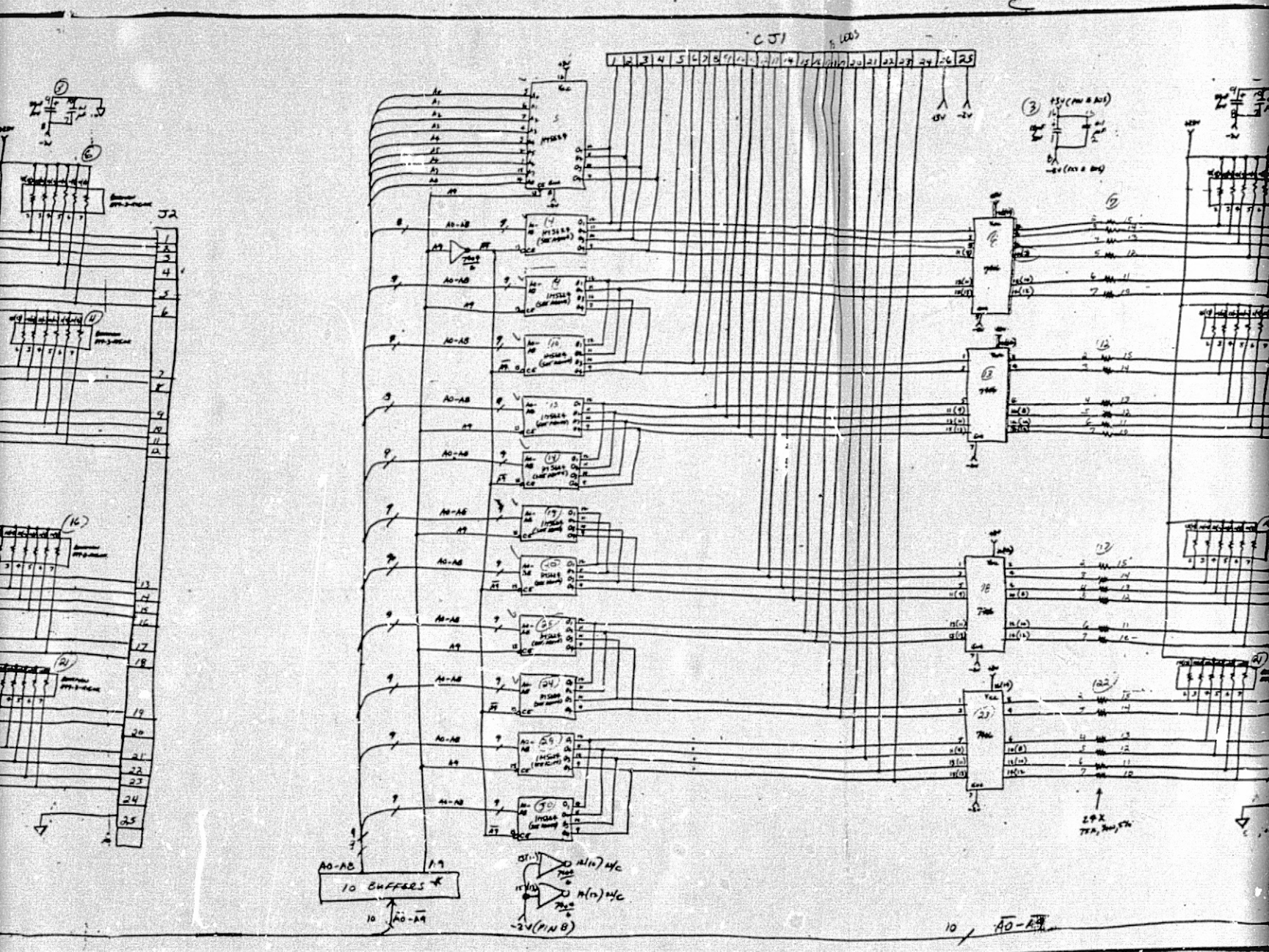

FOLDOUT FRAME 5

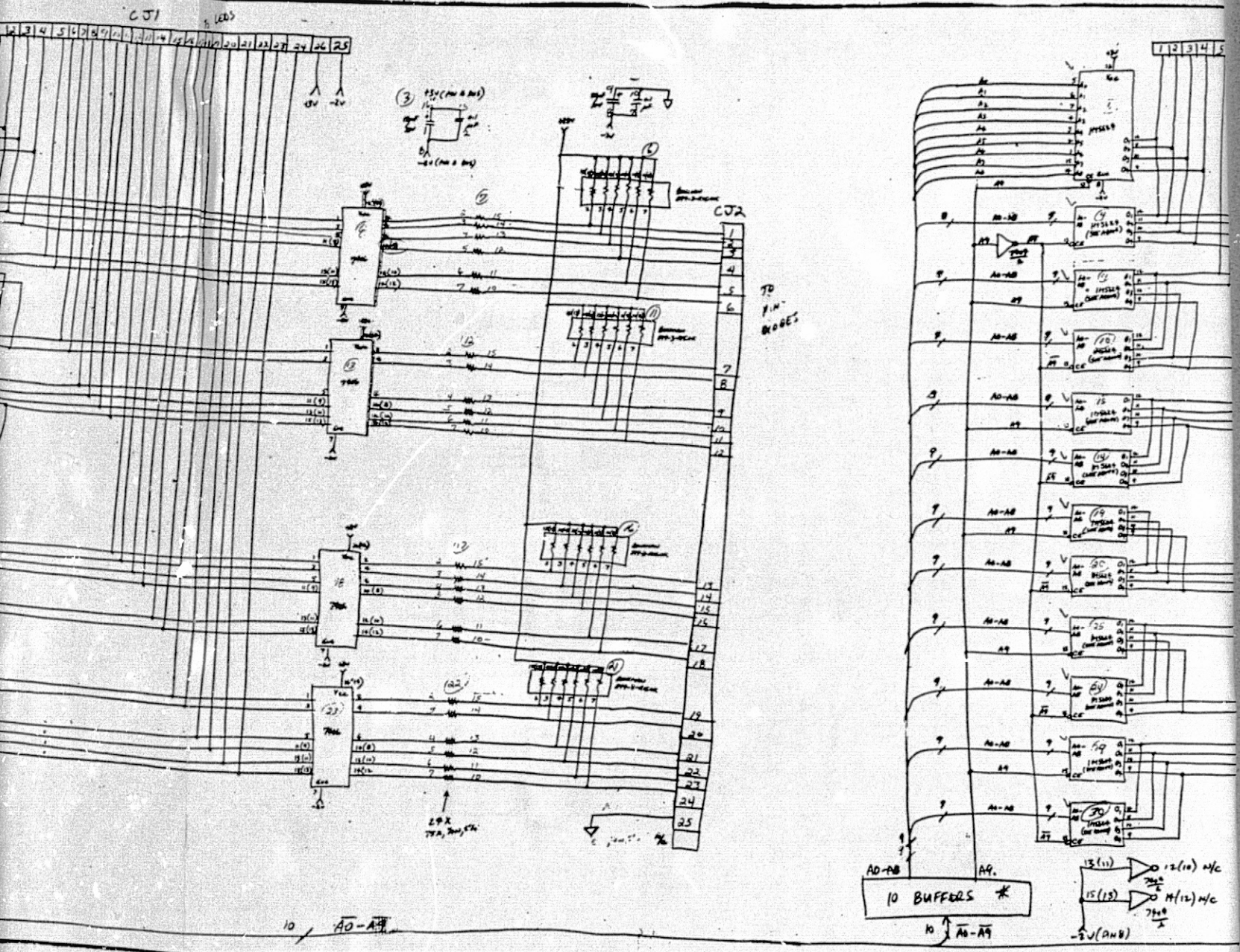

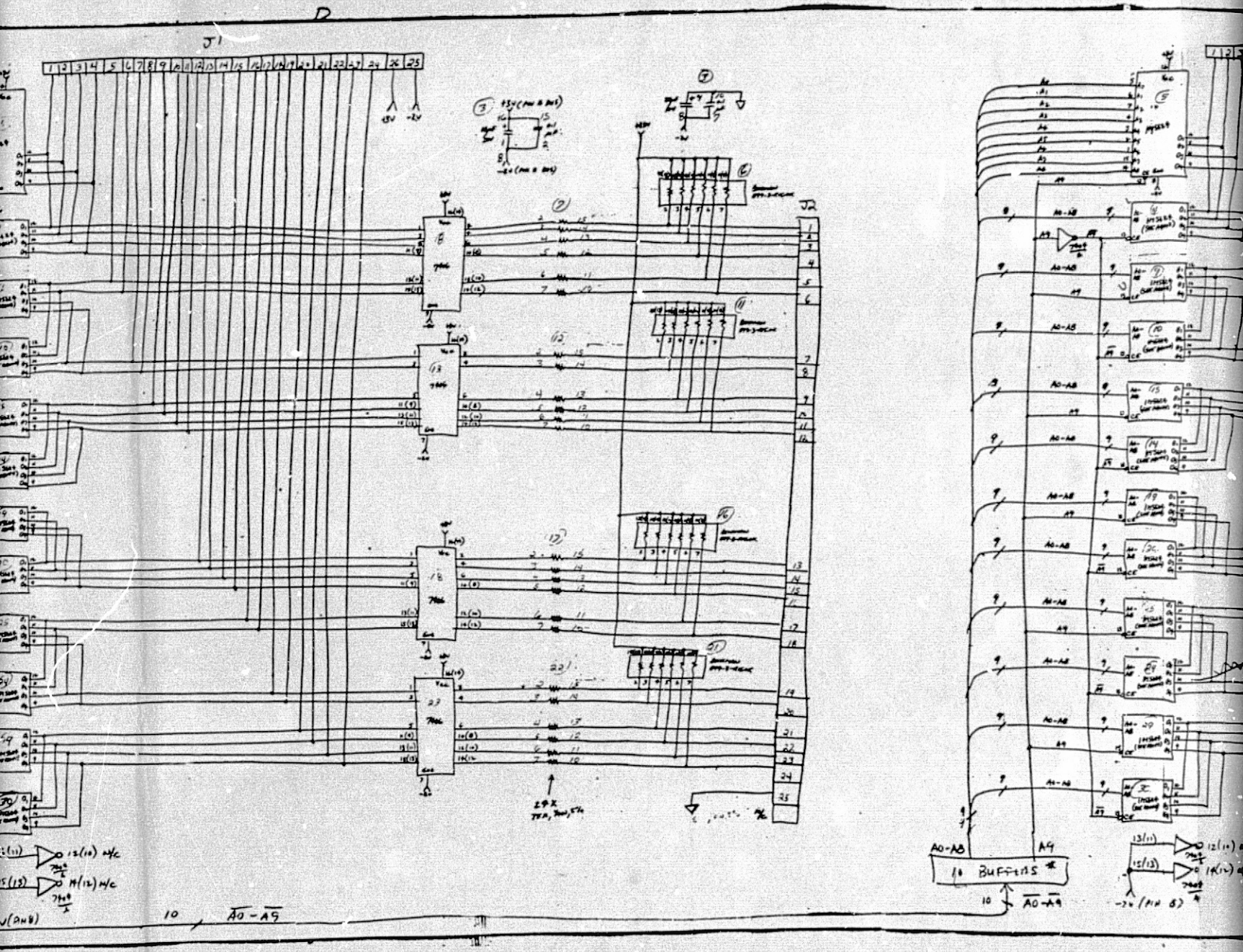
J1
J2
A0-A8
A9
10 BUFFERS
10
A0-A9
-2V (PIN 8)

FOLDOUT FRAME 2

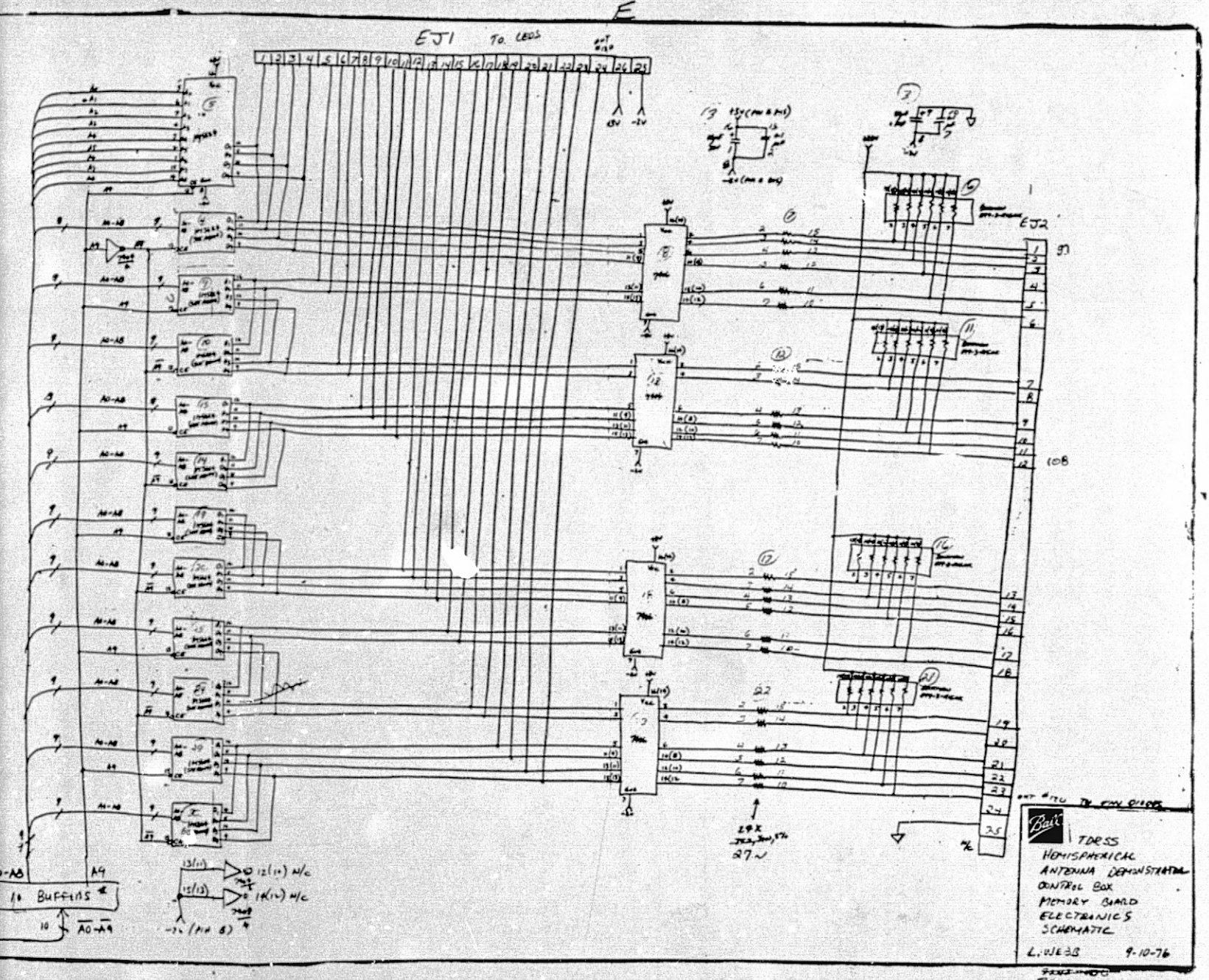

FOLDOUT FRAME

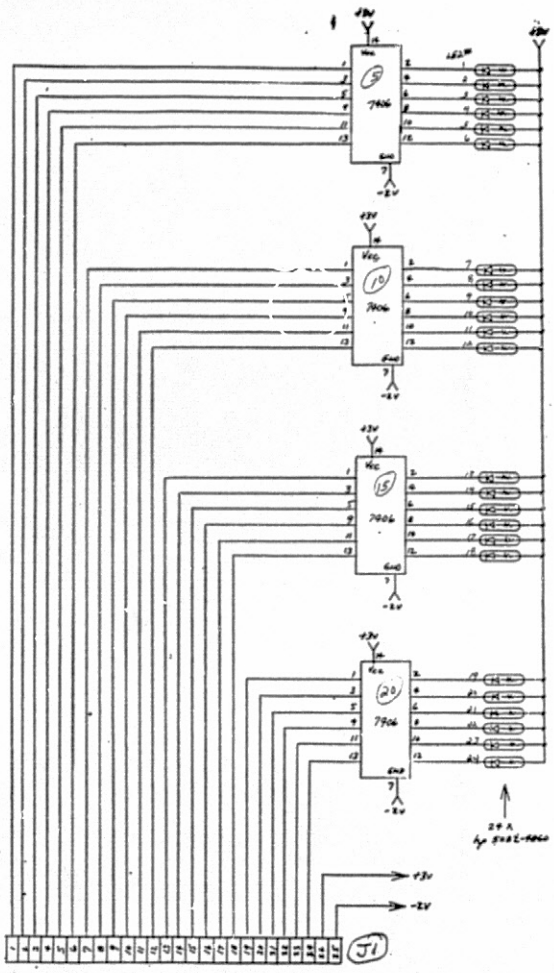

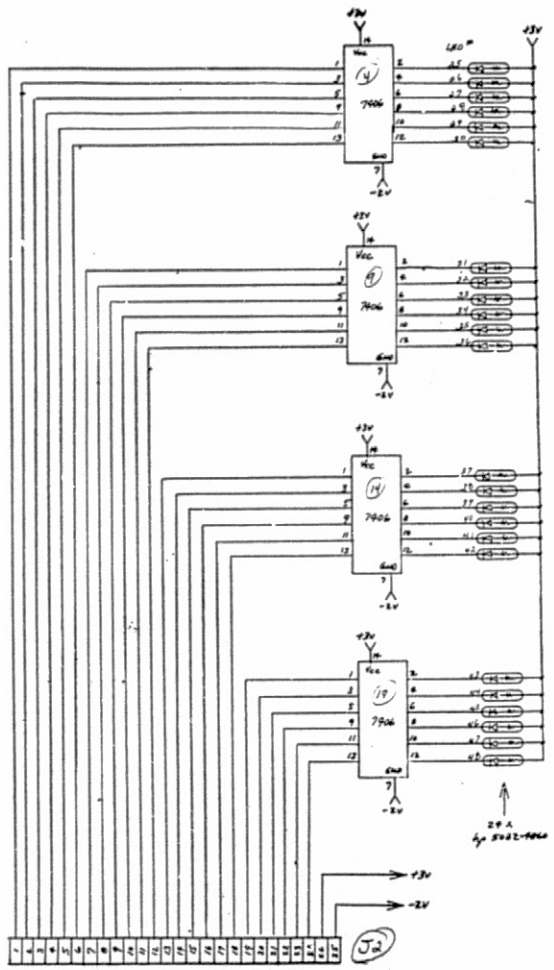

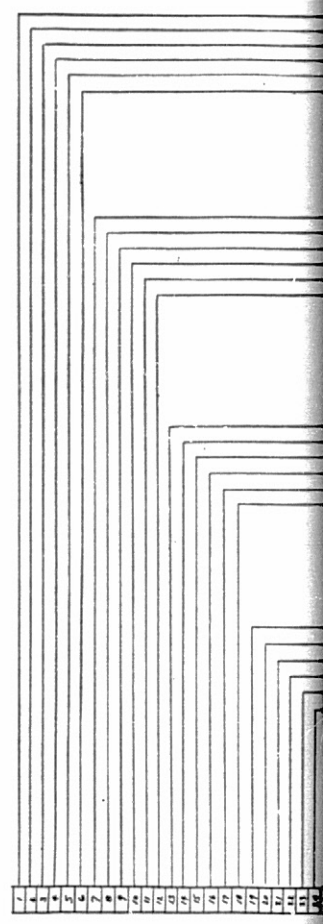

REPRODUCIBILITY OF THE
IS POOR

FOLDOUT FRAME 2

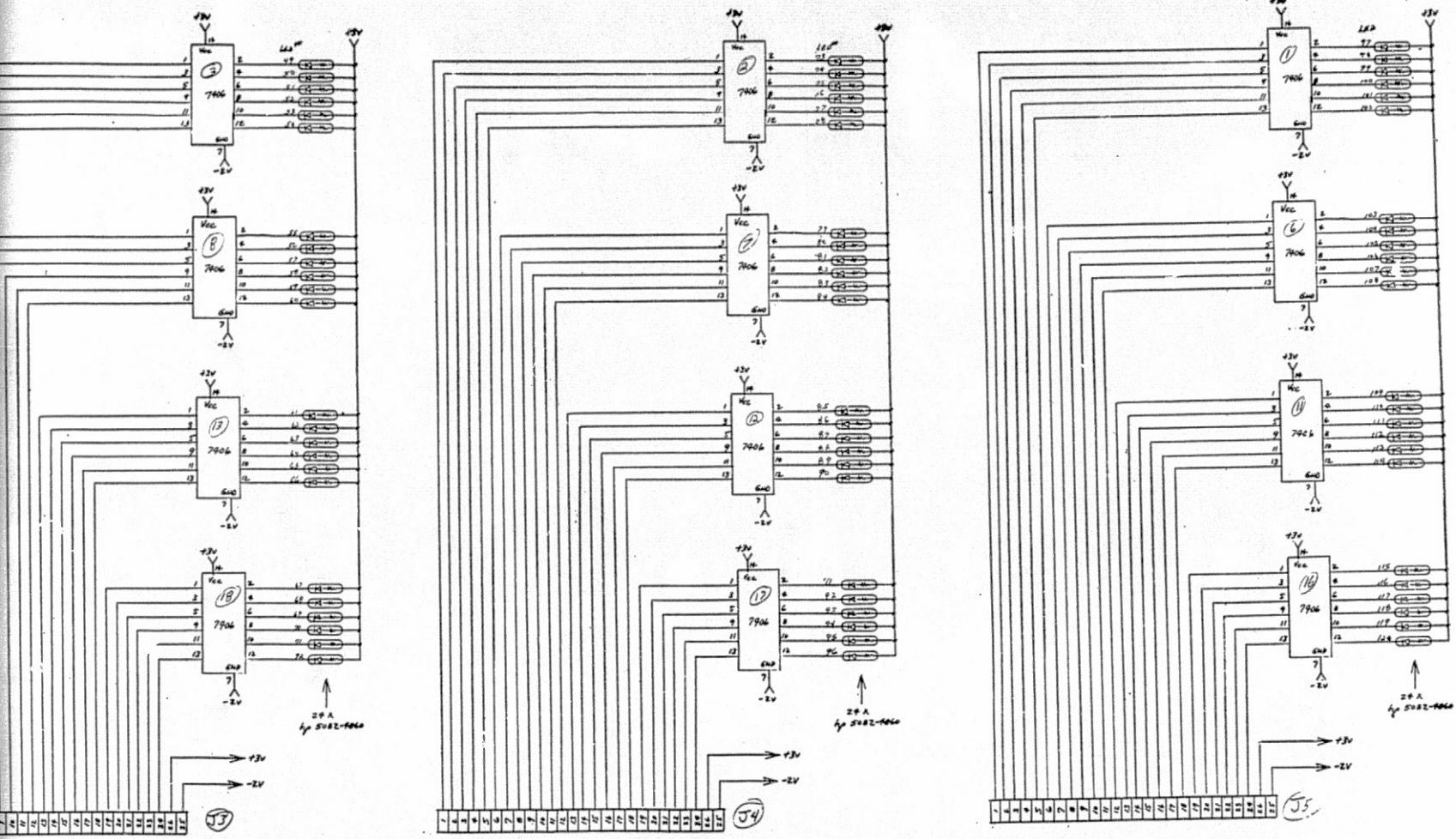

Ball

HEMISPHERICAL COVERAGE
MEDIUM GAIN ANTENNA
CONTROLLER DEMONSTRATOR
SUITCASE WIRING

L. WEBB 11-3-76

Appendix F

RADIATION DISTRIBUTION PATTERNS FOR GPS ARRAYS

FOLDOUT FRAME

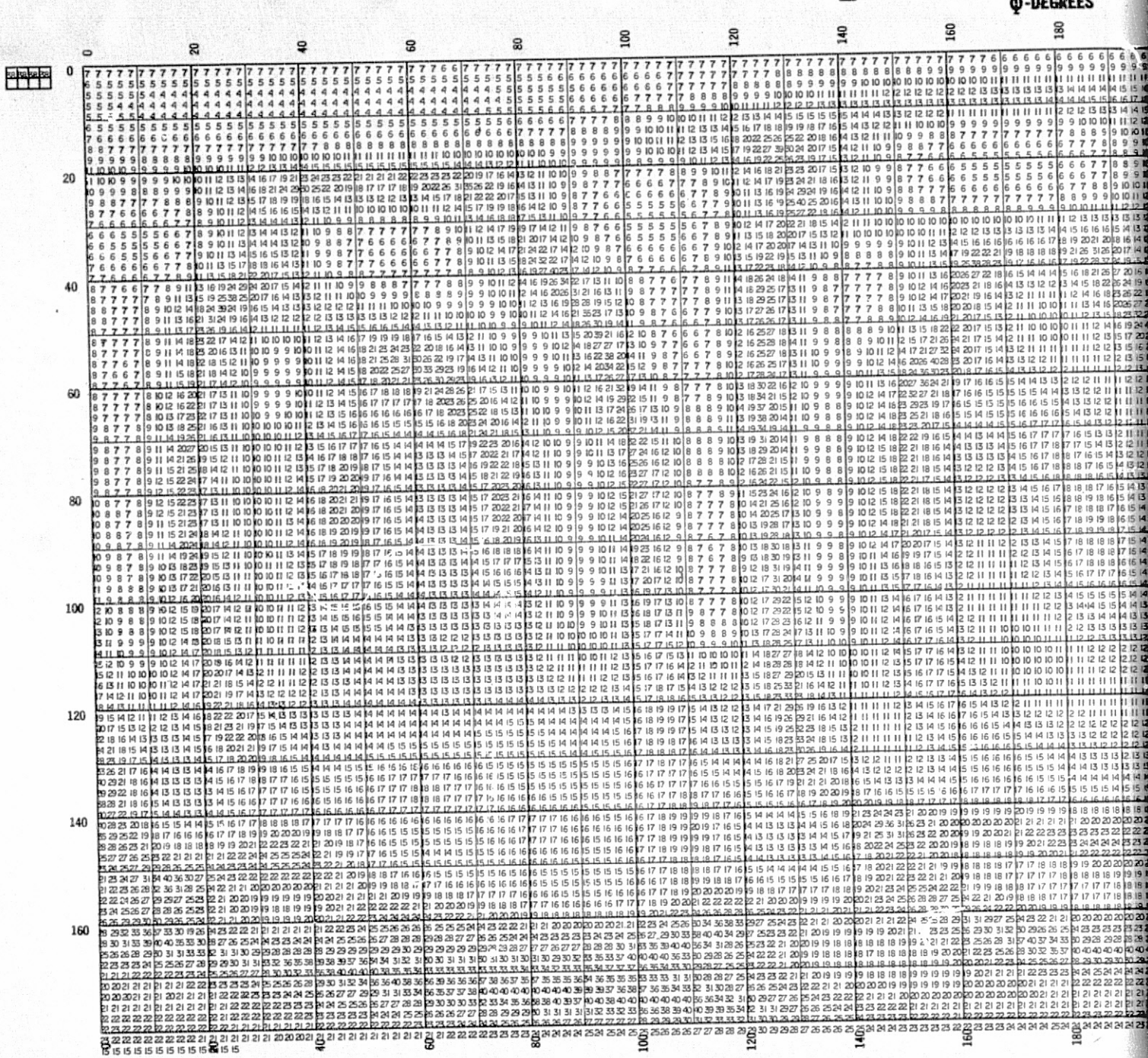

TEST PROGRAM OR VEHICLE: ESSA/GPS PROJECT: 3542

DATE: 9 AUG 77 PATTERN NO: 1 ORGANIZATION: ENGRS:

ANTENNA TYPE: 3 ELEMENT TURNSTILE ARRAY FREQ. RANGE: PATTERN MEASUREMENT FREQ: 1227 MHz.

PREDOMINANT POLARIZATION: RHC MODEL SCALE: LOCATION OF POINT Py ($\phi = 0$, $\theta = 90°$):

REPRODUCIBILITY OF THE
ORIGINAL PAGE IS POOR

FOLDOUT FRAME 2

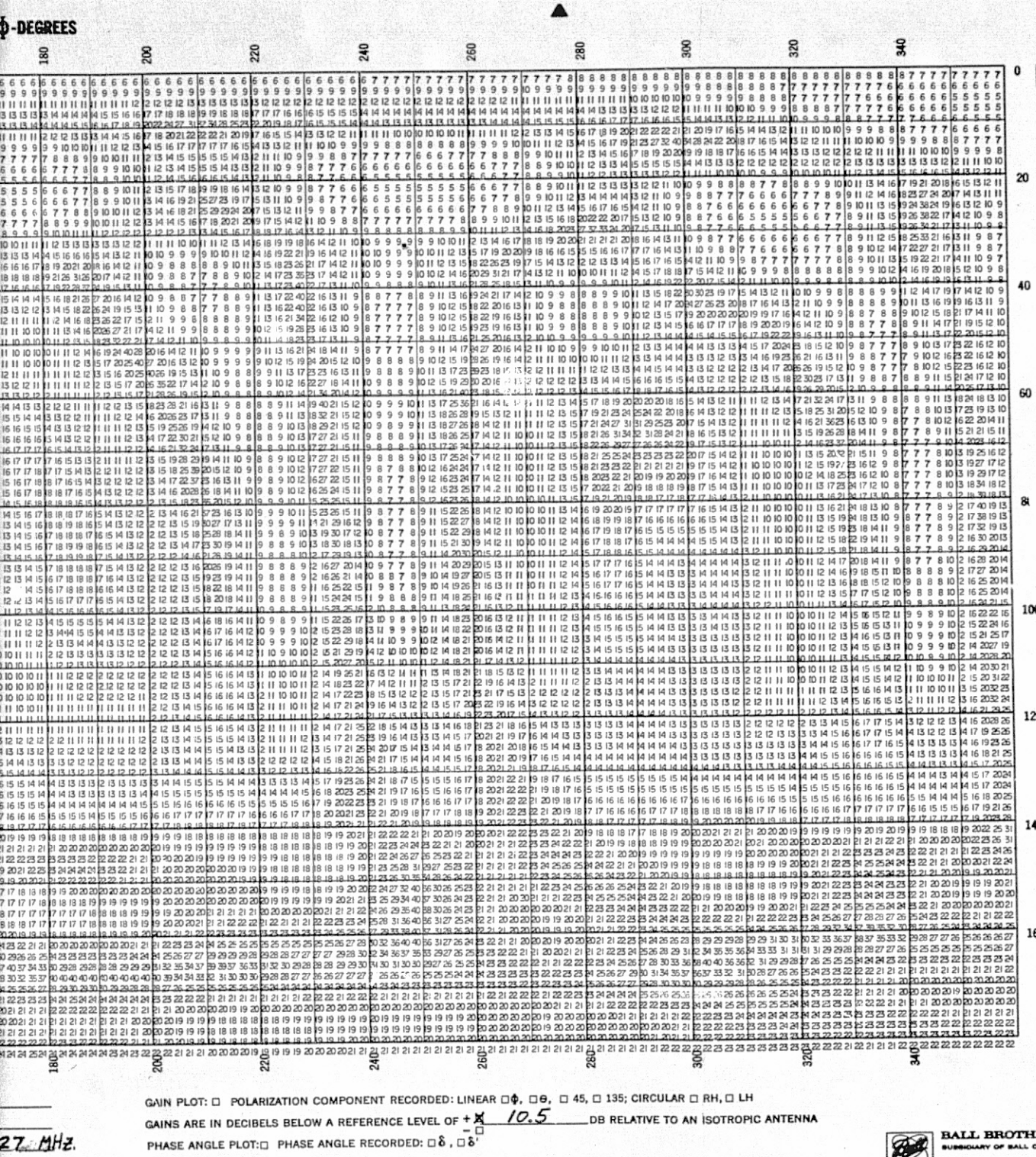

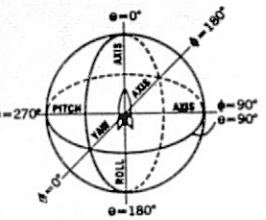

GAIN PLOT: □ POLARIZATION COMPONENT RECORDED: LINEAR □φ, □θ, □ 45, □ 135; CIRCULAR □ RH, □ LH

GAINS ARE IN DECIBELS BELOW A REFERENCE LEVEL OF + X 10.5 DB RELATIVE TO AN ISOTROPIC ANTENNA
− □

27 MHz.

PHASE ANGLE PLOT: □ PHASE ANGLE RECORDED: □δ, □δ'

PHASE ANGLES IN DEGREES ARE RECORDED VALUES MULTIPLIED BY 10.

BALL BROTHERS RESEARCH CORPORATION
SUBSIDIARY OF BALL CORPORATION
BOULDER, COLORADO

F-2

REPRODUCIBILITY OF THE
ORIGINAL PAGE IS POOR

FOLDOUT FRAME

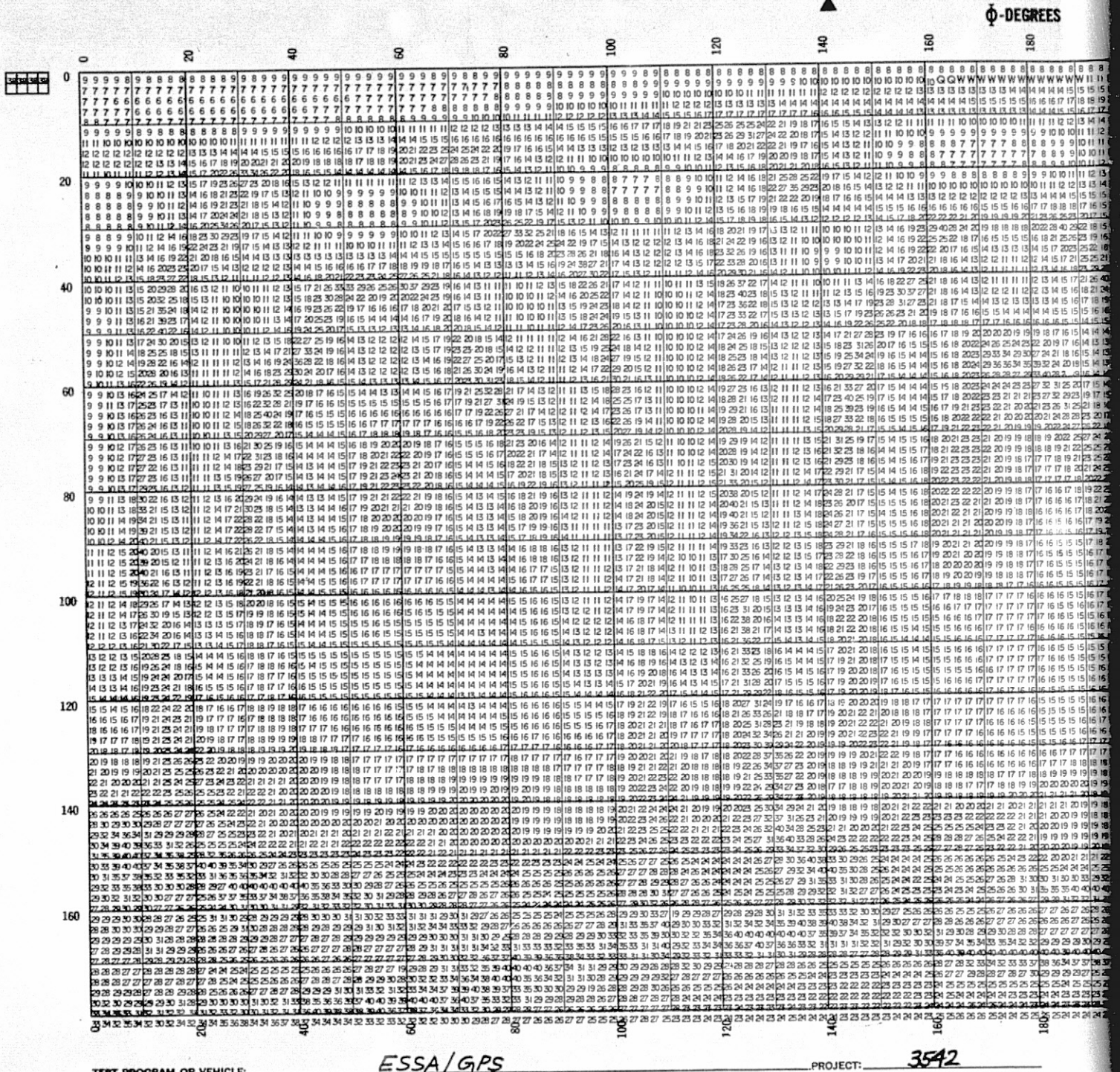

TEST PROGRAM OR VEHICLE: ESSA/GPS PROJECT: 3542

DATE: 8/10/77 PATTERN NO: 2 ORGANIZATION: ENGRS:

ANTENNA TYPE: 3 ELEMENT TURNSTILE ARRAY FREQ. RANGE: PATTERN MEASUREMENT FREQ: 1575 MHz

PREDOMINANT POLARIZATION: RHC MODEL SCALE: LOCATION OF POINT P'y (Φ=0, Θ=90°):

REPRODUCIBILITY OF THE
IS POOR

FOLDOUT FRAME 2

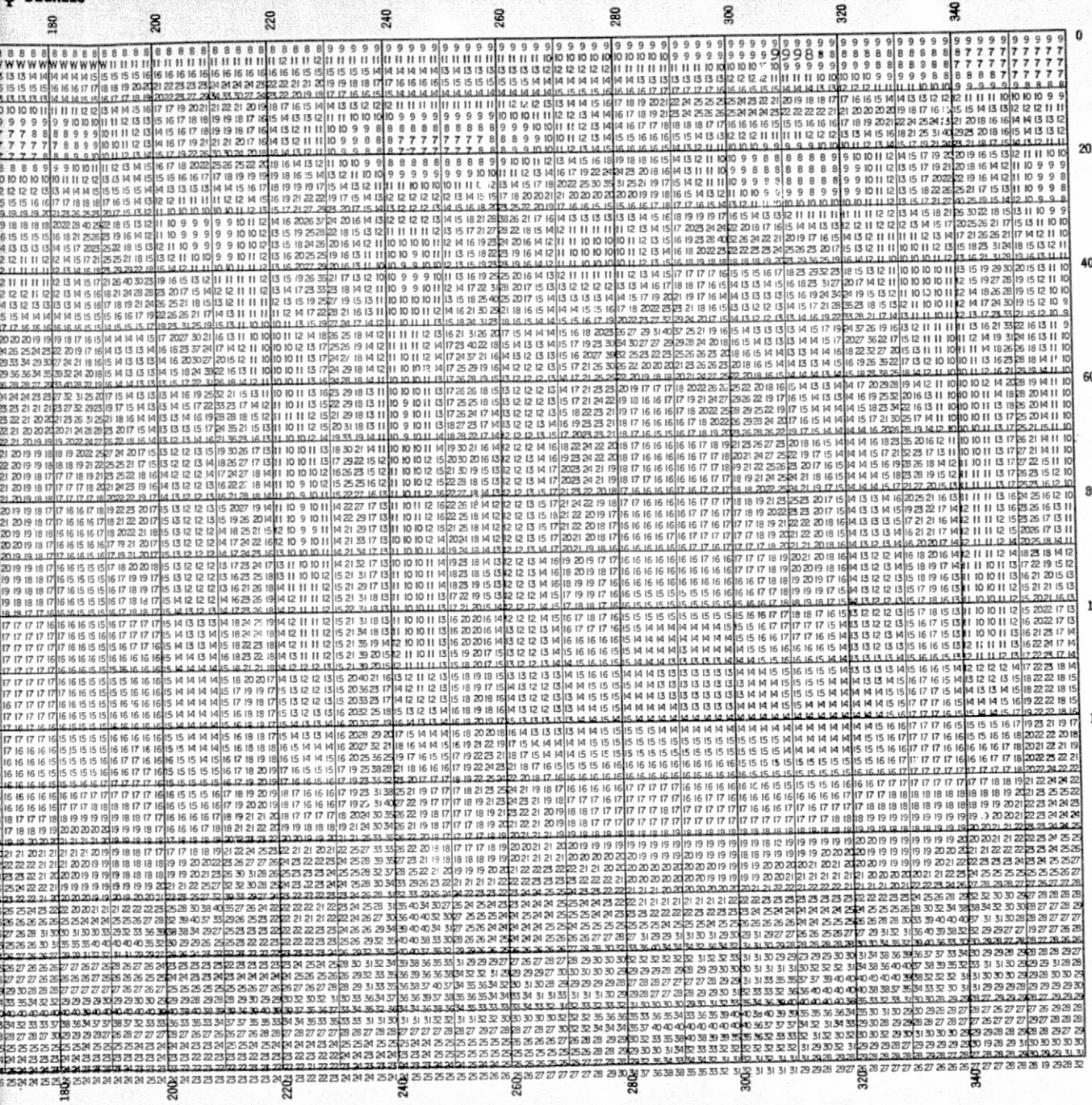

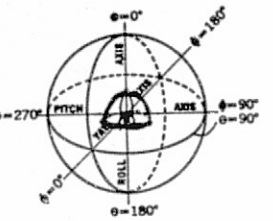

GAIN PLOT: □ POLARIZATION COMPONENT RECORDED: LINEAR □φ, □θ, □ 45, □ 135; CIRCULAR □ RH, □ LH

GAINS ARE IN DECIBELS BELOW A REFERENCE LEVEL OF + 12.0 DB RELATIVE TO AN ISOTROPIC ANTENNA

PHASE ANGLE PLOT: □ PHASE ANGLE RECORDED: □δ, □δ'

PHASE ANGLES IN DEGREES ARE RECORDED VALUES MULTIPLIED BY 10.

75 MHz

BALL BROTHERS RESEARCH CORPORATION
SUBSIDIARY OF BALL CORPORATION
BOULDER, COLORADO

F-3

FOLDOUT FRAME

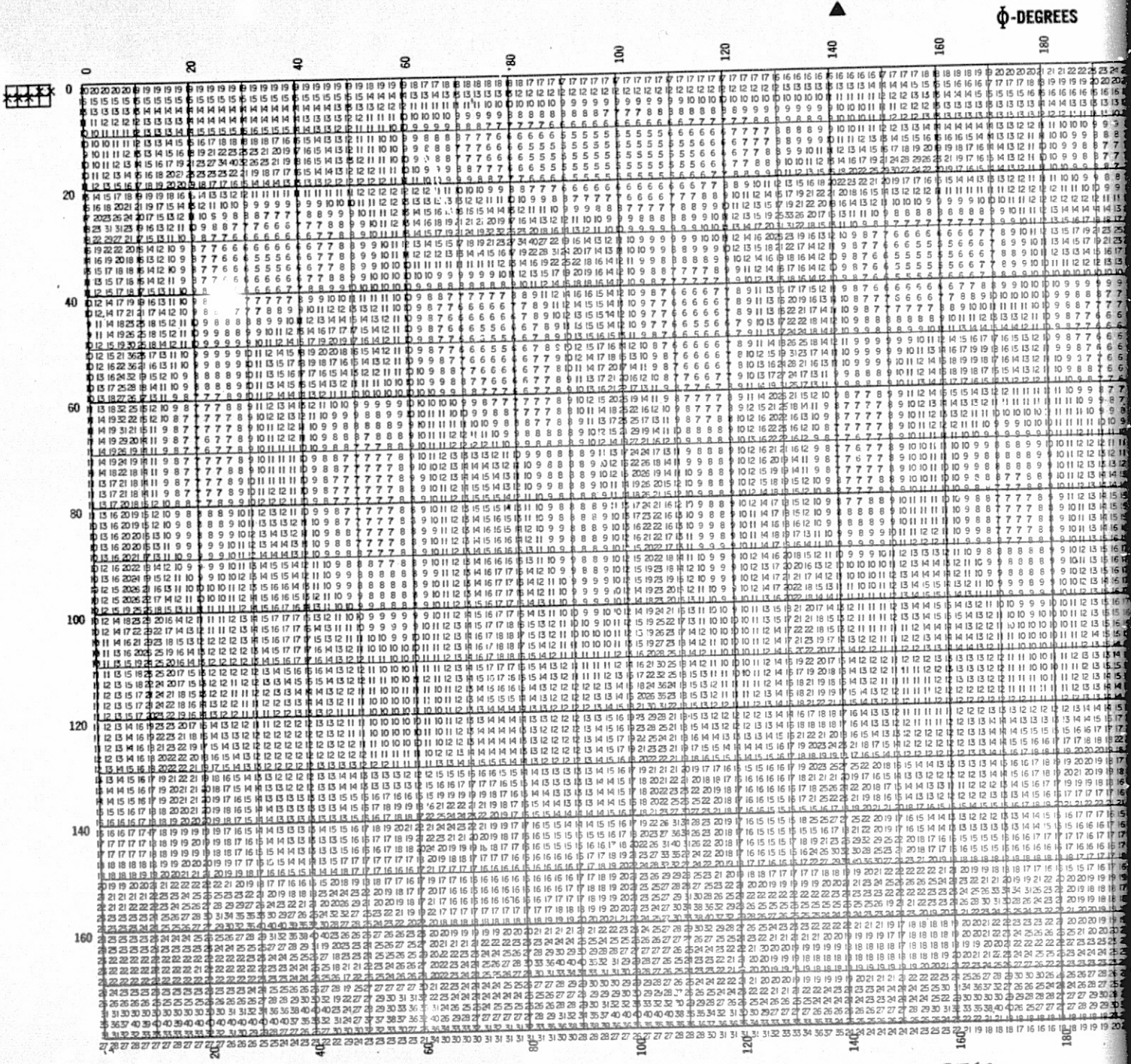

TEST PROGRAM OR VEHICLE: ESSA/GPS PROJECT: 3542

DATE: 8/12/77 PATTERN NO: 3 ORGANIZATION: ENGRS:

ANTENNA TYPE: 3 ELEMENT MICROSTRIP ARRAY FREQ. RANGE: PATTERN MEASUREMENT FREQ: 1227 MHz

PREDOMINANT POLARIZATION: RHC MODEL SCALE: LOCATION OF POINT P'y (Φ=0, Θ=90°):

FOLDOUT FRAME 2

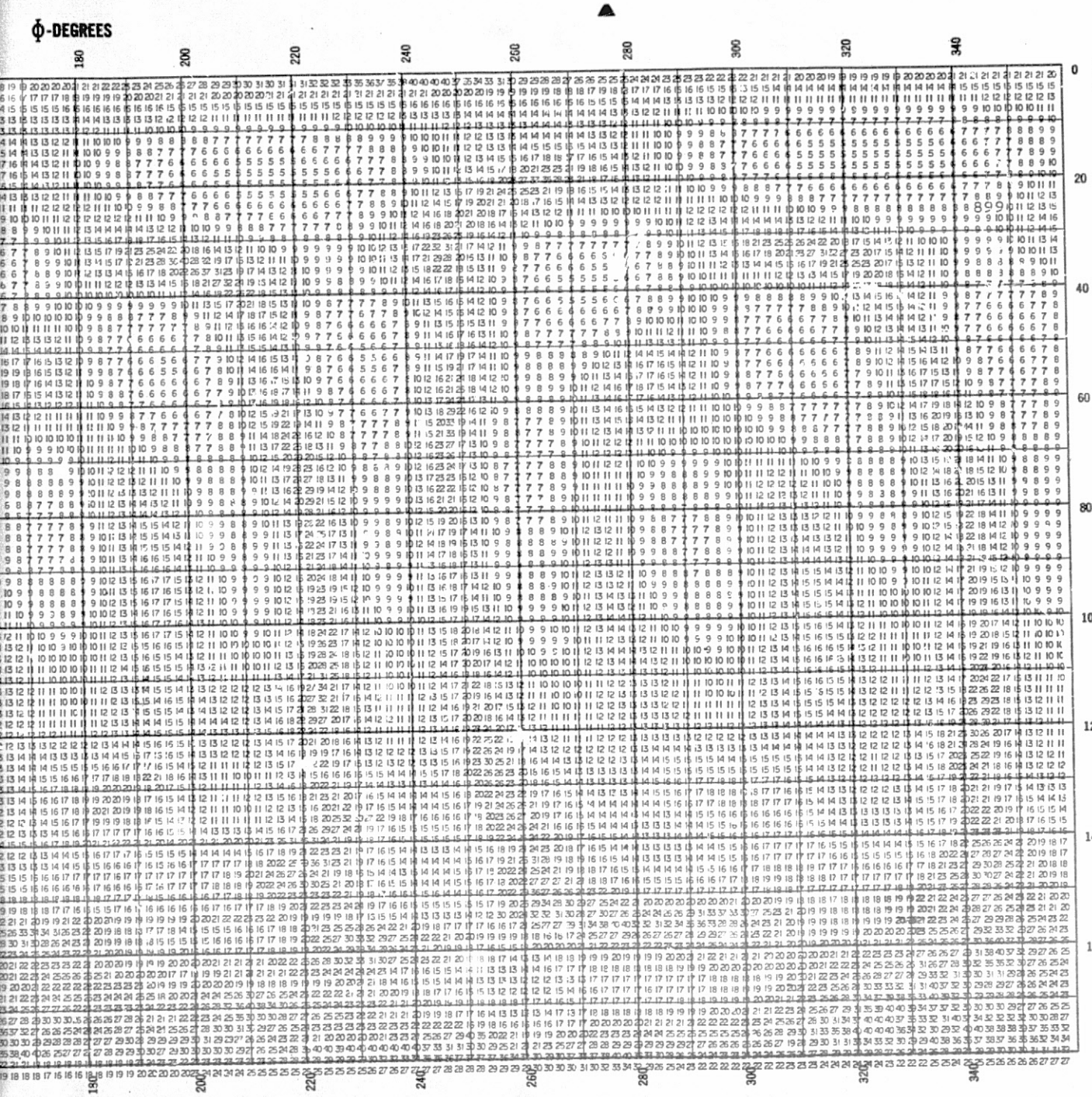

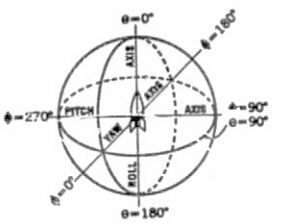

2

1227 MHz

GAIN PLOT: □ POLARIZATION COMPONENT RECORDED: LINEAR □Φ, □Θ, □ 45, □ 135; CIRCULAR □ RH, □ LH

GAINS ARE IN DECIBELS BELOW A REFERENCE LEVEL OF $\pm\square$ 11.9 DB RELATIVE TO AN ISOTROPIC ANTENNA

PHASE ANGLE PLOT:□ PHASE ANGLE RECORDED: □δ , □δ'

PHASE ANGLES IN DEGREES ARE RECORDED VALUES MULTIPLIED BY 10.

BALL BROTHERS RESEARCH CORPORATION
SUBSIDIARY OF BALL CORPORATION
BOULDER, COLORADO

F-4

FOLDOUT FRAME

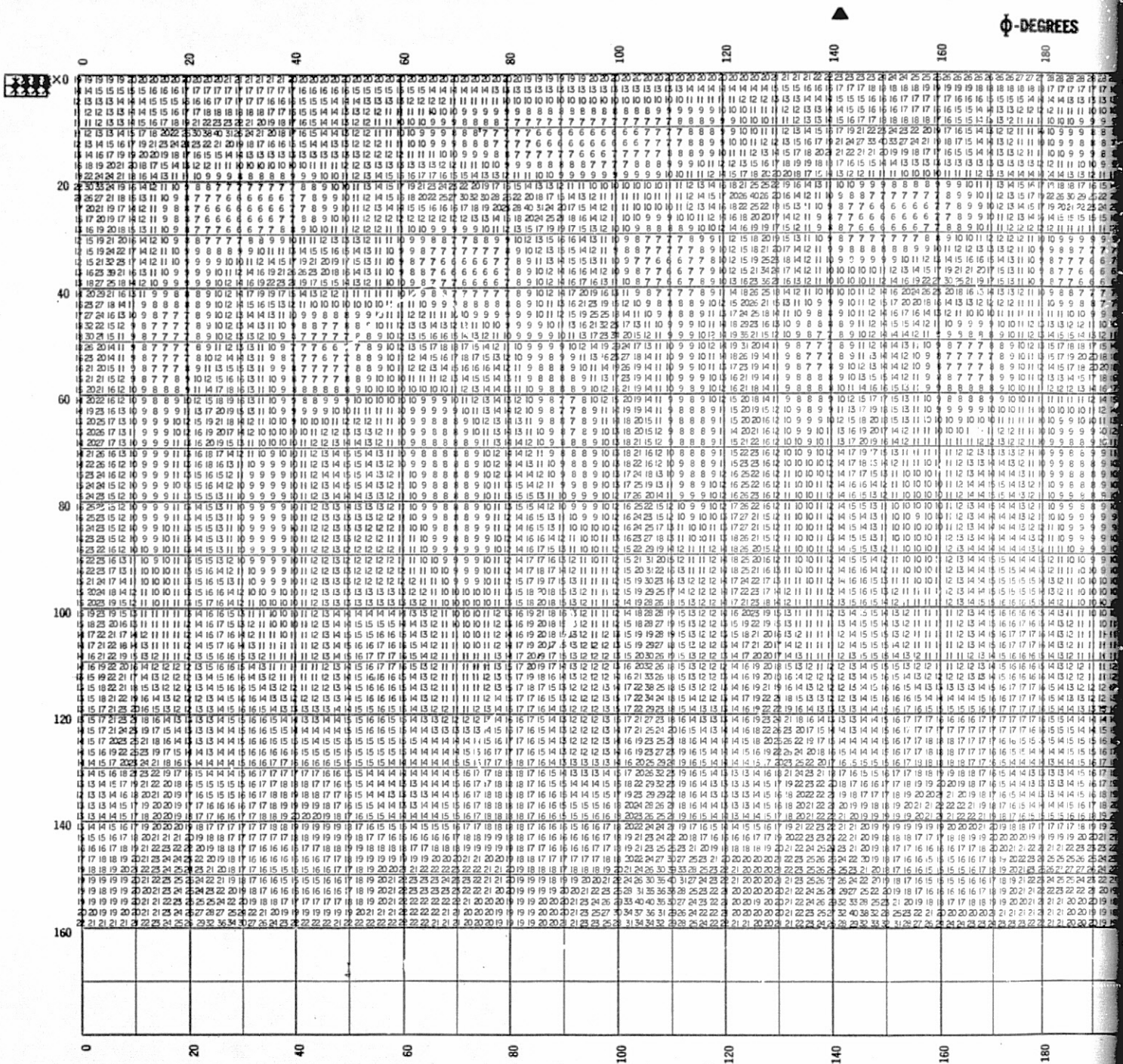

TEST PROGRAM OR VEHICLE: ESSA/GPS PROJECT: 3542

DATE: 8/12/77 PATTERN NO: 4 ORGANIZATION: ENGRS:

ANTENNA TYPE: 3 ELEMENT MICROSTRIP ARRAY FREQ. RANGE: PATTERN MEASUREMENT FREQ: 1575 MHz.

PREDOMINANT POLARIZATION: RHC MODEL SCALE: LOCATION OF POINT P'y (Φ=0, Θ=90°):

FOLDOUT FRAME 12

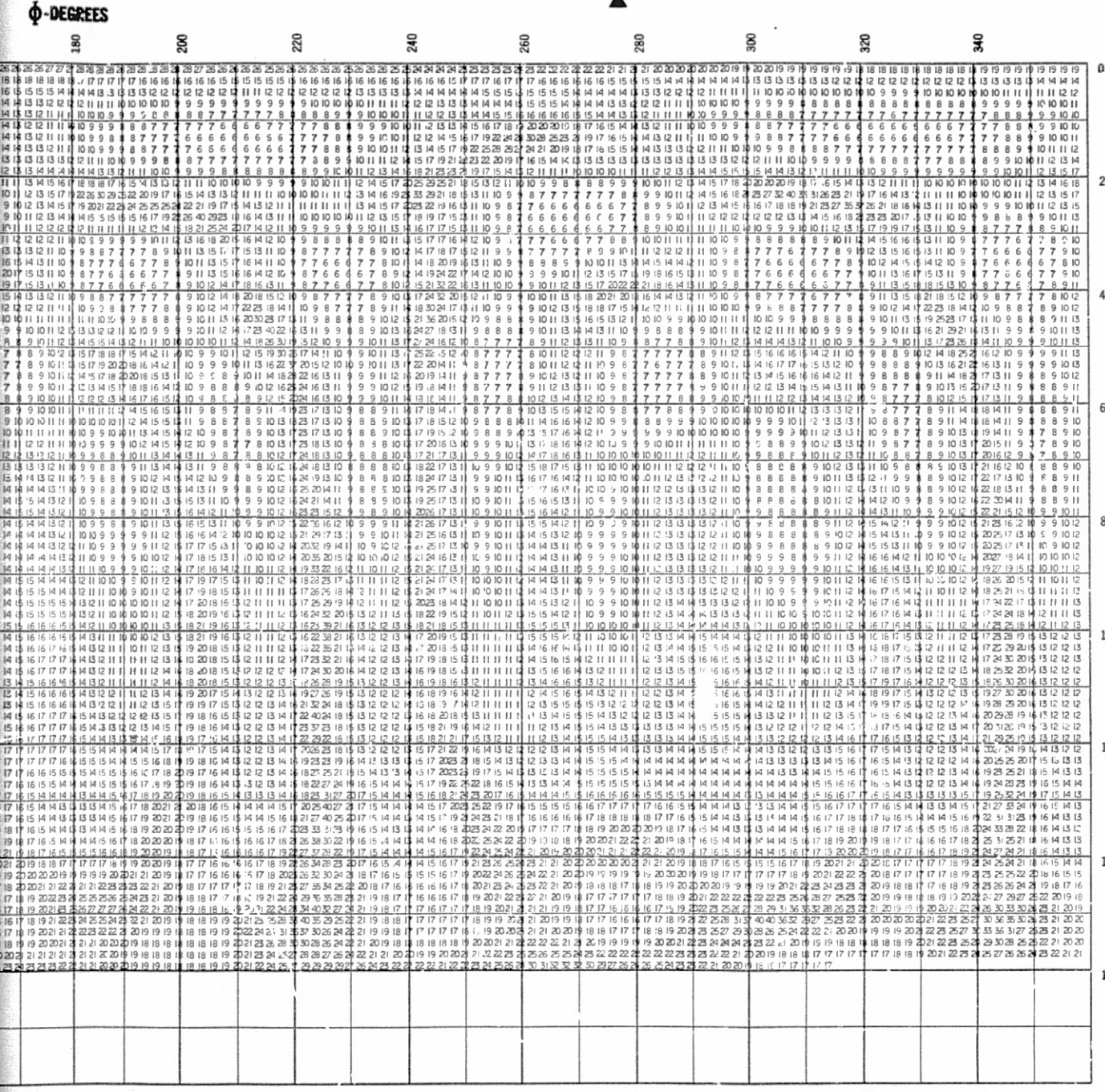

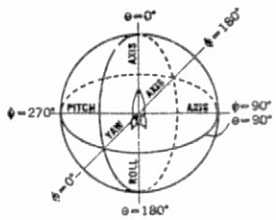

Ball

GAIN PLOT: □ POLARIZATION COMPONENT RECORDED: LINEAR □φ, □θ, □ 45, □ 135; CIRCULAR □ RH, □ LH

GAINS ARE IN DECIBELS BELOW A REFERENCE LEVEL OF ± X 10.8 DB RELATIVE TO AN ISOTROPIC ANTENNA
□

1575 MHz.

PHASE ANGLE PLOT: □ PHASE ANGLE RECORDED: □δ, □δ'

PHASE ANGLES IN DEGREES ARE RECORDED VALUES MULTIPLIED BY 10.

BALL BROTHERS RESEARCH CORPORATION
SUBSIDIARY OF BALL CORPORATION
BOULDER, COLORADO

F-5